



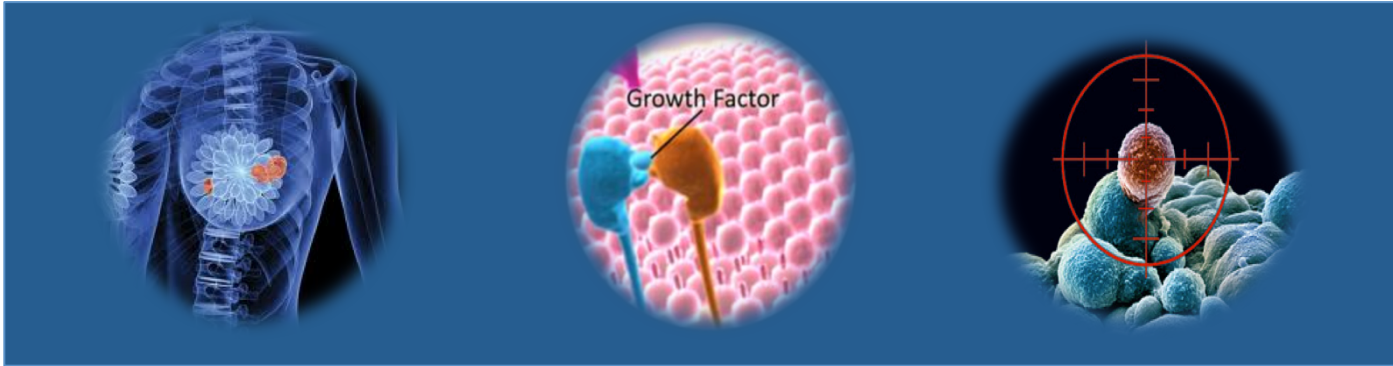
University of Liège  
Faculty of Medicine  
*GIGA-Cancer*



*Metastasis Research Laboratory*

*Prof. Vincent CASTRONOVO*

# Contribution Towards Understanding the Role of Myoferlin During Breast Cancer Progression



**Blomme Arnaud**

Master in Biochemistry, Molecular and Cellular Biology

Thesis submitted in support of the candidature to the  
PhD degree in Biomedical and Pharmaceutical Sciences

Promoters: Dr. Andrei Turtoi and Pr. Vincent Castronovo

Academic year 2014-2015

## Remerciements

Voilà, quatre ans déjà se sont écoulés... Quatre belles années faites de joie et (parfois) de frustrations, mais surtout de rencontres inoubliables. A l'heure d'écrire ce manuscrit (dans l'urgence, pour ne pas changer) il est maintenant temps pour moi de remercier toutes les personnes qui ont contribué de près ou de loin à la réalisation de ce doctorat.

En premier lieu, je voudrai remercier le professeur Castronovo de m'avoir accueilli au sein de son laboratoire. C'est grâce à vous que j'ai eu la chance de faire de la recherche mon métier au cours des quatre dernières années, et j'espère pouvoir continuer cela encore longtemps. Vous m'avez appris la rigueur et la précision au travers de votre exigence, mais surtout j'ai pu, je pense, avoir un aperçu de ce qu'est la vraie vie de chercheur. Je retiendrai de vous (entre autre) votre créativité et votre capacité de réaction face aux questions posées, auxquelles je restais sans réponse. Votre implication permanente dans l'opération Télévie force également l'admiration.

Ensuite je tiens à remercier le docteur Andrei Turtoi, qui a supervisé jour après jour l'entièreté de ce travail. En écrivant ces lignes je me suis rendu compte que je n'ai jamais su si je pouvais te tutoyer ! Je prends le risque de le faire. Un jour tu es arrivé de nulle part et tu m'as proposé de tout quitter et venir travailler avec toi. Bien que cette décision n'ait pas été facile à prendre, je suis convaincu aujourd'hui que j'ai fait un des meilleurs choix de ma vie. Je te remercie pour tout ce que tu as fait pour moi, sache que je ne l'oublierai pas.

Je tiens également à remercier les docteurs/professeurs Akeila Bellahcene et Olivier Peulen pour leurs nombreux conseils avisés, pendant ou en dehors des réunions, qui ont permis l'amélioration quotidienne de ce travail.

Un grand merci également au docteur Paul Peixoto, qui m'aura guidé tout au long de mon doctorat. Tu as joué à la perfection ton rôle de grand frère. Impossible pour moi de ne pas remercier également le docteur Denis Mottet. Tes conseils, tes remarques, les discussions que nous avons pu échanger m'ont été d'une aide précieuse et m'ont aussi permis de grandir. Je ne te souhaite que le meilleur pour la suite.

J'en viens ensuite à Vincent, mon ami Vincent. Je n'ose pas imaginer ce qu'aurait été mon doctorat sans ta présence. Plus qu'un collègue, tu es pour moi un ami inestimable. Tes aptitudes ainsi que ta loyauté forcent le respect. Tu m'as toujours aidé, à toute heure du jour et de la nuit, et j'espère pouvoir un jour te rendre la pareille. Cette thèse, c'est également la tienne et j'espère avoir été à la hauteur.

Ensuite je souhaite remercier tous les membres du LRM, présents ou passés, qui ont rendus ces 4 années inoubliables. Une pensée toute particulière pour Naïma, malgré ton manque d'humour, et Véronique pour votre aide quotidienne. Je remercie également Bruno, David et Muffin pour tous les bons moments passés ensemble. J'aimerais également remercier Pamela, Ana et Brunella, la relève du LRM, pour leur aide précieuse ces derniers mois.

Je remercie également les membres des différentes plate-formes de l'université de Liège, toutes les personnes qui ont collaboré à cette étude ainsi que les membres du jury d'avoir pris le temps de considérer ce travail.

Enfin j'aimerais remercier mon petit frère, Benoit, d'avoir toujours été là. Sache que je suis probablement la personne la plus fière de toi sur cette terre. Evidemment, je remercie mes parents Marie-Anne et Christian, qui m'ont toujours soutenu peu importe le contexte. Vous seuls étiez là dans les moments difficiles et c'est grâce à vous que j'ai trouvé la motivation de continuer dans cette voie. Cette thèse je vous la dédie, et j'espère que vous en serez fiers.

Je ne pourrai pas conclure ces remerciements sans remercier ma compagne, Jennifer, et ma petite Naomi, pour tous les sacrifices que cette thèse a représenté. Je vous remercie pour votre patience et votre soutien quotidien. Merci pour tout.

Arnaud

# Index

<b>1. <i>Index</i></b>	<b>3</b>
<b>2. <i>Abbreviations</i></b>	<b>7</b>
<b>3. <i>Introduction</i></b>	<b>9</b>
<b>3.1. Discovery of myoferlin as novel accessible biomarker</b>	<b>9</b>
<b>3.2. The ferlin family</b>	<b>11</b>
3.2.1. <i>C2 Domain</i>	12
3.2.2. <i>FER and Transmembrane domains</i>	12
<b>3.3. Ferlins and their biological functions</b>	<b>12</b>
<b>3.4. Myoferlin</b>	<b>13</b>
3.4.1. <i>Myoferlin in muscle cells</i>	13
3.4.2. <i>Myoferlin and angiogenesis</i>	14
3.4.3. <i>Myoferlin in cancer</i>	15
<b>3.5. Vesicle trafficking in cancer progression</b>	<b>16</b>
3.5.1. <i>Role in cell polarization</i>	16
3.5.2. <i>Role in receptor recycling and degradation</i>	18
3.5.3. <i>The example: EGFR</i>	19
3.5.4. <i>Role in microvilli formation</i>	20
3.5.5. <i>Role in cell metabolism &amp; significance of caveolin</i>	20
<b>3.6. Cancer cell metabolism: A brief overview</b>	<b>23</b>
3.6.1. <i>Tumor cells exhibit a glycolytic phenotype</i>	23
3.6.2. <i>Mitochondrial metabolism is altered in cancer cells,                 but essential for tumorigenesis</i>	23
3.6.3. <i>Alterations of energy-supplying pathways in cancer</i>	25
<b>3.7. AMP activated protein kinase, the “master regulator” of cell metabolism</b>	<b>25</b>
3.7.1. <i>AMPK deregulation in metabolic disease</i>	26
3.7.2. <i>AMPK deregulation in cancer</i>	27
3.7.3. <i>AMPK in cancer: Friend or foe?</i>	27

---

<b>4. <i>Aims of the study</i></b>	<b>29</b>
<hr/>	
<b>5. <i>Materials and methods</i></b>	<b>31</b>
<hr/>	
5.1. Patients	31
5.2. Proteomic analysis	31
5.3. MS analysis and data processing	32
5.4. Histology and Immunohistochemistry	33
5.5. Survival Analysis	34
5.6. MDA-MB231, MDA-MB468 cell culture, siRNA- and shRNA-mediated knockdown	34
5.7. Migration and invasion assay	35
5.8. Cell proliferation assay	35
5.9. Cell growth assay	36
5.10. Chicken chorioallantoic membrane (in vivo) tumor assay	36
5.11. EGF stimulation	36
5.12. Western blot	36
5.13. EGF-mediated EMT assay	37
5.14. RT-qPCR	37
5.15. Flow cytometry analysis of cell surface EGFR	38
5.16. Immunofluorescence	38
5.17. Density Gradient Centrifugation	38
5.18. Lactate measurement using nuclear magnetic resonance (NMR)	39
5.19. WST-1 assay	39
5.20. Isolation of mitochondria	40
5.21. Oxygen consumption measurements	40
5.22. ATP measurement	41
5.23. Apoptosis assay	41
5.24. Mitochondrial membrane potential and ROS measurement	41
5.25. Electron microscopy and immunogold labeling	42
5.26. Immunoprecipitation	42
5.27. Isolation of tumor cells	43
5.28. Murine <i>in vivo</i> experiments	43

5.29. Oil-Red-O staining of xenografted tumors	43
5.30. Statistical analysis	43
5.31. Adhesion assay	44
<b>6. <i>Results Part 1: Myoferlin is a consistent feature of human breast cancer</i></b>	<b>45</b>
6.1. Proteomic investigation identifies myoferlin as a membrane protein in human breast adenocarcinoma	46
6.2. Myoferlin is highly expressed in hormone-receptor positive breast cancer	48
6.3. Myoferlin gene-expression correlates with IHC data and patient survival	49
6.4. Myoferlin levels have different significance in individual breast cancer subtypes	50
6.5. Myoferlin affects migration, invasion, and survival of triple negative breast cancer cells.	51
6.6. Myoferlin depletion slows tumor growth <i>in vivo</i> .	52
<b>7. <i>Results Part 2: Myoferlin is a key regulator of EGFR activity in breast cancer</i></b>	<b>55</b>
7.1. Myoferlin regulates EGFR fate upon EGF-mediated receptor activation	56
7.2. Myoferlin silencing in breast cancer cells impaired EGF-induced migration and EMT	57
7.3. Myoferlin depletion affects the degradation of the internalized EGFR	59
7.4. Myoferlin does not affect clathrin cellular distribution/quantity in MDA-MB231 cells	61
7.5. Myoferlin is critical for proper assembly of caveolin in caveolae	62

---

<b>8. <i>Results Part 3: Myoferlin regulates endosomal trafficking and tunes cancer cell metabolism</i></b>	<b>65</b>
<b>8.1. Myoferlin silencing in breast cancer cells leads to lactate accumulation and impaired mitochondrial activity</b>	<b>66</b>
<b>8.2. Loss of Myoferlin induces mitochondrial dysfunction in breast cancer cells</b>	<b>67</b>
<b>8.3. Myoferlin depletion activates AMPK and induces a metabolic shift towards glycolysis</b>	<b>71</b>
<b>8.4. Myoferlin silencing sensitizes cells to drugs targeting metabolism</b>	<b>74</b>
<b>8.5. Myoferlin colocalizes with endosomal system and trafficking vesicles</b>	<b>77</b>
<b>8.6. Myoferlin interacts with caveolin-1 in caveolae and is essential for caveolin oligomerization</b>	<b>81</b>
<b>8.7. Myoferlin silencing impairs microvilli formation and endosome traffic</b>	<b>82</b>
<b>8.8. AMPK activation following myoferlin silencing is caveolin dependent</b>	<b>84</b>
<b>8.9. Myoferlin silencing reduces tumor growth and metastasis <i>in vivo</i></b>	<b>85</b>
<b>9. <i>Discussion</i></b>	<b>89</b>
<b>10. <i>Conclusions and perspectives</i></b>	<b>97</b>
<b>11. <i>Supplementary data</i></b>	<b>99</b>
<b>12. <i>Literature</i></b>	<b>103</b>
<b>13. <i>Annexes</i></b>	<b>114</b>

---

## List of abbreviations

ADP: Adenosine diphosphate	MS: Mass spectrometry
AMP: Adenosine monophosphate	NMR: Nuclear magnetic resonance
ATP: Adenosine triphosphate	OVN: Overnight
BSA: Bovine serum albumin	OXPPOS: Oxydative phosphorylation
CAM: Chorioallantoic membrane	PAGE: polyacrylamide gel electrophoresis
CBL: Casitas B lineage lymphoma	PBS: Phosphate buffer saline
cDNA: complementary DNA	PE: Phycoerythrin
CFH1: Cadherin-1	PI: propidium iodide
DAB: 3,3'-diaminobenzidine tetrachlorhydrate dihydrate	PR: Progesterone receptor
DCA: Dichloroacetic acid	PVDF: Polyvinylidene difluoride
DNA: Deoxyribonucleic acid	RNA: Ribonucleic acid
DTT: Dithiothreitol	RT-qPCR: Quantitative reverse transcription polymerase chain reaction
EDTA: Ethylene diaminetetraacetic acid	RT: Room temperature
EGF: Epidermal growth factor	SDS: Sodium dodecyl sulfate
EGFR: Epidermal growth factor receptor	TBS-T: Tris buffered saline tween
emPAI: Exponentially modified protein abundance index	TCI: Triple resonance cryprobe
EMT: Epithelial to mesenchymal transition	TMRE: Tetramethylrhodamin ester
ER: Estrogen receptor	TMSP: Trimethylsilyl propanoic acid
FBS: Fetal bovine serum	TNE: Tris-NaCl-EDTA
FCCP: Carbonyl cyanide-4- (trifluoromethoxy)phenylhydrazone	TX100: Triton X-100
FITC: Fluorescein isothiocyanate	VEGFR2: Vascular endothelial growth factor receptor 2
HBSS: Hank's balance salt solution	VIM: Vimentin
HER2: Human epidermal growth factor receptor 2	WB: Western Blot
HPLC: High performance liquid chromatography	
IGFR: Insulin growth factor receptor	
IHC: Immunohistochemistry	

# **Introduction**

### **Discovery of myoferlin as novel accessible biomarker**

Today, owing to mass spectrometry, shotgun proteomics and DNA/RNA microarray analyses, the list of reported potential tumor biomarkers is increasing rapidly. Despite this abundance, very few of such modulated proteins have found their way into the clinical validation phase and even fewer are used as reliable therapeutic targets or diagnostic markers [1-4]. Although this may seem discouraging, a major and indispensable step in many aspects of cancer research relates to the identification of specific and sensitive marker proteins. They form a base for the development of effective diagnostic, prognostic and therapeutic agents. To be considered as a good target, a tumor-associated biomarker has to fulfill several mandatory criteria: it has to be highly expressed in the tumor site but absent from healthy tissues. An ideal biomarker has also to be accessible through the blood circulation, in order to facilitate the delivery of directed antibodies or ligands that will specifically target the tumor. In the context of targeted therapies, such biomarkers are coupled with a cytotoxic compound that will allow a selective damaging of the tumor environment, sparing normal surrounding tissues. In the current work we embarked on such discovery study for breast cancer. We aimed to find a novel accessible biomarker which would fulfill the above criteria. However, considering the previous studies in the field we sought to develop a new method that would enable us to better exploit the targetable proteome of the breast cancer.

We and others believe that one of the most promising ways of identifying new and clinically useful biomarkers is to narrow down the number of proteins to the essential group of interest. Modulated proteins accessible from the bloodstream are an example of such a group. These proteins are mostly membrane-based or embedded in the surrounding extracellular matrix. They are of particular interest because they have increased potential to be reached by systemically delivered monoclonal antibodies loaded with pharmacological compounds. The available proteomic techniques tailored to tackle this protein group of interest do this by primarily exploiting the physical location of the protein and are to a lesser extent, focused on their chemical properties. To this end, the use of chemically modified biotin that labels accessible proteins through their free amino groups combined with streptavidin affinity chromatography represents a powerful method [5]. Modified biotin possesses on one end the biotin group and on the other a ligand that will react with proteins. Usually the ligand-protein reaction is based on NHS ester chemistry which targets the primary amines, and results in labelling of N-terminal and lysine amino acid residues. Following the rationale that the tissue cells are intact, the biotinylation reagent will not penetrate the cell membrane and hence will label only the proteins found on the outer side of the membrane and

in the extracellular matrix. This method has proved to be particularly useful to enrich accessible proteins and has successfully been used in our laboratory to identify biomarkers from tumoral kidney [6], breast [7], colon [8] and glioma [9]. Nevertheless, accessible proteins that do not bear such free amino groups will escape the inventory.

Another way to enrich proteomic samples in accessible proteins is to exploit the known fact that most membrane and extracellular proteins are glycoproteins [10]. Hence, the analysis of glycoproteins in tandem with the biotinylation method would offer a real possibility of covering a supplementary segment of accessible, but previously unidentified, proteins. Lectin column affinity purification, combined with concanavalin A, is one of the enrichment techniques that have been developed to isolate glycoproteins [11]. However, restricted specificities of individual lectins towards certain classes of glycans oblige to use several lectins in combination to ensure maximal isolation of glycopeptides; therefore increasing the risk of error. An alternative method is the hydrazide capture of preliminarily oxidized glycans, which appears to be more reproducible and less biased toward certain subsets of the glycoproteome in comparison to the lectin technique [12-14]. This approach has already been applied to cell lines [15] and recently also to normal tissue samples [16].

In the current work, we have developed an original method that combines three sequential steps consisting in protein biotinylation and glycopeptide analysis followed by the sequencing of neither glycosylated nor biotinylated peptides (rest-proteins) [7]. The latter helps to assign those glycopeptides that cannot be related with enough confidence to a specific protein. Additionally, we have shown that the rest-fraction also contains a number of unique and potentially accessible proteins making this step an integral part of the approach. The method was designed such that a minimal amount of material or information is wasted. Following this approach we have identified a number of novel potentially accessible biomarkers which have unknown functions in cancer [17]. One of these novel proteins is myoferlin, which has caught our attention due to its quality of being a transmembrane protein with an extracellular domain. According to the existing knowledge, this protein belongs to the ferlin family of protein and is involved in the process of cell membrane fusion and repair [18], as well as vesicle-mediated endocytosis [19]. Thus far little is known regarding the potential role of myoferlin in cancer and we therefore aimed to shed light on this protein specifically in breast cancer.

## The ferlin family

The term ferlin is derived from the *fer-1* gene, in *Caenorhabditis elegans*, a FERTilization factor essential for spermatogenesis. Mutations of this gene lead to defects in membranous organelle fusion and infertility [20-22]. Another related gene in *Drosophila melanogaster*, termed the *misfire* gene, is involved in developmental processes such as sperm activation and early embryogenesis [23, 24].

Ferlins are an ancient family of proteins, with homologs of the *fer-1* gene discovered from phytoplankton to human, and having been reported in all eukaryotic kingdoms and in protozoans [25]. Surprisingly, ferlins have not been found in higher plants, amoeba and yeast. The ancient origin of ferlins underlies their important role in cellular trafficking; as a comparison, clathrin and caveolin came much later in evolution [26].

Ferlins are large proteins (over 200kDa) which feature multiple C2 domains (see below) and a short C-terminal transmembrane domain (**Fig. 1**). Nowadays, the ferlin family of proteins is composed of six mammalian genes: dysferlin, otoferlin, myoferlin, FER1L4, FER1L5 and FER1L6. Of these, the role of the last three members is currently not well understood. The ferlins can be further separated into two groups, based on the presence or not of the dysferlin (DysF) domain [27]. In addition, many of these proteins can undergo alternative splicing and are therefore present in multiple isoforms.

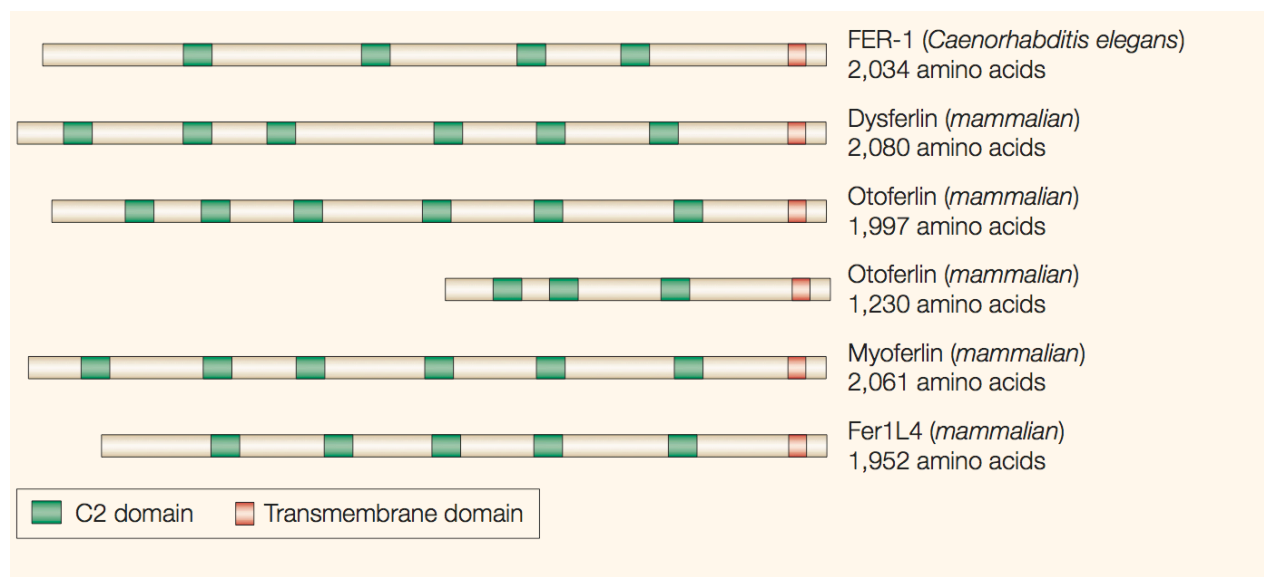


**Figure 1:** The Ferlin protein family. Members of the ferlin family contain multiple C2 domains and a short C-terminal transmembrane domain. From McNeil et al., 2005 [28].

### *C2 domain*

All ferlin proteins contain at least 5 to 7 C2 domains. C2 domains are primarily involved in protein-membrane targeting processes. Majority of these domains is able to interact with calcium ions and have specialized segments mediating phospholipid and protein binding. C2 domains display a canonical eight beta-strands structure with a type II strand topology. Apart from ferlins, two other families of protein contain multiple C2 domains: multiple C2 domain transmembrane proteins (MCTPs) [29] and synaptotagmins [30]. The multiple C2 domains (from C2A to C2F) in ferlins are structurally different from each other, but share a significant homology to analogous C2 domain in other ferlins [25]. The latter suggests a specialized function for each domain.

### *FER and transmembrane domains*

In addition to multiple C2 domains, ferlins present short ferlin-specific motifs (FerA and FerB) and can contain a DysF domain, whose functions are yet unknown. They also contain a short C-terminal single pass transmembrane domain.

## **Ferlins and their biological functions**

*Fer-1*, in *C. elegans*, was the first ferlin identified in 1997. It plays a role in calcium-sensitive membranous organelle fusion during spermatogenesis [31]. Mutations in this gene in different models (*C. elegans* [21], *D. melanogaster* [23] and in sea urchin eggs [32]) lead to impairment of several calcium-regulated processes such as membrane fusion, exocytosis, embryo development and wound repair. *FER-1* mutants are infertile and present locomotion defects as well as muscle loss.

Dysferlin is mainly expressed in muscle, heart and brain, but can also be found in placenta [33-35]. Mutations in the dysferlin gene result in autosomal forms of muscular dystrophy [36] and can be associated with cardiomyopathy [37, 38]. Studies in dysferlin-null mice highlight an important role of this protein in calcium dependent membrane repair of muscle cells [39]. Interactions with other dystrophy-related genes, like caveolin-3 [40], calpain-3 [41], annexins A1 and A2 [42], have been reported. Dysferlin, together with myoferlin, regulates cellular trafficking and recycling of the insulin growth factor receptor (IGFR) in muscle cells [43, 44], suggesting a broader role in muscle growth. Finally, in endothelial cells, dysferlin regulates the trafficking of the platelet endothelial cellular adhesion molecule-1 (PECAM-1), influencing cell adhesion and angiogenesis [45].

Otoferlin is another disease-related ferlin. This protein is expressed in brain and in the

inner ear (vestibular system and cochlea) [46]. Otoferlin has been shown to play an important role in auditory neurotransmission, through calcium-activated exocytosis of synaptic vesicles [47]. Mutations in otoferlin result in progressive hearing loss ending in deafness [48]. Biochemically, otoferlin has been shown to bind SNARE proteins and enhance synaptic vesicle fusion [49].

### **Myoferlin**

Myoferlin has first been identified in cardiac and skeletal muscle, where it was found both at the plasma membrane and in the nucleus of mouse muscle cells [50]. The protein has 8 different isoforms (alternative splicing), ranging from 17 to 230 kDa, of which 5 harbor a short transmembrane and an extracellular domain. Currently no information is available on whether these isoforms have different functions. Myoferlin is highly homologous to dysferlin (68%) [51], but unlike the latter myoferlin also contains a SH3 domain that mediates interaction with other proteins. Interestingly, a number of phosphorylation sites are conserved in both dysferlin and myoferlin, leaving room for a potential role of these proteins in cell signaling.

#### *Myoferlin in muscle cells*

Myoferlin has been reported at the membrane sites of myoblast-myoblast and myoblast-myotube fusions [18, 50], playing essential role in muscle development and regeneration [28, 52]. Analysis of myoferlin-null mice showed that mutant animals developed smaller muscles, lacking large diameter myofibers as compared to wild-type animals. The myoferlin-null mice were also unable to fully regenerate muscle after injury [18]. Following these important functional observations, the question concerning the myoferlin gene regulation was quickly raised. McNally and colleagues suggested that myoferlin could be regulated by NFAT. The authors have shown that a 1543 bp fragment of the myoferlin promoter, containing multiple NFAT binding sites, was sufficient to induce an overexpression of the protein at a similar level than the one observed during muscle injury [53]. Additional studies by the same group demonstrated that muscles from myoferlin-knockout mice were unable to respond to IGF1 treatment, a strong promoter of muscle growth [44]. In normal myoblasts, myoferlin deficiency led to a defect in insulin growth factor-like receptor (IGFR1) trafficking as well as to decreased IGFR1 signaling, evidenced by decrease in activated AKT and MAPK. In absence of myoferlin, IGFR1 accumulated in large vesicles promoting degradation instead of recycling.

*Myoferlin and angiogenesis*

Alongside its importance in muscle cells, a growing body of literature points at a novel myoferlin function in endothelial cells (EC) regulating angiogenesis and Tyrosine Kinase Receptor (RTK) trafficking. Bernatchez et al. identified myoferlin in purified caveolae-enriched membrane microdomains/lipid rafts isolated from human umbilical vein and bovine aortic endothelial cells [54]. The protein localized in puncta throughout the cell and at the cell surface. Using short interfering RNA the authors demonstrated that myoferlin loss leads to defective membrane repair, and affects vascular endothelial growth factor (VEGF) induced proliferation, migration and permeability. The effects of myoferlin deficiency were further linked to down-regulation of the VEGFR2 protein and subsequent alteration of the downstream signaling pathway. Decrease in VEGFR2 levels resulted from an increased proteasomal degradation of the receptor via enhanced polyubiquitination. Pull-down experiments demonstrated that myoferlin associates with dynamin-2 and VEGFR2 through the SH3 domain, forming protein complexes that blocks casitas B-lineage lymphoma (CBL) dependent ubiquitination of the receptor.

Along the same lines, myoferlin silencing was shown to decrease the expression of TIE-2, a tyrosine kinase receptor expressed mainly in the vascular endothelium [55]. However, regulation of TIE-2 in absence of myoferlin did not depend on CBL or on proteasomal degradation. Interestingly, injection of a myoferlin siRNA/lipid mixture *in vivo* into the ears of CD1 mice did not affect ear vasculature but was sufficient to abolish VEGF-induced edema, confirming the importance of myoferlin in VEGF-induced angiogenesis. In a further study, caveolin-1 was reported as another major interactor of the myoferlin/dynamin-2 complex [56]. This study pointed at the implication of myoferlin in receptor-dependent endocytosis. Indeed, myoferlin overexpression increased caveolae/lipid-rafts mediated endocytosis of cholera toxin B and, to a lesser extent, clathrin-dependent endocytosis of transferrin. In contrast to this, silencing of myoferlin dramatically reduced both processes. Immunofluorescence and immunoprecipitation experiments respectively showed that myoferlin and caveolin-1 colocalize and physically interact together. Moreover, silencing of myoferlin interactors caveolin-1 or dynamin-2 also impaired endocytosis as well as membrane resealing after injury, suggesting that all these interacting proteins can regulate overlapping but distinct cellular functions. Collectively, these findings point at the specialized function of myoferlin in controlling essential membrane cell-signaling processes, especially those involved in the vesicular trafficking of growth factor receptors.

### *Myoferlin in cancer*

Although increasing number of studies continues to further our understanding of myoferlin function in normal cells, to date, only little is known concerning its role in tumor cells. Three high-throughput studies have initially reported the overexpression of myoferlin at the mRNA level in lung [57] and breast cancer [58] as well as at the protein level in pancreas cancer [17]. In 2011, a study published by Eisenberg and colleagues has highlighted the pro-invasive functions of myoferlin in breast cancer [59]. Using an electrode-impedance-based invasion assay, they showed that MDA-MB231 stably transfected with shRNA against myoferlin exhibited reduced invasive capacity than their control counterparts. Based on predictive mathematical simulations, they further proposed that this effect could be mediated by downregulation of several matrix metalloproteinases production or secretion and impairment of RTK recycling processes.

Following this, Li and colleagues demonstrated that myoferlin expression was correlated with invasiveness of breast cancer cell lines [60]. They also showed that myoferlin-deficient MDA-MB231 exhibited a more epithelial-like morphology, suggesting that a mesenchymal to epithelial change occurred in these cells. Higher expression of epithelial markers together with lower levels of mesenchymal markers strengthened this hypothesis. Myoferlin depletion was also found to negatively affect invasive capacities of the cells, and to lead to decrease in the secretion of several MMPs. Recently, another study from the same group proposed that myoferlin loss was able to redirect the migratory phenotype of breast cancer cells from single cells migration to collective migration [61]. Using wound healing assays and live cell imaging, they observed that cells lacking myoferlin remained as a cohesive monolayer and underwent directional migration, while control cells separated from each other and migrated randomly to close the gap. MYOF-deficient cells also exhibited increase in cell-substrate adhesion and displayed an altered cytoskeletal structure. Finally, alteration of the invasion properties of the cells *in vitro* led to a decrease in tumor growth and invasiveness *in vivo*, with MYOF-KO tumors being very circular and restricted to their injection site.

Concomitantly with this work, a paper from the Bernatchez's group was the first to describe an important role for myoferlin in tumorigenesis, using a mouse model of lung cancer [62]. In this study, myoferlin expression has been reported in a series of cancer cell lines, regardless of their metastatic potential, and both in xenografted mice tumors of Lewis Lung Carcinoma and in human lung carcinoma. *In vivo*, periodic intratumoral injection of siRNA directed against myoferlin significantly reduced the size of xenografted LLC tumors

without affecting angiogenesis. However, myoferlin silencing decreased cell proliferation of both LLC cells *in vitro* and LLC tumors *in vivo*. In this rapidly dividing type of tumor cells, attenuated proliferation was not a result of increased apoptosis, but was rather due to defects in proliferation-induced membrane repair, highlighting the role of myoferlin in tumorigenesis.

Taken together, the latest data linking myoferlin to cancer suggest an important role of this protein in tumor growth and invasiveness. Certainly there is a potential place for myoferlin to serve as therapeutic target, however this will depend on our ability to understand the underlying mechanism. Therefore we were particularly motivated to answer the question how does myoferlin regulate invasion and proliferation capacity of cancer cell. In our quest for the mechanism we have started from the initial observation that myoferlin is essential for membrane fusion biology and endocytosis. An important aspect of the latter is membrane vesicle trafficking, which is a highly important physiological process controlling receptor-mediated signaling, endocytosis and exocytosis. To further investigate the role of myoferlin in cancer, we first sought to understand how vesicle trafficking influences tumor development and progression.

### **Vesicle trafficking in cancer progression**

Vesicular trafficking regulates components of the plasma membrane in all cell types. In normal cells, membrane vesicles are coordinated by specialized networks of microtubules and F-actin filaments to ensure a correct distribution of membrane proteins, lipids, or metabolites and their targeting to plasma and organelles membranes.

#### *Role in cell polarization*

Epithelial cells require to be polarized [63, 64]. They need to keep both an apical and a basolateral membrane with proper characteristics, and to compartmentalize functional components like receptors, channels and adhesion molecules, in correct sub-cellular areas [65, 66]. These tasks are mediated through vesicle trafficking and impairment of the latter represents the initial step leading to loss of cell polarity. This will in turn cause alterations in protein distribution and cell morphology changes (**Fig. 2**).

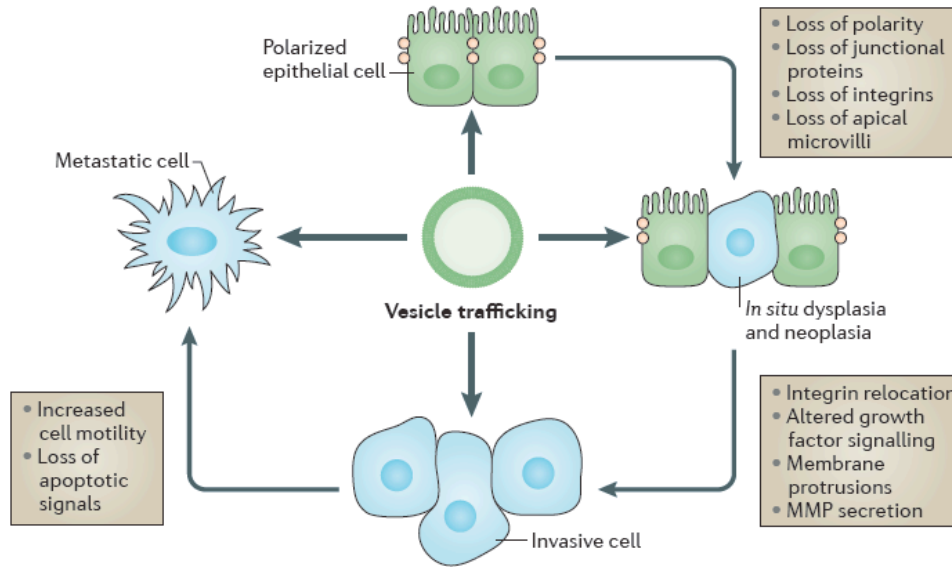


**Figure 2:** Vesicle trafficking impairment can induce tumorigenesis of epithelial cells. Adapted from Goldenring, 2013 [67]

The loss of polarity does not directly lead to carcinogenesis. It initially results in aberrant activation of signaling pathways due to misplaced or overexpressed receptors, disrupted trafficking to lysosomes or impaired recycling of the receptor (see below) (**Fig. 3**) [68]. Furthermore, incorrect distribution of adhesion molecules [69] and junction components [70-72] leads to increased permeability of the mucosa and exposes the cell to external stresses (cytokines and inflammation). These events lead to accumulation of cellular damages resulting from aberrations in cell signaling pathways and are a promoter of cancer development.

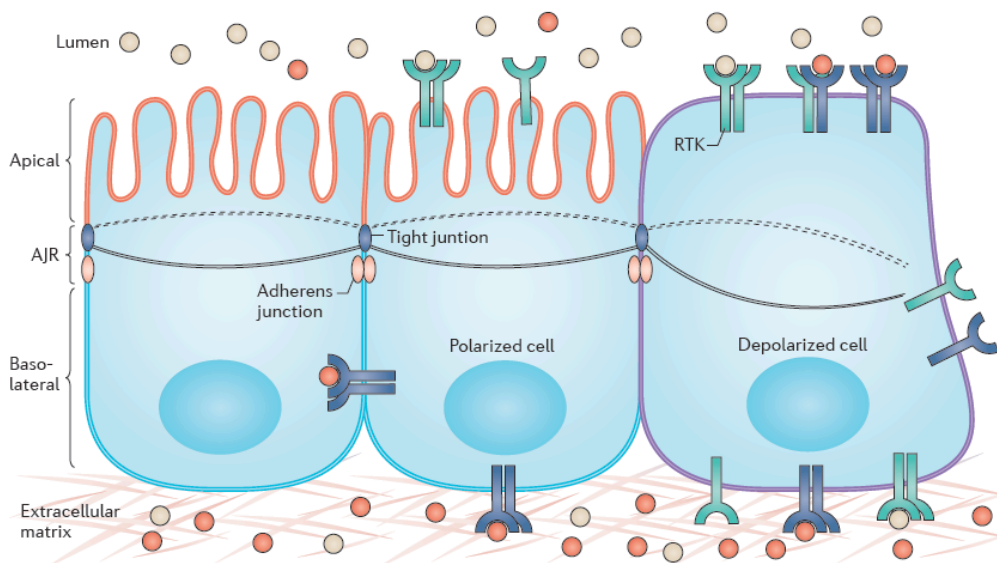


**Figure 3:** Loss of cell polarity results in aberrant cell distribution of Tyrosine Kinase Receptors (RTKs). Adapted from Casaletto et al., 2012 [73]

### Role in receptor recycling and degradation

Vesicular trafficking is involved in *de novo* synthesis of membrane proteins (among which also receptors) and their transport from the Golgi apparatus to the membrane [74]. A further aspect of vesicle trafficking is receptor endocytosis. Receptor-dependent signaling relies on a complex equilibrium between synthesis of the new receptor, recycling of the existing one and degradation [75]. Accordingly, once a receptor binds a ligand, it is endocytosed from the membrane and can be either targeted for degradation to lysosomes, or recycled to the plasma membrane (**Fig. 4**).

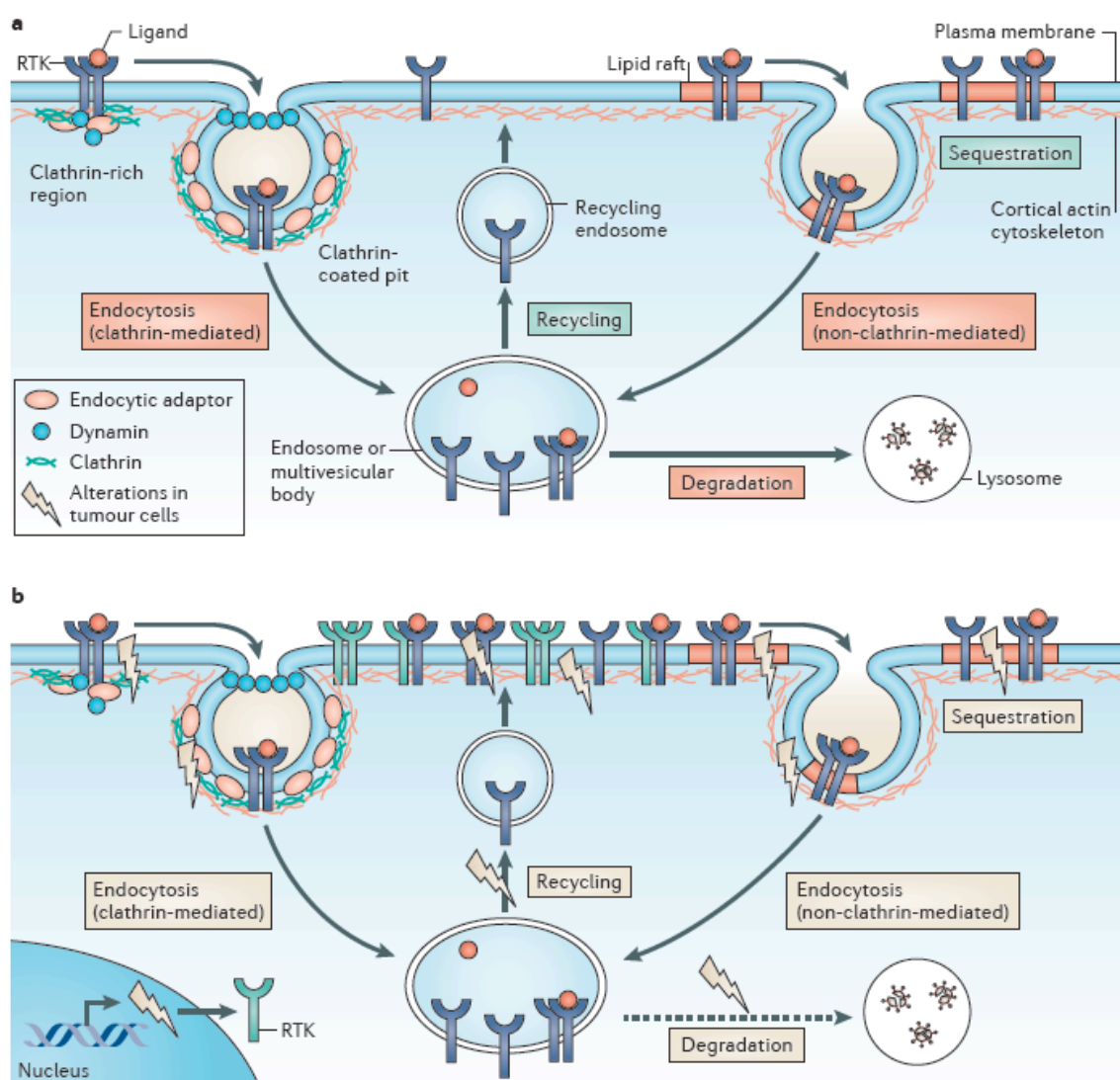


**Figure 4:** Vesicle trafficking involves clathrin and non-clathrin-mediated endocytosis. Once endocytosed, receptor can be directed either to degradation or to recycling. Changes in vesicle trafficking will alter the fate of the receptor and induce different cell signaling. Adapted from Casaletto et al, 2012 [73]

The two major processes described in receptor internalization are the clathrin (CME) or nonclathrin (NCE) mediated endocytosis. After detachment from the membrane, small vesicles will often fuse into multivesicular bodies, called endosomes, which will then differentiate in recycling endosomes or further fuse with lysosomal structures.

One of the most prominent classes of receptors in cancer that functionally benefit from the process of endocytosis, are the receptor tyrosine kinases (RTK). RTK signaling is consistently enhanced in cancer and this has initiated the development of targeted therapies against RTKs [76]. These therapies consist mainly in inhibitors of RTK phosphorylation, that will block the receptor's downstream signaling pathways, or in antibody-based therapies, that prevent association of the receptor with a ligand. However, spatial and dynamic regulation of the receptors confers adaptation to the tumor cells, and can lower the efficiency of such therapies. Increased expression of the receptor and enhanced diversity of dimerization partners will have dramatic effects on the efficacy of ligand-blocking therapies [77-79]. Defects in vesicle trafficking will allow aberrant signaling of the receptors inside intracellular vesicles, where they are protected from antibodies or inhibitors.

### *The example: EGFR*

Epidermal growth factor receptor (EGFR) is an RTK whose activation and signaling contributes to major cancer key hallmarks including proliferation, invasion, and metastasis [80]. As such, EGFR and its downstream signaling is currently one of the most explored pathways in terms of targeting and anticancer treatments. Unfortunately, current therapies aiming to interfere with EGFR signaling components are rather disappointing in clinics, reflecting our limited mechanistic understanding. Today, a wealth of evidence suggests that an essential aspect of EGFR activity regulation consists of receptor internalization (endocytosis) and intracellular targeting [81]. This process goes beyond simple recycling of the EGFR and attenuation of the signaling. In fact, it provides an important spatial and temporal component to the activity of the receptor. Endosomes containing EGFR (or other activated RTK), depending of their composition, can either continue to signal in a specific cell compartment or be rapidly degraded in other. At least 2 mechanisms of RTK internalization, respectively, identified as CME and NCE-mediated endocytosis, have been described to play essential roles in defining EGFR fate upon ligand-based activation [81, 82]. The activation of one particular endocytic pathway depends at least in part on EGF concentration [82], and each of the two leads to a different outcome for the receptor (e.g., degradation or recycling). The NCE process is particularly blurry with yet many unknown players that participate/regulate it.

Present literature frequently points at caveolin as a protein that is involved in the NCE; however, the presence of this protein is not always a compulsory factor [81, 82]. This leaves an important question open concerning the identity of proteins participating in NCE.

#### *Role in microvilli formation*

Invasive cells require the redistribution of adhesive molecules [83] and the secretion of degrading enzymes, such as the matrix metalloproteinases [84, 85]. These cells are characterized by active turnover of cytoskeleton and membrane remodeling [86]. This allows dynamic extension of cell protrusions to promote cell migration. Along these lines, vesicle trafficking is also essential for the formation of such specialized structures also referred to as microvilli. Microvilli are organized plasma membrane protrusions that increase exchange surface area and facilitate absorption and secretion [67]. As a consequence, invasive cells are highly sensitive to alterations in vesicle trafficking and impairing this process will strongly reduce the migratory capacities and the metastatic potential of aggressive cells [69, 87, 88].

#### *Role in cell metabolism & significance of caveolin*

Vesicle trafficking is crucial to cellular metabolism. Perturbations in the function of growth receptors (e.g. IGFR) as well as impaired nutrient uptake due to deficient endocytosis are some of the most evident causes [89, 90]. Of the transport vesicles involved in the traffic, caveolae assume some of the most relevant roles [91]. They have been repeatedly reported as interaction partners of myoferlin [56, 92] and shall therefore be considered in particular detail in the following sections.

Caveolae are non-coated small vesicles, ranging from 25-150 nm, enriched in cholesterol and sphingolipids [93]. Their main component is caveolin, a protein which exists in three different isoforms [94]. Caveolin-1 and 2 are ubiquitously expressed while caveolin-3 expression is muscle specific [95]. Among the three, only caveolin-2 is suggested to have redundant functions and is therefore the less studied. They are synthesized in the endoplasmic reticulum and then undergo several rounds of oligomerization, stabilized by cholesterol, to finally form large hetero or homo-oligomeric structures - the caveolae [96, 97]. Inside these lipid-raft structures, caveolins can also be involved in signal transduction. Caveolae are enriched in signaling molecules such as Src kinases and interaction with caveolin-1 generally leads to inhibition of the signal [98]. Caveolae serve as focal points to concentrate signaling molecules and to rapidly modulate their activity in response to environmental stimuli.

***Caveolae are metabolic platforms*** that have been found to be crucial for stimulated-nutrient uptake, like glucose. For example, translocation of glucose transporter GLUT4 to the plasma membrane in response to insulin is mediated through caveolae in adipocytes. Glucose is therefore temporarily stocked and transported in these vesicles [99-101]. Recently, colocalization of GLUT1 and GLUT3 in caveolae of spermatogenic cells demonstrated that glucose uptake through caveolae is not restricted to insulin-sensitive cells. Presence of glycolytic enzymes within the caveolae further suggests that the glucose already starts to be metabolized in these vesicles [102].

Lipid metabolism is highly dependent on caveolae. Indeed, fatty acid uptake from the membrane is mediated by caveolae. Majority of the proteins composing caveolae are able to directly bind fatty acids (caveolin, cavin, FATP, CD36), and disruption of caveolae abolishes fatty acid uptake, highlighting their importance in this process [103-106]. Subclasses of caveolae in adipocytes have also been shown to synthesize triacylglycerol by conversion of fatty acids. They have the capacity to accumulate lipid droplets and contain all the enzymes required for rapid lipolysis. Caveolin specifically binds cholesterol and synthesis of this protein is directly coupled to cholesterol levels [107, 108]. Through this interaction, caveolae are involved in the uptake of free cholesterol or cholesteryl ester from High Density Lipoprotein (HDL), but also in the transport of cholesterol through the plasma membrane and its efflux from the cell [105, 109, 110].

***Caveolin regulates cell metabolism*** through its involvement in cholesterol homeostasis. Importantly, impaired caveolin-1 function leads to depletion of cholesterol in the plasma membrane, while overexpression of the protein facilitates cholesterol efflux [111, 112]. Additionally to caveolae, soluble form of caveolin is proposed to be essential for intracellular cholesterol regulation. In general, caveolin-1 controls free cholesterol levels and regulate its trafficking from the membrane towards organelles and vice versa [113]. Importantly, caveolin trafficking is also regulated by cholesterol. Therefore, a positive loop between cholesterol and caveolin is created to regulate cholesterol homeostasis.

Owing to its importance in lipid and cholesterol trafficking, caveolin is inevitably linked to cell metabolism. A striking example is the regulation of mitochondrial function by caveolin. Caveolin-deficient mice display altered mitochondrial and metabolic function [114]. Recently, Bosch et al. [115] have proposed that caveolin could regulate mitochondrial function through cholesterol efflux at the plasma membrane. Indeed, cholesterol enters mitochondria through specialized areas of the ER, called the mitochondria associated membranes. In absence of caveolin-1, transport of cholesterol to the membrane is impaired

and MAMs are overloaded with cholesterol [116]. The latter will cause an increase of cholesterol percentage in the mitochondrial membrane, which will ultimately impair mitochondrial function. Increase of caveolin is also observed in response to lipid metabolism defects, such as steatosis [117]. High caveolin expression is associated with a translocation of the protein into mitochondria. In the organelle, the protein will help to transport molecules (ions, proteins, etc) and to prevent oxidative stress, ultimately preserving mitochondrial function [118]. Increased translocation of caveolin inside mitochondria is also seen in adipocytes and in muscle in response to cellular stresses.

In cancer, caveolin has been strongly linked to regulation of tumor metabolism. Caveolin-1 is generally considered as a tumor suppressor [119-121], even if it was also reported to promote tumor growth in certain studies [122, 123]. Caveolin-1 expression has been shown to be suppressed by oncogenes [124] and induced by other tumor suppressors such as p53 [125]. Recent studies have focused their attention on the particular role of caveolin-1 in tumor-associated fibroblasts. The new data demonstrate that loss of caveolin-1 in tumor stroma is a better predictor of clinical outcome in breast [126-128] and prostate [129] cancers than tumor cell caveolin-1. Loss of caveolin-1 alone was sufficient to turn fibroblasts into cancer-associated fibroblasts (CAFs) [130]. However, the main finding is the discovery of caveolin function in regulating metabolism of tumoral stroma. The concept has been termed as “Reverse Warburg Effect” (for a detailed review see [91]). In this model, breast cancer cells inhibit caveolin-1 expression in fibroblasts by increasing oxidative stress. The latter is mediated at least in part by H<sub>2</sub>O<sub>2</sub> secreted by the cancer cells. In fibroblasts, loss of caveolin-1 releases the inhibition of eNOS activity and induces oxidative stress through overproduction of nitric oxide (NO). Increase in oxidative stress in turn decreases caveolin-1 expression through increased autophagy establishing a vicious cycle. Oxidative stress resulting from caveolin-1 defects will activate transcription factors such as HIF1- $\alpha$  and NF- $\kappa$ B and promote a shift of the metabolism from oxidative phosphorylation to glycolysis. Aerobic glycolysis and increased autophagy will lead to increased accumulation of metabolic intermediates, such as lactate and nucleotides, that will fuel mitochondria of cancer cells, promoting cell growth and tumor progression.

### **Cancer cell metabolism: A brief overview**

#### *Tumor cells exhibit a glycolytic phenotype*

In 1926, Otto Warburg demonstrated that cancer cells favor glycolysis over oxidative phosphorylation (even under aerobic conditions) to produce their ATP [131]. He assumed that this metabolic adaptation, called “aerobic glycolysis” was a common feature of malignant cells and suggested that cancer is related to impaired mitochondrial metabolism [132]. Development of tumor imaging by positron emission tomography, based on the high rate of glucose uptake of cancer cells, emphasizes the importance of Warburg’s observation [133]. The glycolytic phenotype often correlates with aggressiveness of the tumor and poor prognosis [134-137].

Even though glycolysis is less efficient, the glycolytic production of ATP is more rapid and can confer cancer cells several adaptive advantages. The high rate of glycolysis in most tumors not only compensates for mitochondrial dysfunction but also provides a constant supply of metabolic intermediates and reducing equivalents that can be used to support cell growth and antioxidant defense. Increased glycolysis is also accompanied by increased stability of the mitochondrial membrane and reduced leakage of apoptosis-inducer cytochrome-c. High intracellular glucose concentrations enable the cell to redirect the accumulated glycolytic end-product pyruvate toward lipid synthesis [138], which is necessary for membrane assembly. Extracellular accumulation of lactate, resulting from increased glycolysis, will in turn lead to acidification of the surrounding environment and is thought to confer a competitive advantage to tumor cells [139]. Using less mitochondria for energy production will finally help cancer cells to acquire resistance to mitochondrial-mediated apoptosis [140].

#### *Mitochondrial metabolism is altered in cancer cells, but essential for tumorigenesis*

Although looking at Warburg’s theory, one may think that cancer cells do not require mitochondria, we know today that this is not the case and that using mitochondria and glycolysis are in balance to each other. Contrary to Warburg’s idea, aerobic glycolysis seen in cancer cells is not only due to defects in mitochondrial oxidative phosphorylation. Although mutations in mitochondrial genes are common in cancer cells, they alter mitochondrial bioenergetics rather than to completely inactivate mitochondrial energy metabolism. It has been shown that complete deletion of mitochondrial DNA decreases tumorigenicity instead of promoting it [141, 142]. In addition, expression of mtDNA isolated from cancer cells into normal cells induces carcinogenesis [143-145]. These results suggest that mtDNA is required

for tumor development, but has to be mutated in specific sites to promote cancer phenotype. In addition to mutations in mtDNA, cancer-specific mutations in nuclear genes encoding for mitochondrial enzymes of the tricarboxylic acid cycle (TCA), like succinate dehydrogenase [146, 147], fumarate hydratase [148, 149] and both isoforms of isocitrate dehydrogenases [150-152], are also frequent in cancer. These mutations lead to accumulation of metabolites (succinate, fumarate, hydroxyglutarate) that will activate signaling responses contributing to tumorigenesis. Excess of succinate and fumarate will for example lead to stabilization of HIF1 $\alpha$  or induction of NRF2 stress response.

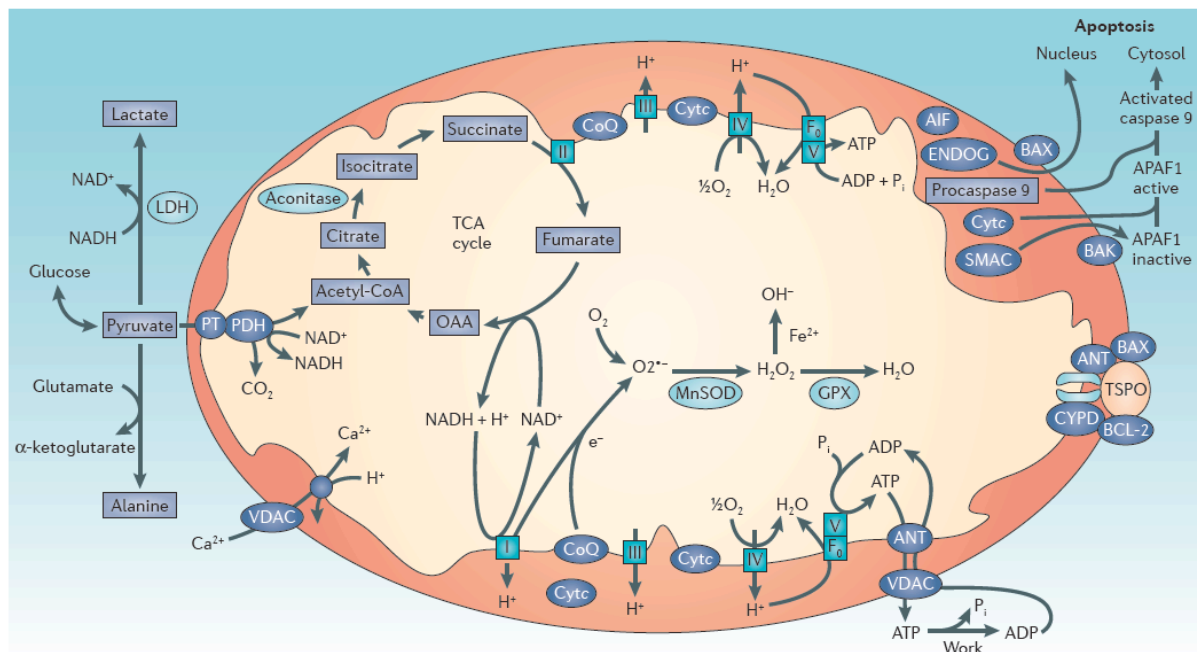


**Figure 5:** Physiological processes of mitochondria

Mutations in isocitrate dehydrogenase genes will alter the cellular redox state by altering NADPH regulation through accumulation of  $\alpha$ -ketoglutarate. Deregulation of NADPH flux, an important constituent of antioxidant defenses, increases oxidative stress and stimulates cancer cell proliferation. Reduction of mitochondrial calcium uptake by cancer cells decreases the activation of mitochondrial intrinsic apoptosis pathway; render them more resistant to cell death [153]. In general, cancer cells need altered but functional mitochondria, usually with reduced oxidative phosphorylation (OXPHOS), to initiate and sustain tumorigenesis. Alteration in the bioenergetics of mitochondria will activate signaling pathways that will ultimately serve to reprogram the nucleus of the cell to induce cancer phenotype. This response is called the “retrograde signaling” [154].

### *Alterations of energy-supplying pathways in cancer*

Alterations in bioenergetics in cancer result from this crosstalk between mitochondria and nucleus of cancer cells. The shift from oxidative to glycolytic metabolism commonly involves activation of canonical signaling pathways. The PI3K-AKT pathway is one of them. When activated, this pathway stimulates glucose uptake, enhances the expression of glycolytic genes, maintains the constitutive function of hexokinases and activates mTOR [155]. This pathway also inhibits the expression of carnitine palmitoyltransferase, the rate-limiting step of fatty acid oxidation [156].

Induction of the hypoxia inducible factor 1, HIF1- $\alpha$ , signaling pathway is also frequently observed in cancer. HIF-1 $\alpha$  stimulates key steps of glycolysis, and regulates genes that control angiogenesis, cell survival and invasion [157]. HIF1- $\alpha$  lowers mitochondrial function by promoting the pyruvate dehydrogenase kinase 1 (PDHK1) overexpression. This in turn inhibits pyruvate entry in the TCA cycle through inactivation of the pyruvate dehydrogenase (PDH) complex. HIF-1 $\alpha$  can also promote the transcription of genes encoding for the lactate dehydrogenase (LDH) [158, 159], which facilitates the conversion of pyruvate to lactate. Interestingly, stimulation of this pathway can be triggered solely by mitochondria in response to accumulation of metabolites, such as succinate, or to oxidative stress. Analogously, dysfunction of mitochondria can lead to activation of AKT through modification of the redox state.

Mutations in the tumor suppressor p53 have also an impact on metabolism. Mutated p53 causes down-regulation of mitochondrial respiration as a result of cytochrome c oxidase (COX) deficiency [160]. Shift of cellular energy metabolism towards glycolysis is strengthened through the inhibition of the TP53-induced glycolysis and apoptosis regulator (TIGAR), which inhibits glycolysis in favor of the pentose phosphate pathway [161].

### **AMP activated protein kinase, the “master regulator” of cell metabolism**

Maintaining the balance between energy production and consumption is key to metabolic homeostasis. This function is performed in the cell, at least in part, by a particular enzyme called AMP activated protein kinase (AMPK). In the current study the metabolic misbalance caused by myoferlin removal is in part compensated through activation of AMPK that directs cancer cell to other sources of ATP. Therefore we will briefly touch upon the function of AMPK and its relationship to cancer.

AMPK is an evolutionary conserved serine/threonine kinase composed of three subunits, each of them existing in multiple isoforms ( $\alpha$ 1,  $\alpha$ 2,  $\beta$ 1,  $\beta$ 2,  $\gamma$ 1,  $\gamma$ 2,  $\gamma$ 3) encoded by

separate genes [162]. AMPK is a tightly regulated enzyme, whose activation is extremely sensitive to small intracellular changes of AMP/ATP ratio. When intracellular ATP is low, AMP (or ADP) can bind and activate the protein. Phosphorylation by kinases and conformational protection from phosphatases are required for a proper activation [163]. AMPK can be phosphorylated by at least three different kinases in response to external stimuli (e.g. cytokines, hormones, growth factors, etc): the tumor suppressor LKB1, the calmodulin dependent protein kinase kinase  $\beta$  (CAMKK  $\beta$ ), and the TGF- $\beta$ -activated kinase 1 (TAK1) [164]. Several pharmacological compounds (metformin, phenformin, AICAR, resveratrol) can also activate AMPK, but their specificity is still controversial [165].

#### *AMPK controls cell metabolism, cell growth and autophagy*

Activation of AMPK stimulates catabolic pathways (e.g. fatty acid oxidation and glycolysis) to generate more ATP when energy demand is high. It also inhibits ATP-consuming anabolic processes in order to conserve cellular energy. AMPK can regulate cellular metabolism via direct effects on metabolic enzymes. AMPK inhibits fatty acid synthesis and stimulates  $\beta$ -oxidation via the direct phosphorylation of the enzymes acetyl-CoA carboxylases (ACC) and hydroxymethylglutaryl-CoA (HMG-CoA) reductase, which are rate-limiting steps of fatty acid and sterol synthesis [166, 167]. In fat, AMPK also directly phosphorylates the lipases hormone sensitive lipase (HSL) and adipocyte triglyceride lipase (ATGL) [168, 169]. In muscle, AMPK has been shown to control glucose metabolism. It increases glycolysis via phosphorylation of phosphofructokinase 2 (PFK2) [170] and is involved in GLUT4 trafficking to enhance glucose uptake [171]. In addition to an acute control of metabolism, AMPK also phosphorylates transcriptional factors and histones, mediating a long-term adaptive response (for example: SREBP1, PGC-1 $\alpha$ , class IIa HDACs, H2B histones, for a detailed review see [163]). In condition of nutrient deprivation, AMPK inhibits cell growth, mainly via suppressing the mammalian target of rapamycin complex 1 (mTORC1) pathway. Roles for AMPK in control of autophagy, cell polarity and cytoskeleton dynamics have also been reported [163].

#### *AMPK deregulation in metabolic disease*

Over the last years, pharmacological activation of AMPK has been used in the treatment of metabolic diseases, such as type-2 diabetes, with encouraging results. Considering the link between metabolic disorders and cancer development, treatment associated with AMPK activation appeared as one of the anticancer therapeutic options. Most

convincing data supporting this idea have been given by the clinical use of metformin in diabetic patients. Indeed, retrospective studies of type-2 diabetic patients revealed that patients treated with metformin have a lower risk to develop cancer than normal patients, or patients undergoing other type of treatments (sulfonylureas, insulin) [172, 173]. Moreover, several other studies demonstrated that pharmacological activation of AMPK decreased cancer cell proliferation *in vitro* and attenuated tumor growth *in vivo* [174].

### *AMPK deregulation in cancer*

In cancer, it is now well established that the tumor suppressor LKB1 is the main activator of AMPK, and that the latter is essential to mediate LKB1 tumor-suppressive functions. AMPK situated at the center of an antitumor network, being activated by LKB1 and having as direct downstream targets recognized tumor suppressors such as p53, TSC2 and p27 [175]. Mutations in LKB1 occur frequently, leading to attenuated AMPK signaling pathway and correlating with bad prognosis in breast [176] and lung [177] cancers. Somatic mutations of AMPK are rarely found in cancer, possibly due to the redundancy of the isoforms composing the protein, and are not sufficient to drive tumorigenesis alone. However, deletion of AMPK can help oncogene-induced tumorigenesis [178]. Activation of AMPK can have been also reported to promote tumor growth [179] suggesting that the function of AMPK may depend on the biological/cellular context.

### *AMPK in cancer: friend or foe?*

In cancer cells, AMPK has been shown to inhibit HIF-1 $\alpha$ , which is a key to Warburg effect. AMPK can also activate p53, which inhibits glycolysis [180]. Study of AMPK knockout mice showed that absence of AMPK leads to a HIF-1 $\alpha$ -mediated induction of the Warburg effect, which ultimately promoted oncogene-induced tumor growth [178]. However, studies in hypoxia have reported that AMPK was also able to activate HIF-1 $\alpha$ , instead of inhibiting it [181]. Similarly, Wu and colleagues demonstrated that AMPK activation following nutrient deprivation resulted in increased aerobic glycolysis [182].

Because of this dual role, it has been suggested that loss of AMPK could help to promote carcinogenesis in the early steps of tumor development. In contrast to this, long-term inactivation of the protein could be deleterious to the fitness of the cells to adapt to new environments. An elegant summary is given by Faubert et al [175], who reviews the role of microenvironment on AMPK activity: when nutrients are available, AMPK loss confers tumor an advantage, for example by increasing HIF-1 $\alpha$  driven glucose and glutamine

metabolism. When nutrients are scarce, AMPK activation leads to metabolic stress resistance in cancer cells, allowing them to adapt and survive in the new environments.

# **Aims of the study**

## **Aims of the study**

This study was inspired from the results obtained through two newly developed proteomics techniques, focusing on the identification of novel accessible biomarkers in human pancreas and breast cancer. Both studies have brought forward myoferlin as one of the most significantly up-regulated biomarkers that was subsequently validated in large patient cohorts. The results were particularly motivating to further characterize the function of myoferlin as a novel cancer-associated protein in tumor progression.

Along these lines, our first objective was to demonstrate that myoferlin was relevant for the breast cancer development. We aimed to assess whether this protein could be used as a predictive marker for clinical outcome of the patient. Based on existing literature which describes the role of myoferlin in receptor dependent endocytosis and trafficking in normal cells, we next asked the question if myoferlin was involved in the regulation of the EGFR, a potent oncogene in human cancer. Finally, because of an important observation that myoferlin deficient cells change the pH of their culture medium *in vitro*, we decided to explore the global impact of myoferlin silencing on the metabolism of cancer cells.

# **Materials and Methods**

### Patients

All experiments undertaken with patient material complied with the regulations and ethical guidelines of the University of Liège (Liège, Belgium). All tissue samples were obtained from the Pathology Department of the University Hospital of Liege. The proteomic analysis was conducted using tumoral (ductal adenocarcinoma) and adjacent normal tissue samples, collected from 3 patients. The patients were female, 61 to 78 years of age, and with tumor grade 2 to 3 (Bloom grading). The immunohistochemical (IHC) validation was conducted on a collection of breast cancer tissues comprising 90 tumoral (patients with breast ductal adenocarcinoma, grade 2 and 3 with no known metastases at the time point of surgery) and 10 normal adjacent tissues. To study the correlation between myoferlin and breast cancer subtypes, we used additional 25 patients per subtype (ER+/PR+, HER2+ and triple-negative). The Western blot-based validation was conducted on samples originating from 4 patients with breast ductal and 4 with lobular carcinoma (not included in the mass spectrometry or IHC analysis) as well as their matched normal tissues.

### Proteomic analysis

The analytic approach has been developed and described previously [183]. Briefly, fresh human breast cancer biopsies were immediately sliced and soaked in freshly prepared EZ-link Sulfo NHS-SS biotin (1 mg/mL, Pierce) solution. Following a 20 minutes incubation at 37°C, the samples were snap-frozen in liquid nitrogen and converted to powder. Protein extraction was conducted as previously described [183]. The protein extracts were mixed with 100 µL/mg streptavidin resin (Pierce) and incubated for 2 hours under rotational conditions at room temperature. The supernatant was retained for the subsequent glycoproteomic analysis (fraction 1) and the streptavidin beads were washed thoroughly. The biotinylated proteins were eluted (fraction 2) using 100 mmol/L dithiothreitol (DTT; 30 minutes at 60°C). Fraction 1 was also reduced in 100 mmol/L DTT. Following this, both fractions were alkylated with 150 mmol/L iodoacetamide (30 minutes at room temperature) and the proteins were then precipitated with 20% trichloroacetic acid at 4°C overnight. Subsequently, the proteins were dissolved (as complete as possible) in 50 mmol/L NH<sub>4</sub>HCO<sub>3</sub> and digested using trypsin (Promega; 1:50 protease/protein ratio at 37°C) overnight. The biotinylated peptides (fraction 2) were further processed using mass spectrometry. Fraction 1 was used for the isolation of glycopeptides.

### MS analysis and data processing

Peptides originating from biotinylated and glycosylated fractions were desalted using C18 ZipTip pipette tips (Millipore, Billerica, MA, USA) and subjected to mass spectrometry analysis. All the peptide samples were analyzed using the 2D-nano-HPLC system Ultimate 3000® (Dionex, Sunnyvale, CA, USA). The HPLC system was connected on-line to the electrospray ion-trap mass spectrometer Esquire HCT ultra® (Bruker Daltonics, Bremen, Germany). For the MS analysis, approximately 5 µg of digested protein sample were loaded onto the Bio-X-SCX column (500 µm i.d. x 15 mm; Dionex; Ref.: 161395). Subsequently, 4 different concentrations of salt injection were performed (45, 75, 150 and 500 mM ammonium acetate). After each salt injection, the eluted peptides from the SCX column were trapped on a C18 pre-column (Acclaim PepMap®, 300 µm i.d. x 5 mm; Dionex; Ref.: 160454) and desalted for 5 minutes at a flow rate of 30 µL/min using solvent A (97.9% water, 2% acetonitrile and 0.1% formic acid). Following this, the peptides were separated on the C18 analytical column (Acclaim® 75 µm x 150 mm; Dionex; Ref.: 162224) using a 140- minutes solvent gradient (t = 0 minute, 0 % B [B: 80% acetonitrile, 19.9% water and 0.1% formic acid; t = 140 minutes, 40% B) at a flow rate of 0.3 µL/minute. The MS scanned the mass range from 200 to 1600 m/z. The 4 most intensive peptides found in this mass range (bearing +1, +2 and +3 charges) were selected automatically and fragmented in the MS/MS modus (m/z range 100-2500). The acquired spectra were processed for peak list generation using the Data Analysis® software version 3.4 (Bruker Daltonics, Bremen, Germany). The MS/MS database search was conducted using the Mascot® search engine version 2.2.2 (Matrix Sciences, Boston, MA, USA). The human non-redundant and non-identical protein database Swissprot® (Swiss Institute for Bioinformatics, Basel, Switzerland) version 57.7 was used and a total of 20,405 entries were searched. The mass tolerances of precursor and fragmented ions were set at 0.6 and 0.3, respectively; fixed modifications were carbamidomethyl; variable modifications were oxidization of methionines, whereas specifically for glycoprotein deamidation on asparagines and for biotinylated proteins a custom-made modification (+ 87.99829 m/z) was used for all the lysine residues. The glycoproteins were identified using the presence of deamidated asparagines at the consensus sequence site (NXS/T, where X can be replaced by any amino acid except proline). Semi-quantitative analysis was performed for the proteins that were identified in both tumoral and normal samples and in more than one individual. Accordingly, the peak-list files from all the fractions were combined into one file for each individual and disease state. These combined files were submitted to the Swissprot® database using the Mascot® search engine. The results yielded protein identifications along

with the exponentially modified protein abundance index (emPAI). The proteins with the increased emPAI abundance ratio (tumoral vs. normal  $\geq 2$ ) were regarded as differentially expressed and included in further analysis. Proteins which were not eligible for emPAI quantification (peptides with scores lower than 100 and/or not present in at least two individuals for each of the disease conditions) were screened for the frequency of presence or absence in all the samples. Those proteins which were identified more frequently in the tumoral conditions than in the normal counterpart (in at least 2 individuals more) were also considered as potentially modulated.

### **Histology and Immunohistochemistry**

The expression of myoferlin was verified in formalin-fixed paraffin-embedded breast tissue sections using immunohistochemistry (IHC). Sections of xenografted tumors were examined histologically using hematoxylin/eosin staining. The vimentin staining was used to identify tumor cells in mice xenografts and was also performed on paraffin-embedded tissues. Anti-myoferlin was purchased from Sigma Aldrich, (St. Louis, MO, USA; Ref. HPA014245) and anti-vimentin was obtained from Ventana (Tucson, AZ, USA) and was a ready to use formulation.

The tissues were sliced from paraffin blocks (5  $\mu\text{m}$  sections), unparaffined 2 times in xylene for 5 minutes and hydrated in the methanol gradient (100%, 95%, 70%, and 50%). Blocking of unspecific peroxidase was performed for 30 minutes with 3%  $\text{H}_2\text{O}_2$  and 90% methanol. Following the antibody incubation (anti-myoferlin diluted 1/100 and anti-vimentin undiluted, 4°C, overnight), slides were washed with PBS for 10 minutes. The biotinylated secondary antibody was incubated initially for 30 minutes and subsequently with the avidin biotin complex kit (ABC kit) for an additional 30 minutes. 3,3'-diaminobenzidine tetrachlorhydrate dihydrate (DAB) with 5%  $\text{H}_2\text{O}_2$  was used for colorization. The slides were counter-stained with hematoxylin. Two independent evaluators examined tissue positivity using a semi-quantitative approach. The samples were scored for the percentage of positivity (divided into four classes: 1 = 0-25%, 2 = 25-50%, 3 = 50-75% and 4 = 75-100%) and for intensity (0 = no staining, 1 = weak, 2 = moderate and 3 = strong). Following this, both parameters were multiplied and yielded a unique score. Box-Plots were generated using Sigma Plot software (Systat Software, Inc., Chicago, IL, USA; version 10.0). Statistical significance of the Myoferlin expression was assessed using Mann-Whitney-U-Test.

### Survival Analysis

Kaplan Meier survival curves were plotted using publicly available online tools KM-plotter (<http://kmplot.com/analysis>). The statistical analysis was automatically conducted with the online software.

### MDA-MB231, MDA-MB468 cell culture, siRNA- and shRNA-mediated knockdown

The MDA-MB231 (HTB-26) and MDA-MB468 (HTB-132) cells were obtained from American Type Culture Collection. The cells were authenticated through DNA profiling of 8 different and highly polymorphic short-tandem repeat loci (DSMZ, Braunschweig, Germany). Both cell lines were cultured in Dulbecco's Modified Eagle Medium (DMEM; Life Technologies) supplemented with 10% heat-inactivated fetal calf serum (MP Biomedicals) and L-Glutamine (MP Biomedicals) at 37°C, 5% CO<sub>2</sub>, and 95% humidity. The cells were used between passages 5 and 20 reaching near-confluence and were harvested with trypsin.

For transient silencing, the cells were transfected using Lipofectamine (Lipofectamine 2000 reagent, catalog no. 11668-019, Life Technologies) with small-interfering RNA (Thermo Scientific, Rockford, IL, USA) directed against myoferlin (siRNA#1: CCCUGUCUGGAAUGAGA and siRNA#2: CGGCGGAUGCUGUCAAAUA) or caveolin (CGAGAAGCAAGUGUACGAC) at a concentration of 10 nmol/L/siRNA. ON-TARGETplus Non-Targeting Pool (Dharmacon) was used as a negative control [further referred to as Irrelevant (Irr.) siRNA]. The principal effects (migration, invasion, EGF stimulation, lactate measurements and WST-1 experiments) were evaluated using both myoferlin siRNA oligomers. As both displayed similar levels of silencing, the remaining experiments were conducted using siRNA #1. Sixteen hours after transfection, culture medium was changed and 48-72 hours later, the cells were lysed and used for all Western blot analyses. For fluorescence-activated cell sorting (FACS), cells were detached with 5 mmol/L EDTA.

For stable myoferlin depletion, the breast cancer cell line MDA-MB231 was transduced with lentiviral short hairpin RNA (shRNA) particles. shRNA plasmids targeting myoferlin : ( sequences xxx cloned into pLKO (Sigma) ) and control shRNA targeting a sequence unrelated to known mouse genome sequences (Sigma, SHC005) were used. Lentiviral vectors were generated with the help of GIGA Viral vectors platform. Briefly, Lenti-X 293T cells (Clontech, Mountain view, CA, USA) were co-transfected with shRNA, pSPAX2 (Addgene, Cambridge, MA, USA) and a VSV-G encoding plasmids [184]. Viral supernatants were collected 48h, 72h and 96h post-transfection, filtrated and concentrated

100x by ultracentrifugation. The lentiviral vectors were then titrated with qPCR Lentivirus Titration (Titer) Kit (#LV900, ABM, Richmond, BC, Canada). MDA-MB231 cells were stably transduced with control and anti-myoferlin shRNA lentiviral vectors. Stably transduced clones cells expressing either shRNA anti-myoferlin or vector control were isolated and maintained in medium supplemented with 10 µg/ml of Puromycin (ant-pr-1, Invivogen, Toulouse, FR). To avoid clone-specific effects, pooled cultures were used for all the experiments. Cells that were used in murine *in vivo* experiments were additionally transduced with lentiviral vector to express the luciferase gene.

### **Migration and invasion assay**

$2 \times 10^5$  cells were suspended in serum-free resuspension medium (0.1% BSA, 1% penicillin/streptomycin) and seeded into the upper part of a Transwell filter (diameter 6.5mm, pore size 8µm, Costar, Cambridge, MA) coated with gelatine (100 µg/ml) for migration assay or precoated with Matrigel for invasion assay (BD Biosciences, Bedford, MA). The lower compartment was filled with a migration medium composed of DMEM containing 1% BSA, 1% pen/strep and either 6% or 10% BSA (for migration and invasion respectively). For EGF-induced migration, cells were starved overnight in DMEM and EGF was added into both resuspension and migration media at a concentration of 10 ng/ml. After 6, 10 or 24 hours incubation at 37°C, migrating cells were fixed and stained with Diff-Quick kit (Medion Diagnostics, Düringen, Switzerland; Ref.: 130832). Pictures of each insert were taken at a 5X magnification and percentage of migrating cells was further quantified by densitometry using the ImageJ software (National Institute of Health, USA, public access). Three wells (technical replicates) per condition and replicate were counted.

### **Cell proliferation assay**

Transfected MDA-MB231 cells were pulsed at different time points with 33 mM BrdU for 30 minutes, suspended in PBS (supplemented with 10% FBS) and then fixed with 70% ice-cold ethanol. DNA was denatured with denaturing solution (4 N HCl and 0.5% Triton X100) for 30 minutes at 37 °C. Following one PBS wash, the pellet was suspended in PBS (with 10% FBS) and anti-BrdU antibody (clone BU-33; Sigma) was added to the cells; the cell suspension was then incubated for 1 hour at RT. Next, the cells were washed 1 time with PBS and the secondary antibody (Alexa-488 goat anti-mouse, Molecular Probes) was added to the cells, followed by 1 hour incubation at RT and in the dark. After a final wash, the cells were collected, suspended in PI solution (3mM EDTA, 0.05% Tween 20, 50 mg/ml PI,

50 mg/ml RNase A in PBS, pH 8.0). The cells were subjected to flow cytometry as described above.

### **Cell growth assay**

The MDA-MB231 cells were cultured and transfected as described above. Cells were detached with trypsin and 30,000 cells were plated into 24-well plate. At respective times, the cells were sonicated in 1mL PBS for 10 seconds. 100  $\mu$ L of this extract was agitated for 30 minutes in a 96-well plate along with an equal volume of Hoechst solution (Calbiochem, ref. 382061) in absence of light. The plates were read (Ex.: 352 nm/ Em.: 461 nm) using the Spectra Max Gemini XS (Molecular Devices). The data were analyzed in Excel (Microsoft).

### **Chicken chorioallantoic membrane (in vivo) tumor assay**

On embryonic day 11, 100  $\mu$ L of a suspension of  $2 \times 10^6$  of MDA-MB231 cells in culture medium mixed (1:1) with Matrigel (BD Biosciences) were deposited in the center of a plastic ring on the chorioallantoic membrane (CAM) of a developing embryo. Tumors were harvested on embryonic day 18 and were either fixed in 4% paraformaldehyde solution (30 minutes) for histology analysis or snap frozen in liquid nitrogen for Western blot analysis. Tumor volume was assessed using the formula  $V = (4/3) \cdot \pi \cdot (H/2) \cdot (L/2) \cdot (W/2)$  where **H**, **L**, and **W** denote height, length, and width of the tumor.

### **EGF stimulation**

Cells, 32 hours after transfection, were starved overnight (16 hours) in serum-free DMEM and stimulated with a pulse of 10 ng/mL of EGF (PeProTech) for different periods of time (up to 120 minutes). Cells were then washed once with PBS and subsequently subjected to protein extraction.

### **Western blot**

Pulverized tissue samples or MDA-MB231 and MDA-MB468 cell pellets were lysed in SDS-based buffer (1% SDS, supplemented with protease and phosphatase inhibitors) and quantified using BCA quantification kit (Pierce, Thermo Scientific, Rockford, IL, USA). 20  $\mu$ g of protein were then diluted with Laemmli buffer (60 mM Tris-HCl pH 6.8, 25% glycerol, 2% SDS, 14.4 mM of 2-mercaptoethanol and trace of bromophenol blue) and boiled for 5 minutes. Protein samples were loaded and separated by SDS-PAGE followed by electro-transfer on PVDF membrane. Next, the membranes were blocked in TBS-T containing 5%

nonfat dried milk (Bio-Rad, Hercules, CA, USA; Ref. 170-6404) and incubated with the selected primary antibodies. Myoferlin was detected using the antibody described above. Antibodies against caveolin 1 (Ref.: 3238), p-CAV1 (Ref.: 3251), STX6 (Ref.: 2689), EGFR (Ref.: 2232), pEGFR (Ref.: 4407), AKT (Ref.: 9272), p-AKT (Ref.: 9271), AMPK (Ref.: 2795), p-AMPK (Ref.: 2535), p-ACC (Ref.: 3661) were purchased from Cell Signaling (Danvers, MA, USA). PDH (ab168379), p-PDH (ab92696), p-PDHK1 (ab109460) were purchased from Abcam (Cambridge, UK). Anti-COX1 was purchased from Invitrogen (Ref.: 459600, LifeTechnologies, Gent, BE), anti-HIF1A from BD Biosciences (Ref.: 610958, San Jose, CA, USA), vimentin (v6389) was obtained from Sigma. Anti NDUFB5 was obtained from Genetex (GTX111880, Irvine, CA, USA) and anti-mitofilin from Santa Cruz (sc-390707, Dallas, TX, USA). Following three TBS-T washes, the membranes were incubated for 1 hour at room temperature with specific secondary antibody conjugated to horseradish peroxidase. After sufficient rinsing, the immunoblots were visualized using the chemiluminescent substrate (ECL Western blotting substrate, Thermo Scientific, Rockford, IL, USA). The blots were normalized either with  $\alpha$ -tubulin (Sigma; Ref.: T5168) or HSC70 (Santa Cruz, Dallas, TX, USA; Ref.: sc-7298) proteins.

### **EGF-mediated EMT assay**

MDA-MB468 cells served as an EGF-inducible EMT model and were described in detail elsewhere [185]. Briefly, 48 hours post-transfection, the cells were trypsinized and plated at a confluence of 200,000/well in a 6-well plate. The culture medium was supplemented with EGF for a final concentration of 20 ng/mL. Cells were allowed to grow for further 24 to 48 hours before protein and RNA extraction.

### **RT-qPCR**

RNA was extracted using the High Pure RNA Isolation Kit (Roche, Mannheim, Germany; Ref.: 11828665001) and converted to cDNA using the Transcriptor First Strand cDNA Synthesis Kit (Roche; Ref. 04897030001). 10ng of cDNA was transferred into 96-well plate and mixed with primers, UPL-probe system and 2X Fast Start Universal Probe Master mix (Roche). Following primers were used: vimentin – FRW GCGTGACGTACGTCAGCAATATGA, REV GTTCCAGGGACTCATTTGGTTCCTT and UPL probe 16; e-cadherin - FRW GACACATTTATGGAACAGAAAATAACA, REV AGTGGAATGGCACCAGTGT and UPL probe 19. Relative expressions were normalized to GAPDH - FRW ACCAGGTGGTCTCCTCTGAC, REV TGCTGTAGCCAAATTCGTTG

and UPL probe 25. The qPCR was performed using the LightCycler480 system and the corresponding manufacturers software (Roche Diagnostics).

### **Flow cytometry analysis of cell surface EGFR**

Starved cells were stimulated with EGF as previously described (on ice), gently detached with a 5 mM solution of EDTA and washed twice in cold PBS. They were then incubated for one hour with PE-conjugated mouse antibodies directed against EGF Receptor or corresponding isotype control (BD Biosciences, San Jose, CA, USA; Ref.: 555997 and 555743) and washed two times in PBS (all steps on ice). The cells were analyzed using a FACS-Calibur 2 (BD) and the data were evaluated with the Cell Quest Pro software.

### **Immunofluorescence**

After 16 hours of siRNA-mediated silencing,  $5 \times 10^4$  cells were plated on a 12 mm coverslip (Menzer Glaser; CB00120RA1) and allowed to grow for additional 48-72 hours. For EGF-stimulated cells, 36 hours after replating, cells were starved overnight in medium without serum and then treated with 10 ng/mL EGF and allowed to incubate for a maximum of 120 minutes. Treated cells were fixed for 10 minutes at  $-20^{\circ}\text{C}$  in a methanol/acetone solution (80/20), washed twice with PBS, and blocked in 2% bovine serum albumin (BSA; Sigma-Aldrich, A3059) for 30 minutes. Coverslips were incubated for 2 hours at room temperature with primary antibodies diluted in 2% BSA: anti-caveolin (same as for Western blot), anti-myoferlin (Santa Cruz Biotechnology; sc-51367), anti-EGFR (Santa Cruz Biotechnology; sc-03), anti-pEGFR (Millipore; 05-1004) and anti-mitochondria (Millipore; MAB1273). Subsequently, the slides were washed in 3 PBS–BSA washes and incubated with dye-conjugated secondary antibodies (Life Technologies; A-11056, A-11029, and A-21070) for 45 minutes at room temperature. Following 3 additional washes, nuclei were labeled with 2 ng/mL Hoechst (Merck) for 5 minutes and the coverslips were mounted with Mowiol (Sigma) on glass slides. Images were accrued with laser scanning confocal microscope (A1R, Nikon Instruments).

### **Density Gradient Centrifugation**

Sucrose density gradient (5-20%) was prepared in TNE buffer (20 mM Tris-HCl pH 7.4, 100 mM NaCl, 5 mM EDTA, 0.5% TX100 with protease inhibitors (Roche, Mannheim, Germany) and equilibrated in an SW55 rotor (Beckman Coulter, Krefeld, Germany) overnight at  $237\,020 \times g$  and  $4^{\circ}\text{C}$ . Cells were extracted in TNE buffer and 1mg of protein was loaded on

the top of the sucrose density gradient and subsequently centrifuged for 255 minutes at 237 020 x g and 4°C. After ultracentrifugation, the gradient was fractionated in 25 fractions of 200 µL. 50 µL of individual fractions were vacuum dried, dissolved and boiled in Laemmli buffer. The samples were assayed in WB for caveolin 1 expression (21 kDa band) as described above.

### **Lactate measurement using nuclear magnetic resonance (NMR)**

The NMR spectra were recorded at 298 K on a Bruker Avance spectrometer operating at 500.13 MHz for proton and equipped with a TCI cryoprobe. Deuterated water was used as the internal lock. The data have been processed with Bruker TOSPIN 2.1 software with standard parameter set. Phase and baseline correction were performed manually over the entire range of the spectra and the  $\delta$  scale was calibrated to 0 ppm using the internal standard TMSP.

500 µl of collected culture media were supplemented with 100 µl of deuterated phosphate buffer (pH 7.4), 100 µl of a 35 mM solution of maleic acid and 10 µl of Trimethylsilyl-3-propionic acid-*d*4 (TMSP). The solution was distributed into 5-mm tubes for NMR measurement. <sup>1</sup>H NMR spectra were acquired using a 1D NOESY sequence with presaturation. The Noesy presat experiment used a RD-90°-t1-90°-tm-90°-acquire sequence with a relaxation delay of 4 s, a mixing time *tm* of 10 ms and a fixed *t*1 delay of 4 µs. Water suppression pulse was placed during the relaxation delay (RD). The number of transient is 32 (64K data points) and a number of 4 dummy scans is chosen. Acquisition time is fixed to 3.2769001 s. Lactate dosages were achieved by integrations of the lactate signal at 1.34 ppm using maleic acid as internal standard.

Deuterium Oxide (99.96 % D) and Trimethylsilyl-3-propionic acid-*d*4 (TMSP) were purchased from Eurisotop (St-Aubin, France), Phosphate buffer powder 0.1 M and Maleic acid were purchased from Sigma-Aldrich (St-Louis, MO)

### **WST-1 assay**

48 or 72 hours after transfection, WST-1 reagent (Roche) was diluted 1/10 in the culture medium of living cells, according to manufacturer's instructions. Absorbance at 450 nm was then measured after 30, 60 and 120 minutes of incubation using a Multiskan MS Elisa Plate Reader.

**Isolation of mitochondria**

MDA-MB231 cells were washed with PBS, trypsinised and resuspended in washing buffer (250 mM Sucrose, 1 mM EDTA, 10 mM TRIS, pH 7.4). Cells were then centrifuged for 5 minutes at 1000 rpm and further resuspended in Homogenisation buffer (250 mM Sucrose, 1 mM EDTA, 24 mM TRIS, pH 7.4 supplemented with protease inhibitors (complete EDTA free, Roche) and 0.5 mg Bovine Serum Albumin (Sigma)). Physical breaking of the cells was performed using a glass/teflon tissue grinder and the cell lysate was centrifuged for 3 minutes at 2,700 rpm. Resulting supernatant was collected and enriched fraction of mitochondria was obtained after 3 minutes of high-speed centrifugation at 11,300 rpm. Mitochondrial pellet was washed once with Resuspension buffer (250 mM Sucrose, 1 mM EDTA, 24 mM TRIS, pH 7.4 supplemented with protease inhibitors (complete EDTA free, Roche) to eliminate BSA, centrifuged for 3 minutes at 10,400 rpm and finally resuspended in 200 microliters of Resuspension buffer. Further purification of isolated mitochondria was achieved after sucrose gradient ultracentrifugation. Briefly, mitochondrial suspension was deposited on the top of a discontinuous sucrose gradient (60-32-23%). After one-hour ultracentrifugation (Beckmann Optima LE-80K, Krefeld, Germany) at 32,000 rpm, mitochondria were collected at the interface between the 60 and 32% sucrose layers. Sucrose was sequentially eliminated after several washes with Resuspension buffer followed by centrifugation at 11,300 rpm. Mitochondrial pellet was finally resuspended in appropriate volume of lysis buffer.

**Oxygen consumption measurements**

Oxygen consumption of 48 hours-transfected cells was recorded on a high-resolution oxygraph (OROBOROS INSTRUMENTS, Innsbruck, Austria) with a Clarke electrode at 37°C. Five millions cells were used for each measurement. The measurement was performed under continuous stirring and started just after the closing of the chamber. Routine respiration was measured in culture medium. Leak respiration, which is considered as the proportion of oxygen that is consumed by the cell without producing ATP, was measured in presence of 5 µM oligomycin. ETS<sub>max</sub> (Electron Transport System, reflecting the maximal capacity of the mitochondrial respiratory chain) was obtained in presence of 0.5 µM of the uncoupling agent FCCP (3 pulses of FCCP were made to ensure maximal uncoupling of the respiratory chain). All respiration measurements were corrected for residual oxygen consumption measured in presence of 2.5 µM of rotenone. The slopes of O<sub>2</sub> consumption, representing the routine

respiration of the cells, were calculated with the Oroboros oxygraph software (DatLab 4.0, OROBOROS DatLab software, Innsbruck, Austria)

### **ATP measurement**

Intracellular ATP from breast cancer cells was measured using ApoSENSOR ADP/ATP Ratio Assay Kit from BioVision (Catalog #K255-200), according to manufacturer's protocol. Briefly, transfected cells were washed and lysed in Nucleotide releasing buffer for 5 minutes. Solution was then mixed with ATP monitoring enzyme solution (coupled with luciferase) and allowed to react for 2 minutes. Luminescence was further measured using a Lumat LB 9507 luminometer (Berthold Technologies, BE)

### **Apoptosis assay**

Myoferlin-silenced cells were collected in serum medium at selected time-points. Apoptosis was evaluated using the FITC Annexin V Apoptosis Detection Kit I (BD Pharmingen, San Diego, CA, USA) according to the manufacturer's instructions. Briefly, adherent and floating cells were collected at each time point, washed twice with ice-cold PBS and incubated in the dark with Annexin-FITC and propidium iodide for 15 minutes. Flow cytometry was further performed as described above.

### **Mitochondrial membrane potential and ROS measurement**

Adherent and floating cells were collected, pooled and incubated with the tetra-methyl-rodhamin-ester (TMRE) dye (100 nM final concentration) for 20 minutes in culture medium without serum. Cells were then washed once with ice cold PBS and resuspended in PBS. Fluorescence signal was analyzed using a FACS-Calibur 2 (BD). Two peaks were observable corresponding to depolarized and functional mitochondria. The percentage of each population was evaluated using the Cell Quest Pro software (BD).

For ROS measurement, the cells were collected as indicated and then incubated with MitoSoxRed (5  $\mu$ M) for 20 minutes in HBSS buffer. Cells were then washed once with ice cold PBS and resuspended in PBS. Fluorescence signal was evaluated as outlined above.

### **Electron microscopy and immunogold labeling**

MDA-MB231 cells were fixed for 30 minutes in 2.5% glutaraldehyde (diluted in Sorensen's buffer: 0.1 M Na<sub>2</sub>HPO<sub>4</sub>/NaH<sub>2</sub>PO<sub>4</sub> buffer, pH 7.4) at 4°C and postfixed in 2% OsO<sub>4</sub> (diluted in Sorensen's Buffer 0.1 M). After dehydration in graded ethanol, samples were embedded in Epon resin. Ultrathin sections obtained with a Reichert Ultracut S ultramicrotome were contrasted with 2% uranyl acetate and 4% lead citrate. Observations were made with a Jeol JEM-1400 transmission electron microscope at 80 kV.

For immunolabeling, samples were first fixed for 1 hour in 4% formaldehyde (diluted in Sorensen's buffer 0.1M), rinsed in buffer and dehydrated in graded ethanol baths. After dehydration, samples were infiltrated with increasing concentrations of lowicryl resin. Resin was further polymerized under UV light. Ultrathin sections were washed in phosphate buffer saline (0.1 M PBS, 0.14 M NaCl, 6 mM Na<sub>2</sub>HPO<sub>4</sub>, 4 mM KH<sub>2</sub>PO<sub>4</sub>, pH 7.2) then blocked for 30 minutes in PBS-BSA (1%, pH 7.2) supplemented with normal goat serum (1/30 dilution). Sections were washed in PBS-BSA (0.2%, pH 7.2) and incubated with primary antibody (anti-MYOF, 1/20 dilution in PBS-BSA 0.2% supplemented with normal goat serum 1/50) for 3 hours. After 3 washes in PBS-BSA (1%, pH 7.2) and an additional wash in PBS-BSA (0.2%, pH 8.2), sections were incubated with secondary antibody (anti-rabbit coupled with gold particles, Aurion, NL, diluted 1/40 in PBS-BSA 0.2%, pH 8.2) for 1 hour. Finally, sections were washed 4 times in PBS-BSA (0.2%, pH 8.2) and 4 times in deionized water, stained with uranyl acetate and lead citrate and allowed to dry. Observations were made with a Jeol JEM-1400 transmission electron microscope at 80 kV.

### **Immunoprecipitation**

Cell pellets were lysed in IP buffer (137 mM NaCl, 2mM EDTA, 1% Triton X-100 (v/v), 10% glycerol (v/v) and 20 mM TRIS/HCl, pH 8) supplemented with protease and phosphatase inhibitors (Roche) and centrifuged 14.000g for 10 minutes to remove cell debris. Supernatant was quantified and 500 ug of proteins were mixed with 5 ug of anti-MYOF antibody (Sigma). After overnight incubation at 4°C, antibody-containing samples were mixed with 20 ul of protein A/G magnetic beads (Pierce, ref #88802) and further incubated for 4 hours at 4°C. Beads were collected on a magnetic rack and washed two times with TBS-Tween solution (150 mM NaCl, 25 mM TRIS, 0.05% Tween-20, pH 7.5). Immunoprecipitated proteins were recovered from the beads by incubation in laemmli buffer (60 mM Tris-HCl pH 6.8, 25% glycerol, 2% SDS, 14.4 mM of β-mercaptoethanol and trace of bromophenol blue) followed by a 10 minutes heat shock at 99°C.

### **Isolation of tumor cells**

Dissected tumors were rinsed in DMEM, chopped into small pieces and incubated in enzymatic dissociation mix using the MACS Tumor Dissociation Kit Protocol (# 130096730, Miltenyi Biotec, Leiden, NE). During 1 hour incubation (under slow agitation at 37°C), tumor suspension was mechanically resuspended (20 times through a 1ml cut tip) every 15 minutes to facilitate dissociation. The digested tissue was then diluted in 15 ml of DMEM medium supplemented with 10% serum and filtered through a 70 µm filter. Cell debris were removed from the filtrate by centrifugation of the suspension at 1000 rpm for 5 minutes. Supernatant is mixed with RBC lysis buffer (8,2% NH<sub>4</sub>Cl, 0,8% NaHCO<sub>3</sub>, 0,4% EDTA, pH 8, diluted 10x) to remove red blood cells, and centrifuged 5 minutes at 1000 rpm. The resulting pellet was then resuspended in full culture medium (DMEM with 10% FBS and 5 mM Glutamine) and was further used for respiration experiments.

### **Murine *in vivo* experiments**

100 µl of a suspension of 1x10<sup>6</sup> MDA-MB231 luciferase positive mixed 1:1 with Growth Factor Reduced Matrigel (BD Biosciences) were injected subcutaneously in the flank of 6-weeks old female NOD-SCID mice. Tumor growth was weekly measured using a digital caliper and the volume was assessed using the formula  $V = (4/3) \cdot \pi \cdot (H/2) \cdot (L/2) \cdot (W/2)$  where **H**, **L**, and **W** denote height, length, and width of the tumor. After 4 weeks of development, tumors were removed and mice were kept alive during 6 additional weeks to monitor lung metastasis development. Tumor size as well as metastasis formation were also evaluated every week by imaging of the mice in IVIS Xenogen after intraperitoneal injection of luciferine (ref E1605, Promega, WI, USA).

### **Oil-Red-O staining of xenografted tumors**

Intra-tumoral distribution of lipids was evaluated using Oil-Red-O staining. For the purpose of this staining procedure, non-fixed freshly-frozen tissues were sliced in 5µm, sections allowed to dry and fixed in 10% ice-cold formalin for 10 minutes. Sections were further washed three times in deionized water bath, allowed to dry and placed in absolute propylene glycol (Cat# 398039, Sigma) for another 5 minutes. Slides were stained with Oil-Red-O solution (0,5% diluted in propylene glycol, Sigma) for 10 minutes at 60°C. Staining solution was washed for 5 minutes in 85% propylene glycol followed by two additional washes in deionized water. Slides were counterstained with haematoxylin and mounted using glycerin jelly (Sigma).

### **Statistical analysis**

All experiments were carried out in biological triplicates. The CAM model was conducted in 3 biological and 5 technical replicates. Mice experiment was repeated three times with a cohort of 10 animals/condition. Appropriate statistical analysis was conducted using 2-sided Student **t** test and assuming equal variances. The calculations were conducted with Excel software (Microsoft).

### **Adhesion assay**

Forty-eight hours post transfection, 20,000 MDA-MB231 were placed in pre-coated 96-well plate and left to adhere for 2 hours at 37 °C and 5% CO<sub>2</sub>. The coating of the wells was performed using 10µl of the following substrates: vitronectin (Millipore, ref. CC080), laminin (Invitrogen, ref. 23017-015), fibronectin (Calbiochem, ref. 341635) and collagen (Sigma, ref; C5483); all at concentration of 0.1 µg/ml. Subsequently, the cells were washed with PBS and fixed in a 0.5% cristal violet (Sigma, ref. C3886) in 20% methanol solution for 5 minutes. Stained cells were rinsed with water and air-dried. The colored cells were lysed in 1:1 mixture of absolute ethanol and 0.1M Na-citrate buffer. The cell attachment was evaluated using the Multiskan MS Elisa plate reader (Labsystem) at 560 nm and the data were analyzed in Excel (Microsoft).

# Results

**PART 1: Myoferlin is a consistent feature of**  
**human breast cancer**

## Proteomic investigation identifies myoferlin as a membrane protein in human breast adenocarcinoma

The proteomic approach used here enriches for extracellular and membrane-bound proteins and was previously published by our group [7, 183]. In the current work, comparative mass spectrometry analysis (cancer vs. normal adjacent tissue) identified more than 1,400 proteins, of which approximately 800 were already known to be cell membrane-bound or extracellular. The semiquantitative evaluation identified a number of modulated proteins outlined in **Table 1**.

Gene symbol	Protein names	Accession No.	Presence		Empai Ratio T/N	Subcellular locations	Biological process
			Normal	Tumoral			
AEBP1	Adipocyte enhancer-binding protein 1	Q8IUX7	3	3	3.4±1.4	S; Cy; N	CG
AGRIN	AGRIN	O00468	1	3		S; E	CG
AMPN	Aminopeptidase N	P15144	3	3	2.2±0.0	C; SP; Cy	M
AATM	Aspartate aminotransferase	P00505	0	2		C; MM	M; E
ATLA3	Atlastin-3	Q6DD88	0	2		I; M; MP	-
CAN1	Calpain-1	P07384	1	3		C; Cy	M
CAN2	Calpain-2	P17655	1	3		C; Cy	M
CD276	CD276	Q5ZPR3	0	2		M; SP	I
COCA1	Collagen alpha-1(XII) chain	Q99715	3	3	7.5±1.5	S; E	C; ST
EMIL1	EMILIN-1	Q9Y6C2	3	3	2.5±0.02	S; E	CG
FINC	Fibronectin	P02751	3	3	5.7±1.7	S; E	-
GGT1	Gamma-glutamyl-transpeptidase 1 (CD224)	P19440	1	2		M; SP.	M; E
GGT2	Gamma-glutamyl-transpeptidase 2	P36268	1	2		M; SP	-
ITAV	Integrin alpha-V	P06756	3	3	4.1±2.5	SP	C; ST
IBP3	Insulin-like growth factor-binding protein 3	P17936	0	2		S	C; ST; A
LAMA5	Laminin alpha-5	O15230	1	3		S; E	CG
LRC15	Leucine-rich repeat-containing protein 15	Q8TF66	1	2		M; SP	C; ST
MRC2	Macrophage mannose receptor 2 (CD280)	Q9UBG0	1	3		M; SP	U
MYOF	MYOFerlin	Q9NZM1	0	3		C; SP; NM; Cy	CG
CADM1	Nectin-like protein 2	Q9BY67	0	2		C; SP	-
OLFML1	Olfactomedin-like protein 1	Q6UWY5	0	2		S	U
POSTN	Periostin	Q15063	3	3	5.2±2.7	S; E	C
TENA	Tenascin-C	P24821	2	3	32.0*	S; E	C; ST
TSP1	Thrombospondin-1	P07996	2	3	6.3*	E	CG
TIMP1	Tissue inhibitor of metalloproteinases (TIMP-1)	P01033	1	3		S	CG
BGH3	Transforming growth factor-beta-induced protein ig-h3	Q15582	3	3	3.2±0.6	S; E	C; ST
TM9S3	Transmembrane 9 superfamily member 3 (EP70-P-iso)	Q9HD45	1	3		M; MP	T
CU129	Uncharacterized protein C21orf129	Q96M42	0	3		U	U
CSPG2	Versican (GHAP)	P13611	3	3	7.8±4.3	S; E	CG

**Table 1:** List of up-regulated breast tumor proteins obtained from the analysis of 3 nontumoral adjacent and 3 tumoral specimens. The proteins were selected with respect to their presence in tumoral tissue samples and their absence or reduced presence in non-tumoral tissue samples. For certain proteins present in both the tumoral and the adjacent normal tissue, semi-quantitative data (emPAI ratio) are included if they were significantly overexpressed in the tumor (ratio  $\geq 2.0$ ). All the proteins are potentially accessible as they are located on the outer side of the cell membrane (secreted, extracellular or membrane). Following abbreviations were used: Subcellular location - S: secreted; E: extracellular; M: membrane; C: cell membrane; PIM: plasma membrane; SP: single-pass membrane protein; MP: multipass membrane protein; LA: lipid anchor; MM: mitochondrion matrix; PM: peripheral membrane protein; Cy: cytoplasm; NM: nuclear membrane; U: cell component unknown; Biological process - C: cell communication, ST: signal transduction; I: immune response; M: metabolism; E: energy pathway; T: transport; A: apoptosis; CG: cell growth and/or maintenance; U: biological process unknown.

The number of identified peptides, Mascot score, and sequence coverage for each of the modulated proteins is outlined in supplementary data (**Sup. Table 1**). A number of proteins were identified owing to the glycopeptide enrichment step of the proteomic method used in this study. These are listed in the **Sup. Table 2** along with the glycosylated peptides and the sites of glycosylation that led to their identification.

Myoferlin was identified as a novel breast cancer-related protein in all 3 patient samples used for the proteomic analysis. Next, we sought to confirm myoferlin expression in a larger set of breast cancer patients. We conducted IHC analysis of myoferlin expression in 90 breast adenocarcinoma samples and in 10 adjacent normal breast tissues. The IHC analysis (**Fig. 1A**) largely confirmed the mass spectrometry data and showed that myoferlin overexpression is a consistent feature of human breast cancer.

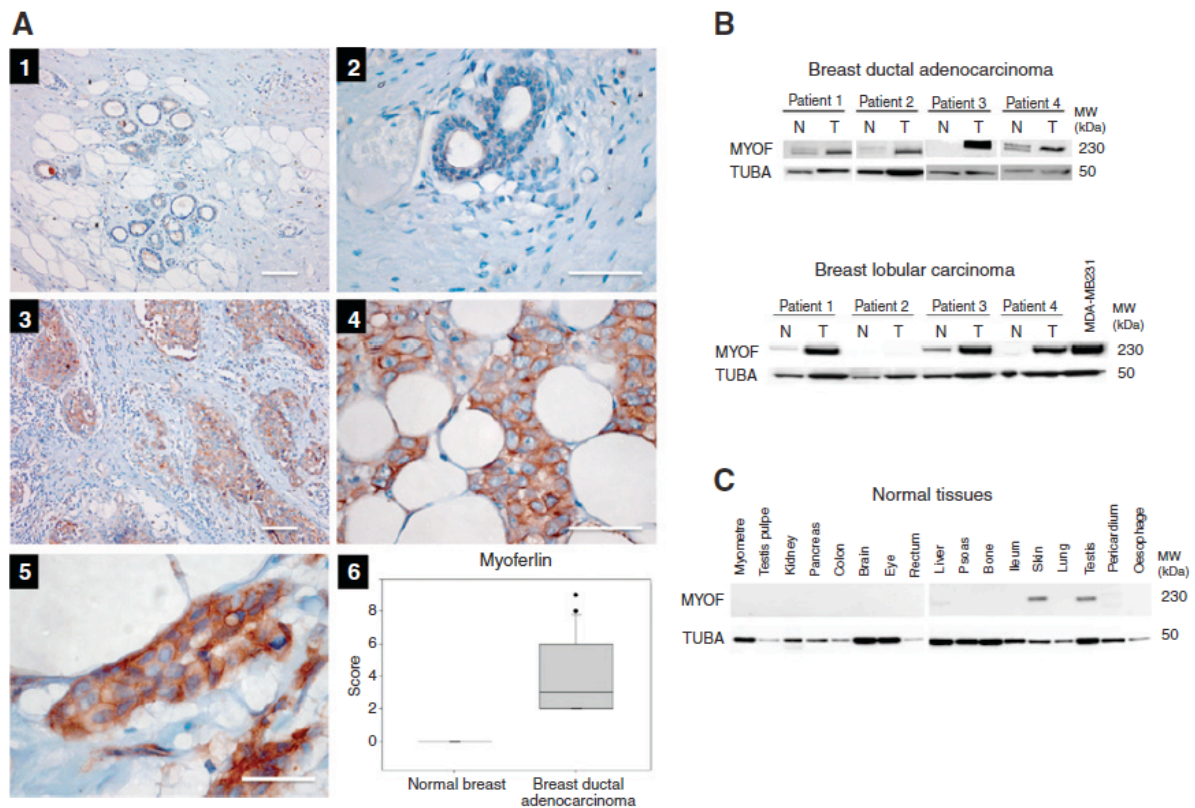


**Figure 1:** Myoferlin is overexpressed in human breast cancer tissue. A, representative immunohistochemical staining of myoferlin (MYOF) expression in human breast malignant tumors; normal breast ducts did not express/had low levels of myoferlin (1–2); breast cancer cells (in situ; 3) as well as cancer cells invading breast fat tissue (4) are both expressing myoferlin; the expression pattern corresponded to a cytoplasm/membrane positivity (5); semiquantitative evaluation (6), as described in Material and Methods, of myoferlin expression in 90 patients with breast ductal adenocarcinoma showed positivity in all examined cases. Magnification used, X100 (1 and 3); X400 (2 and 4); and X600 (5); scale bar, 40  $\mu$ m. B, Western blot analysis of myoferlin expression in 4 matched (tumor/normal) ductal and 4 lobular breast carcinoma patients. C, Western blot evaluation of myoferlin expression in a selection of normal human tissues.

The staining was specifically detected in tumor cells, mostly conferred to the cytoplasm, however a discrete staining of the plasma membrane was observable as well. Normal adjacent breast ducts were predominantly negative. Endothelial cells in the tumor-associated vasculature were positively stained for myoferlin, stromal fibroblasts were not stained except in rare occasions (**Fig. 1A**). Further Western blot analysis (**Fig. 1B**) on paired samples (tumor and adjacent normal tissue from same individual) of breast ductal adenocarcinoma and lobular carcinoma confirmed IHC data. We then conducted a Western blot evaluation of myoferlin expression in a selection of normal human tissues. Interestingly, myoferlin expression was not detectable in all the normal tissues tested (**Fig. 1C**), except testis and skin.

### Myoferlin is highly expressed in hormone-receptor positive breast cancer.

Although breast cancer is commonly referred to as one pathology, we know that many molecular subtypes exist, having different outcomes for the patient and responding to different treatments [186]. We were therefore interested to characterize myoferlin expression in different subtypes of breast cancer.

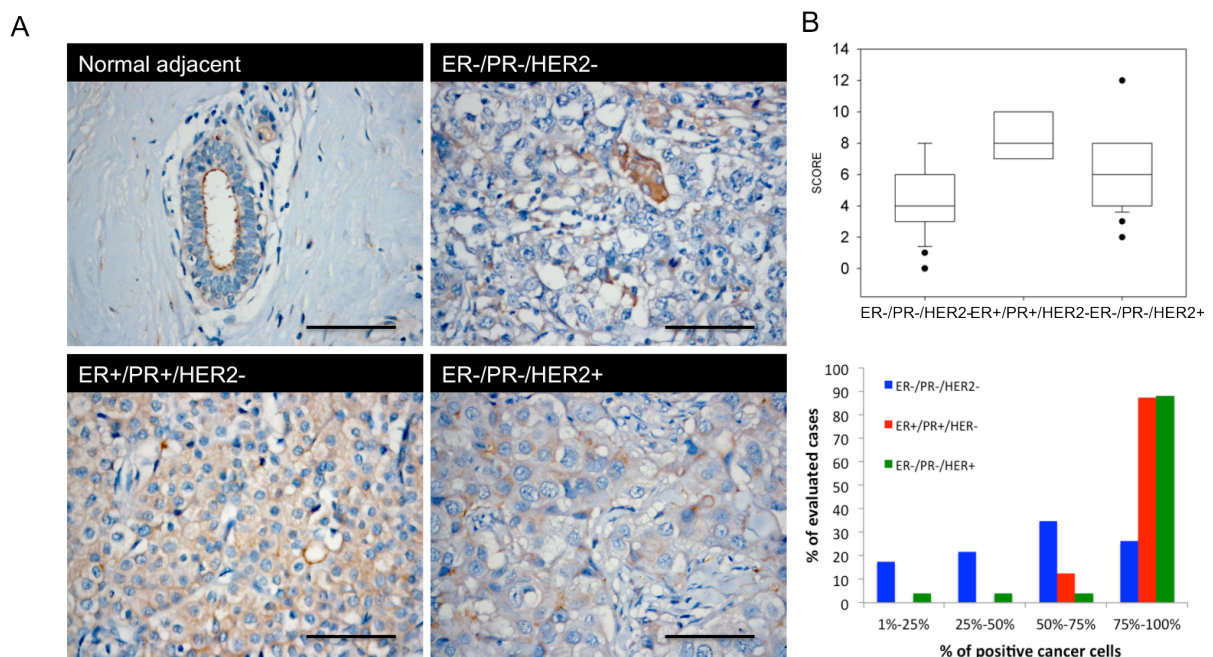


**Figure 2:** Myoferlin is over-expressed in different breast cancer subtypes. A, IHC staining of myoferlin expression in different breast cancer subtypes and normal adjacent breast epithelial cells. B, Evaluation of the IHC staining for myoferlin expression (boxplot) and the extent of staining (bar chart).

We have examined hormone-receptor (HR)-positive HER2-negative (ER+/PR+/HER2-) tumors as well as HR-negative and HER2-positive (ER-/PR-/HER2+) and triple-negative (ER-/PR-/HER2-) tumors. As shown in the **Figure 2**, myoferlin is in general highly expressed

in HR-positive and less expressed in HR-negative tumors. The HR- and HER2-positive tumors displayed a striking uniformity of myoferlin expression (more than 85% of the cases had over 75% of positive cancer cells), even if intensity of the signal was higher in HR-positive cases. The highest degree of heterogeneity was observed in triple-negative breast cancers (25% of patients had more than 75% positive cells). In this tumor subtype areas of negative breast cancer were frequently observed as well as isolated groups of cells with very high myoferlin positivity.

### Myoferlin gene-expression correlates with IHC data and patient survival

We were next intrigued by the question if gene expression data would confirm the observations made at the protein level. To verify this we have employed publicly available algorithm (<http://co.bmc.lu.se/gobo>) recently published by Ringnér et al. [187]. Interrogating gene expression data from over 2000 breast cancer patients (Fig. 3A) has confirmed the principal observations made in the immunohistochemistry study. The highest expression levels were observed in luminal A and B subtypes which are characterized by HR expression. Lowest levels were detected in basal (or triple-negative) and HER2-positive subtypes. Both protein- and gene-expression analysis indicates that tumor subtypes with best prognosis have the highest myoferlin expression levels. This observation is further confirmed by survival analysis based on the overall patient survival and gene-expression data. As outlined in the Figure 3B, and considering the breast cancer patients as one cohort, high myoferlin expression significantly delineates patients with good outcome (logrank  $p \leq 0.01$ ).

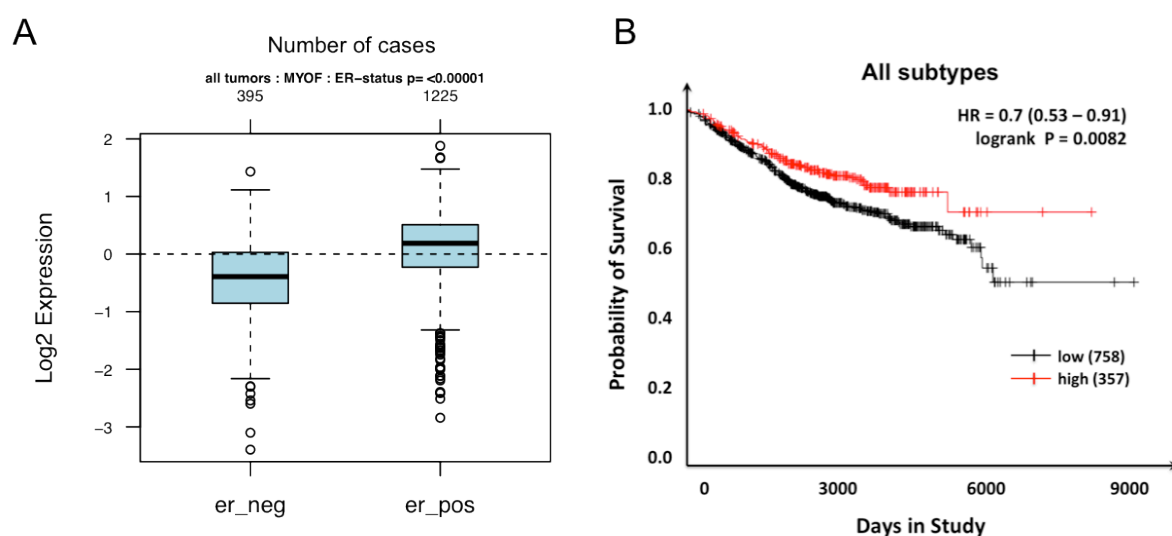


**Figure 3A-B:** Gene expression of myoferlin in breast cancer subtypes and survival analysis. A, Boxplot of normalized log<sub>2</sub> gene expression of myoferlin in different subtypes of breast cancer and B, Kaplan-Meier survival curves of breast cancer patients classified in different subgroups and depending on the myoferlin gene expression levels

### Myoferlin levels have different significance in individual breast cancer subtypes

Having in mind the heterogeneous expression of myoferlin in triple-negative breast cancer, we next sought to examine the relationship between expression and patient survival in each breast cancer subtype individually (**Fig. 4**). Surprisingly, patients with high myoferlin expression and triple-negative or HER2-positive tumors had poorer overall survival. This trend was evident in both subtypes, however the statistical significance could only be established for triple-negative but not for HER2-positive patients. In contrast to this, patients with high myoferlin levels and luminal A or luminal B tumor types showed a better survival that was statistically significant.

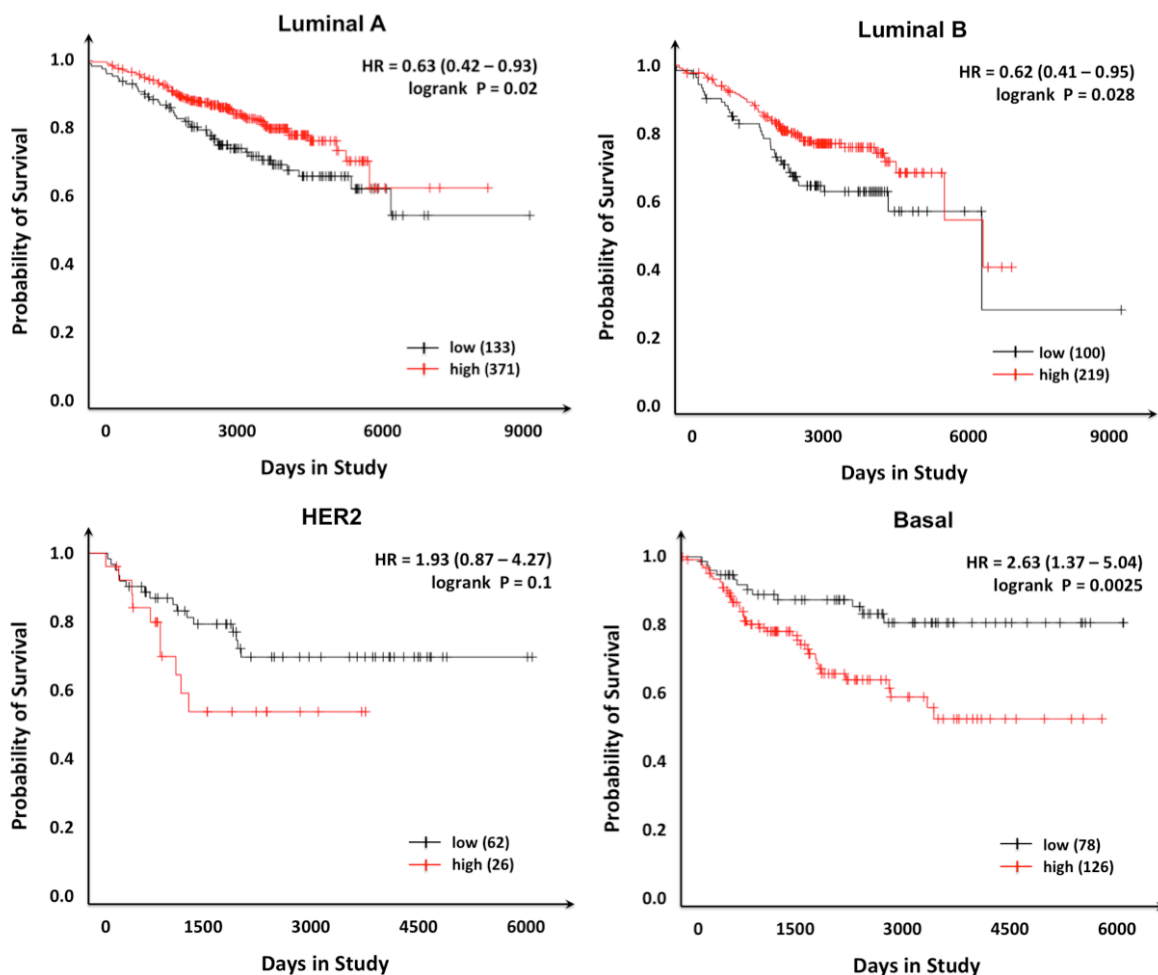


**Figure 4:** Gene expression of myoferlin in breast cancer subtypes and survival analysis. Kaplan-Meier survival curves of breast cancer patients classified in different subgroups and depending on the myoferlin gene expression levels. Hazard ratios (HR) and logrank p values are provided for each subgroup

The survival analysis clearly showed that triple negative patients overexpressing myoferlin were at higher risk comparing to other breast cancer subtypes. This observation was particularly intriguing and we sought to further focus on triple negative breast cancer (TNBC) in order to find a mechanistic explanation.

**Myoferlin affects migration, invasion, and survival of triple negative breast cancer cells.**

In vitro studies in basal conditions (medium with serum) showed that myoferlin depletion induces reduction in cell migration (50%) and invasion (60%) but does not affect cell proliferation (Fig. 5B and C). In addition, myoferlin depletion leads to a modest reduction of cell growth in vitro (10% – 20%; Fig. 5D).

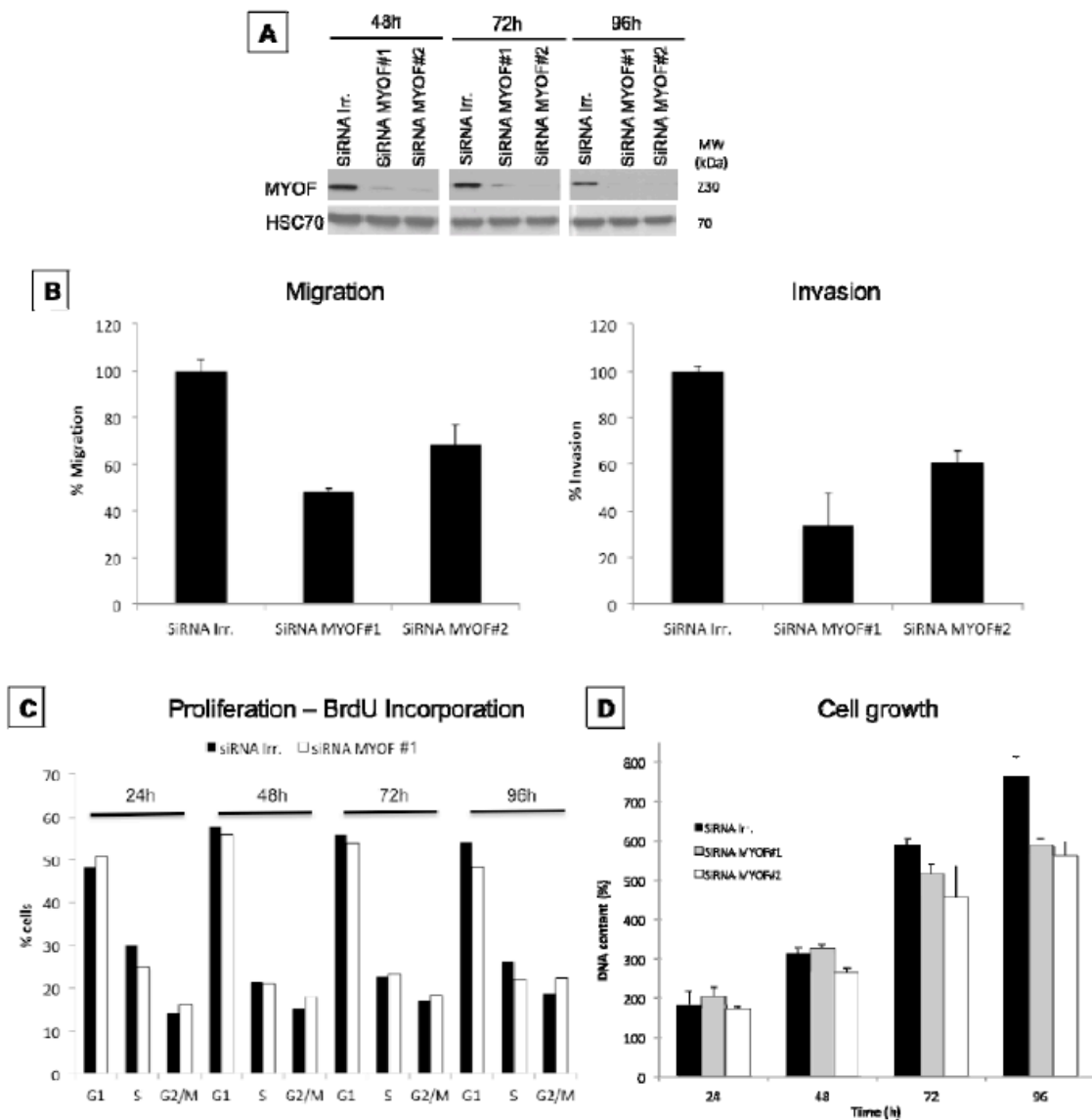


**Figure 5A-D:** Cell migration and invasion analysis following siRNA mediated silencing of myoferlin (MYOF) in MDA-MB231 cells. A, Western blot analysis of myoferlin expression following the silencing with two different siRNAs at different time points post transfection. B, Myoferlin silencing reduced the migration ability of MDA-MB231 cells *in vitro*. Myoferlin depletion in MDA-MB231 cells resulted in impaired invasion in matrigel coated Boyden chamber assay. Error bars indicate standard deviation of means from three biological replicates. C, Assessment of proliferation capacity (adherent cells) using BrdU incorporation and following myoferlin depletion. G1, G2 and S indicate the respective cell cycle phases. Displayed is one representative experiment. D, Measurement of cell growth through quantification of DNA content. Error bars indicate standard deviation of means from three biological replicates.

On the basis of the present *in vitro* data have we next aimed to determine whether the loss of myoferlin in breast cancer cells had an impact on tumor growth *in vivo*.

### Myoferlin depletion slows tumor growth *in vivo*.

We implanted MDA-MB231 cells onto the chorioallantoic membrane (CAM) of the chicken embryos and evaluated the tumor development when myoferlin was depleted (**Fig. 6C**). As shown in the **Figure 6A**, siRNA mediated myoferlin depletion is highly effective, lasting for the entire time period of tumor growth in the present model. On day 7 post-implantation, tumor volumes were measured and showed that myoferlin depletion halved the tumor volume (reduction by 40%) within this short time period (**Fig. 6C**). Histologic analysis of myoferlin-depleted tumors showed general decrease of cellularity characterized by loosely associated cells, lacking orientation typically observed in tissue structures (**Fig. 6D**).

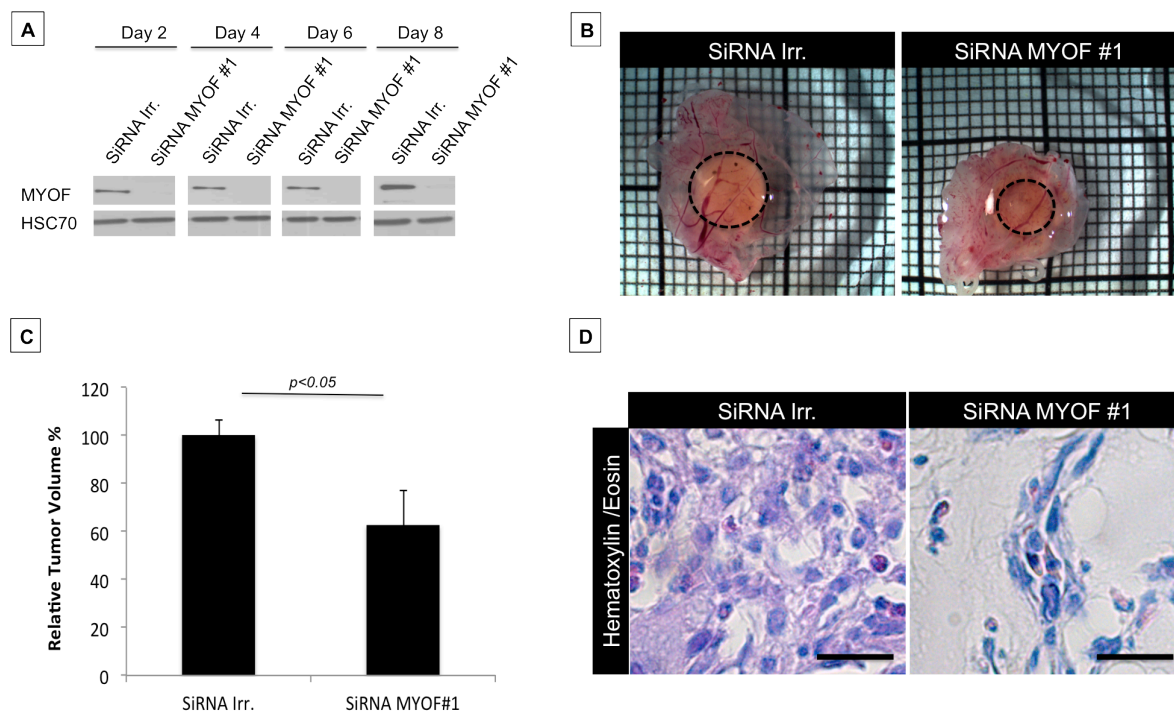


**Figure 6A-D:** Myoferlin depletion reduces breast cancer tumor volume *in vivo*. A, Western blot analysis of MYOF expression in MDA-MB231 cells up to 8 days posttransfection (*in vitro*). B, effect of myoferlin silencing

**Figure 6A-D (continued)** in MDA-MB231 CAM tumor model. Tumors collected at day 7 of tumor development were measured in volume (outlined in Materials and Methods; top). Displayed is macroscopic tumor appearance in both conditions. Representative images of 3 biological and 5 technical replicates. C, Quantitative evaluation of the tumor volume showed a significant decrease in the myoferlin-depleted MDA-MB231 tumors. Error bars indicate SD of means from 3 independent biological replicates with 5 tumors per condition. Statistical significance (P) was evaluated using an unpaired Student t-test. D, histological evaluation of paraffin-embedded CAM tumors. Hematoxylin and eosin staining of the tumor sections show a decreased cellularity in myoferlin-depleted tumors. Pictures were taken at X400 magnification. Data are representative experiments from 3 biologic replicates; scale bars correspond to 20  $\mu\text{m}$ .

Taken together the *in vitro* and *in vivo* data point at a strong pro-invasion, -migration and -survival functions of myoferlin in TNBC cancer. In order to generate the hypothesis for a mechanistic explanation, we were particularly intrigued by the previous reports where myoferlin was reported as a regulator of several RTK in endothelial and muscle cells. Along these lines we hypothesized that myoferlin may assume a similar role in breast cancer. Taking EGFR as one of the most relevant growth factor receptors in triple negative breast cancer we asked the question if myoferlin was implicated in regulating the activity and function of this RTK.

## **PART 2: Myoferlin and EGFR**

## Myoferlin is a key regulator of EGFR activity in breast cancer\*

### Myoferlin regulates EGFR fate upon EGF-mediated receptor activation

Following ligand binding, EGFR undergoes phosphorylation, internalization, and intracellular targeting to modulate downstream signaling. We have investigated whether myoferlin was involved in the EGFR signaling machinery. As shown in **Figure 7A**, upon EGF stimulation, depletion of myoferlin in MDA-MB231 cells led to sustained pEGFR activation, evidenced through prominent phosphorylation of Y1173 residue (the same effect was observed in MDA-MB468, **Fig. 7C**). Following this, we examined whether the downstream targets of the EGFR signaling were also activated. One major key component of the pathway is AKT (RAC-alpha serine/threonine-protein kinase), which is readily phosphorylated upon EGF stimulation. The results in **Figure 7B** show that EGF stimulation of MDA-MB231 cells induced the phosphorylation of AKT on S473 and that this signaling pathway is enhanced and prolonged in myoferlin-depleted cells.

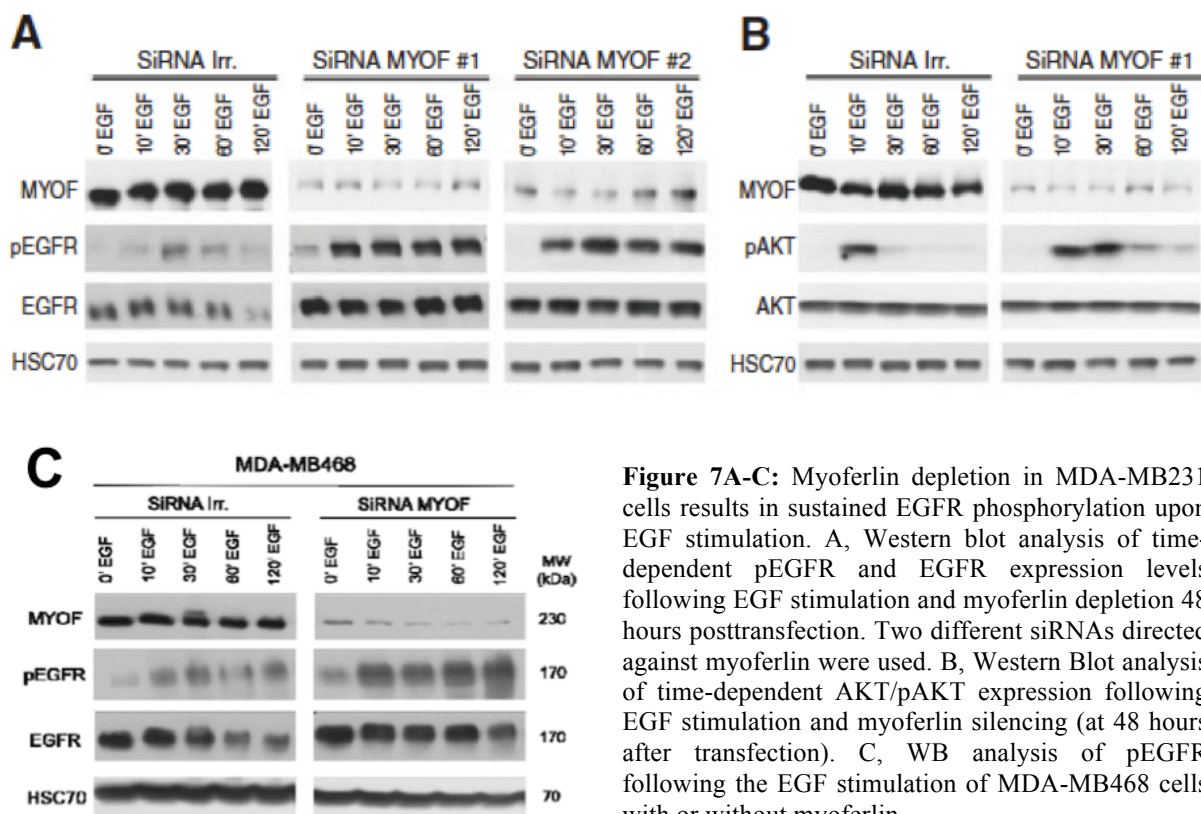


**Figure 7A-C:** Myoferlin depletion in MDA-MB231 cells results in sustained EGFR phosphorylation upon EGF stimulation. A, Western blot analysis of time-dependent pEGFR and EGFR expression levels following EGF stimulation and myoferlin depletion 48 hours posttransfection. Two different siRNAs directed against myoferlin were used. B, Western Blot analysis of time-dependent AKT/pAKT expression following EGF stimulation and myoferlin silencing (at 48 hours after transfection). C, WB analysis of pEGFR following the EGF stimulation of MDA-MB468 cells with or without myoferlin.

As shown in the **Figure 7A**, total EGFR expression levels were increased in comparison with the mock-transfected cells. Further gene expression analysis showed moderately elevated levels of EGFR mRNA (1.5-fold in comparison with the siRNA Irr. at 48 hours) evident in basal condition and further observed during EGF stimulation (**Sup. Fig. 1**). Although the gene expression and protein synthesis levels are not directly comparable, it is unlikely that this moderate increase in EGFR mRNA can justify the prominent increase of protein levels.

Aberrant activation of EGFR in absence of myoferlin may have different functional consequences for the downstream processes. EGFR signaling pathway controls cancer cell differentiation and hence governs associated processes such as migration, invasion, and EMT [188-190]. We have therefore sought to examine the impact of myoferlin depletion on EGFR guided cancer cell migration and EMT.

### Myoferlin silencing in breast cancer cells impaired EGF-induced migration and EMT

Previous studies have shown that MDA-MB231 cells are responsive to EGF stimulus, characterized by enhanced migration [190]. We have examined whether MDA-MB231 cells lacking myoferlin would still show responsiveness toward EGF (**Fig. 8**), and found that myoferlin-depleted cells were unable to migrate (Boyden chamber assay) when pulsed with EGF. This impaired migration toward EGF was also observable in myoferlin-depleted MDA-MB468 breast cancer cells.

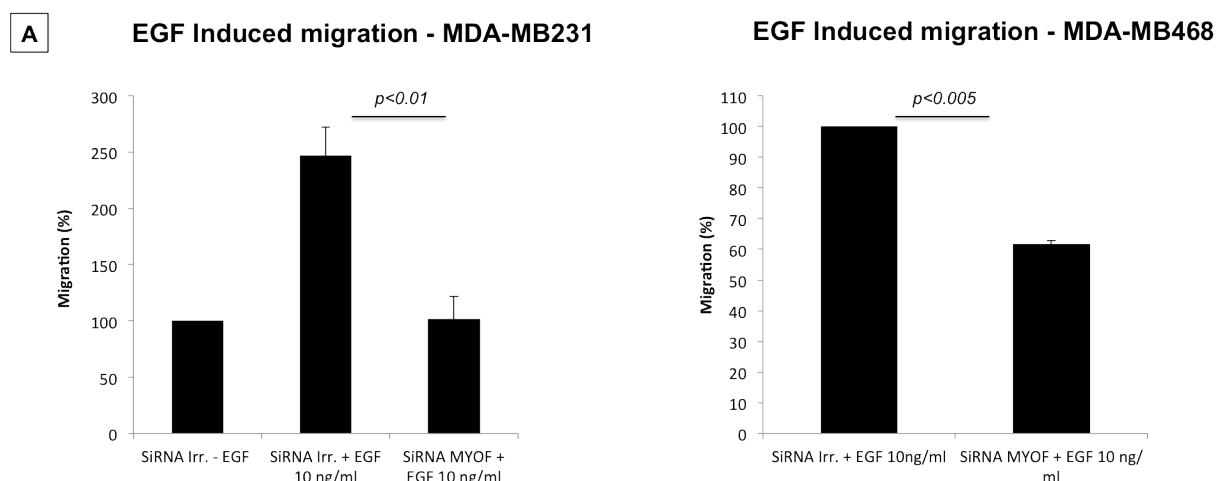


**Figure 8:** Myoferlin depletion inhibits EGF-induced migration in breast cancer cells. A, EGF-induced MDA-MB231 cell migration is stalled in the absence of myoferlin. Similar data are shown with MDA-MB468. Error bars indicate SD of means from 3 independent biological replicates. Statistical significance ( $p$ ) was evaluated using an unpaired Student  $t$  test (for details see Materials and Methods).

To further examine the consequence of myoferlin depletion on EGFR signaling and related biologic processes, we used an EGF-inducible EMT breast cancer cell model. In our recent work [185], we have shown that MDA-MB468 cells are able to undergo EMT *in vitro* following EGF stimulation. Unlike MDA-MB231 cells, which in basal conditions are displaying a prominent mesenchymal appearance, the MDA-MB468 cells are epithelial-like. In presence of the EGF stimulus, MDA-MB468 cells undergo EMT, adopting a mesenchymal phenotype that is primarily characterized by a strong induction of vimentin (VIM) expression coupled to the downregulation of E-cadherin (CDH1) as well as by modulation of other more specific EMT markers (further detailed in ref. [185]). In the present work, we used VIM and CDH1 as surrogate markers of EGF-induced EMT in the MDA-MB468 cells. Myoferlin depletion in MDA-MB468 cells significantly impaired their capacity to undergo EGF-induced EMT with both reduced VIM induction and downregulation of CDH1 expression (**Fig. 9A and B**). These effects were already noticeable 24 hours post-EGF treatment (VIM) and became more pronounced at 48 hours (VIM and CDH1).

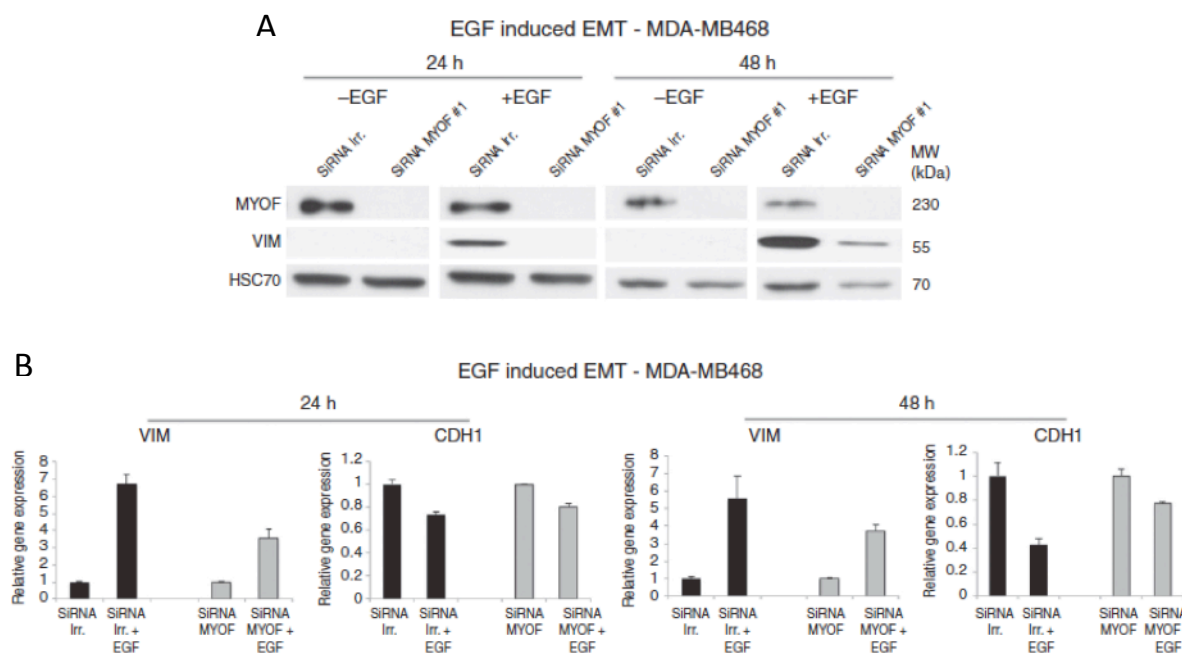


**Figure 9A-B:** Myoferlin depletion inhibits EGF-induced EMT in breast cancer cells. A, myoferlin is essential for EGF-induced EMT in MDA-MB468 breast cancer cells. EGF-mediated vimentin induction is impeded in myoferlin-depleted MDA-MB468 cells (Western blot analysis). Displayed is one representative experiment of 3 biological replicates. B, qRT-PCR analysis of CDH1 and VIM gene expression in EGF-treated MDA-MB468 cells at 24 and 48 hours post-myoferlin silencing. Error bars indicate SD of means from 3 independent biological replicates.

Following these findings we were further interested in elucidating the mechanism on how myoferlin may actively take part in controlling the EGFR signaling. To do so, we

commenced by verifying the internalization process of the EGFR, a key step in initializing the downstream signaling.

### Myoferlin depletion affects the degradation of the internalized EGFR

Quantitative measurement of EGFR levels on the surface of living MDA-MB231 cells during EGF stimulation revealed comparable internalization kinetics between myoferlin-depleted and control conditions (**Fig. 10A**). Further immunofluorescence-based analysis showed that the EGFR was internalized in myoferlin-depleted cells in the same manner as in the control condition. However, after 60 and 120 minutes, the EGFR foci failed to resolve in the absence of myoferlin (**Fig. 10B**).

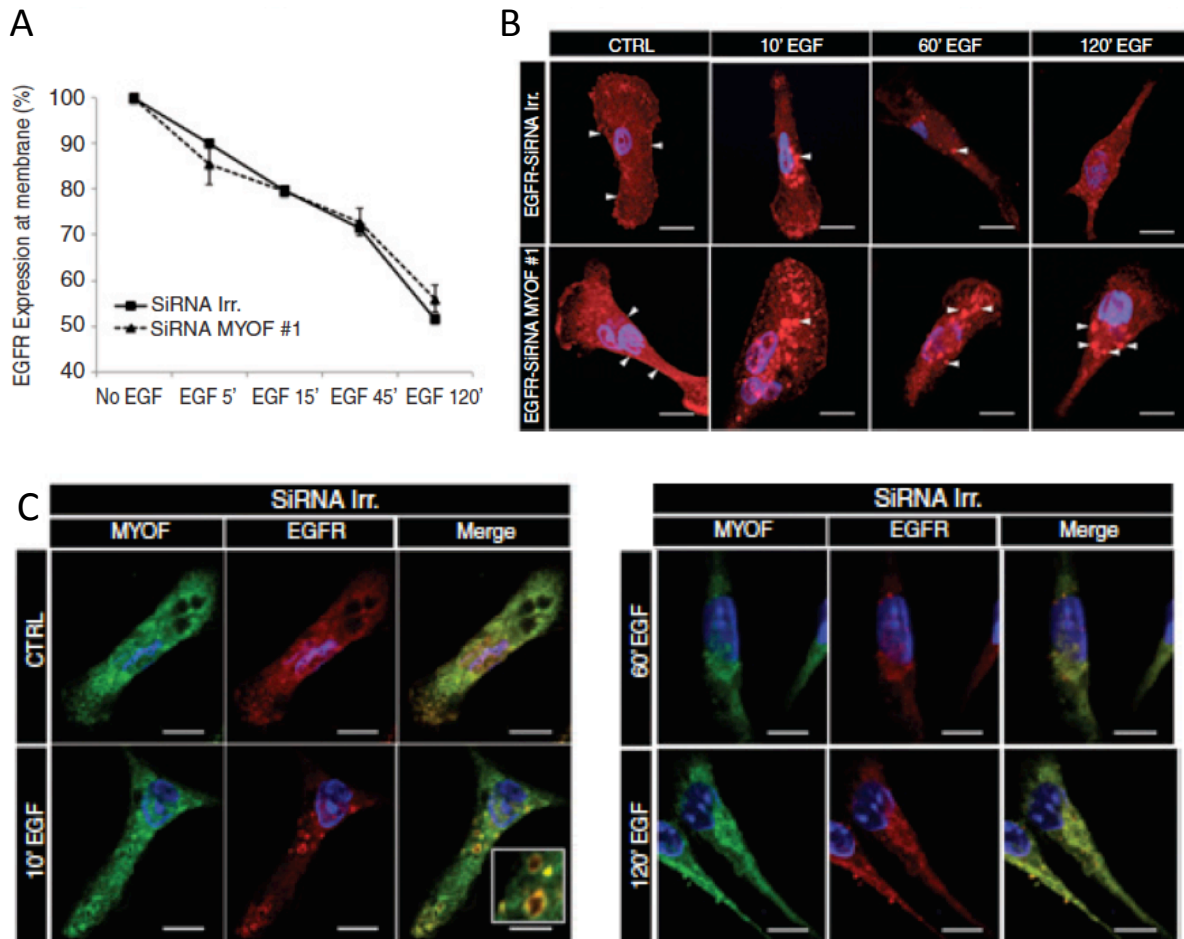


**Figure 10A-C:** Myoferlin depletion in MDA-MB231 cells results in sustained EGFR phosphorylation upon EGF stimulation. **A**, FACS analysis of EGFR surface levels (intact cells) following time-dependent EGF stimulation of myoferlin-depleted MDA-MB231 cells. Error bars indicate SD of means from 3 independent biological experiments. **B**, EGFR immunofluorescence analysis of MDA-MB231 cells following myoferlin depletion and EGF stimulation. White arrows point at EGFR, which at later time-points is internalized and visible as clusters. **C**, EGFR/MYOF immunofluorescence analysis of MDA-MB231 cells following EGF stimulation. The control condition (CTRL) was not treated with EGF. All images were taken at X400 magnification, identical setting of photomultipliers, and are representative of at least 3 biological replicates; scale bars, 5  $\mu$ m.

The observations made above suggest that the elevated EGFR levels in myoferlin-depleted cells are probably linked to their inability to properly degrade the receptor and hence switch off the pEGFR signal. To test this, we inhibited proteolytic activity of the proteasome using MG132 while subjecting the cells to the same EGF stimulation as shown in **Figure 7A**. The comparison of the resulting EGFR/pEGFR expression patterns (**Fig. 11**) showed that impairment of proteasome degradation caused a sustained EGFR expression and activation, similar to what is observed when myoferlin is silenced.

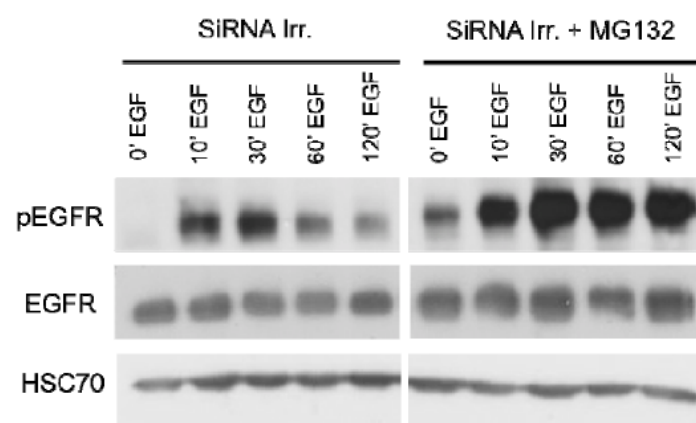


**Figure 11:** Analysis of time dependent pEGFR and EGFR expression patterns (48h post-transfection with irrelevant siRNA) following EGF stimulation and chemical inhibition of the proteasome with MG132. Representative image of 3 biological replicates are shown.

We next examined whether myoferlin is colocalizing with EGFR in basal conditions and in the presence of EGF (**Fig. 10C**). The data show that EGFR does colocalize with myoferlin in MDA-MB231 cells, both in basal and EGF conditions. As displayed in the **Figure 10C**, myoferlin and EGFR are also detectable and colocalized in the endosomal vesicles, structures typically observed following EGF-induced EGFR endocytosis. Considering the existence of 2 EGFR internalization mechanisms (CME and NCE), we next verified whether clathrin or/and caveolin are affected following myoferlin silencing in MDA-MB231 cells.

**Myoferlin does not affect clathrin cellular distribution/quantity in MDA-MB231 cells**

Immunofluorescence analysis showed that myoferlin colocalizes with clathrin in breast cancer cells both in serum and EGF-rich conditions (**Fig. 12A**). As expected, clathrin showed evidence of colocalization with pEGFR during EGF-stimulation (**Fig. 12A**). However, myoferlin depletion neither induced any marked modification of clathrin distribution in the cell (**Fig. 12B**) nor a change in clathrin total protein levels (**Fig. 12C**).

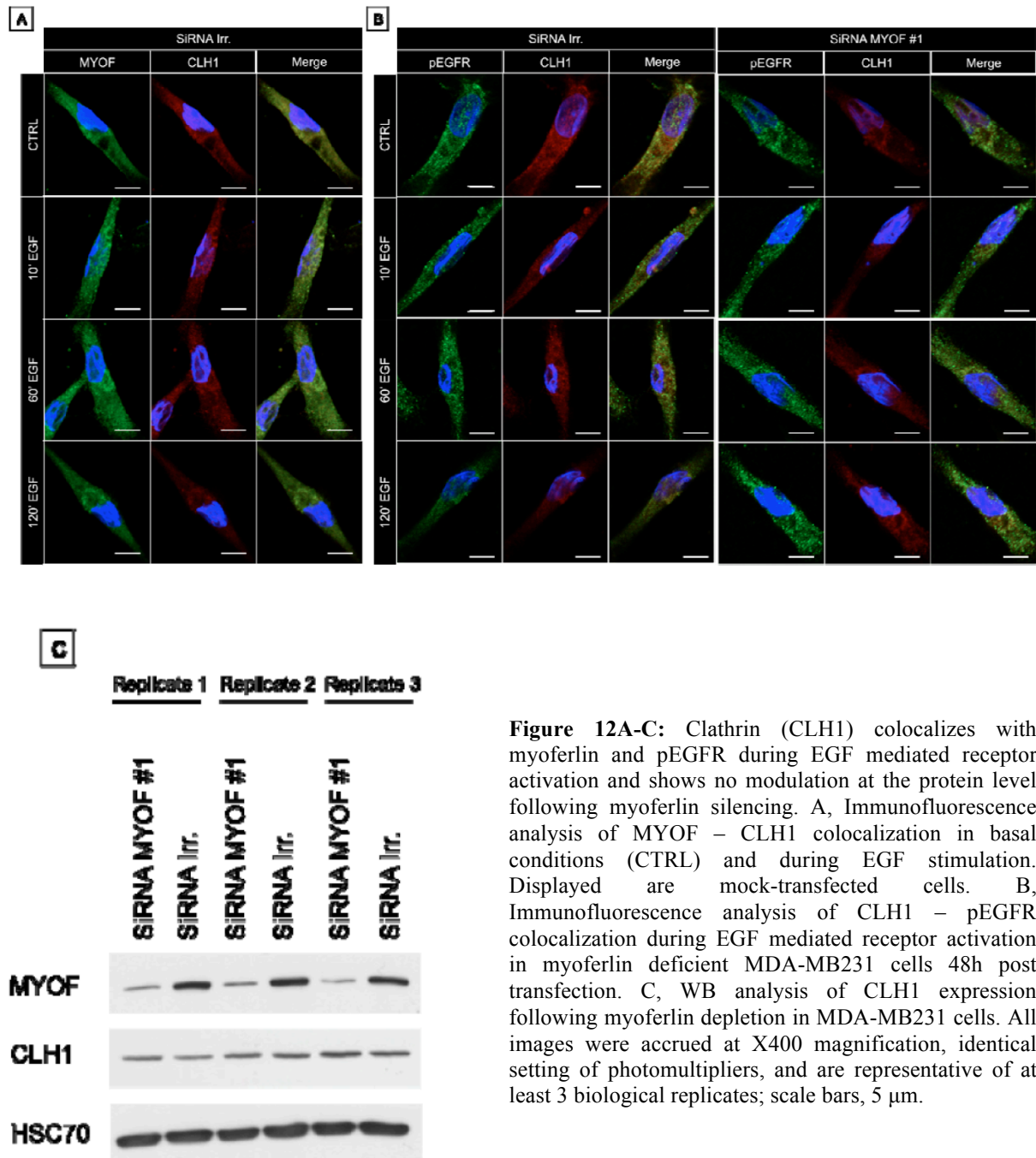


**Figure 12A-C:** Clathrin (CLH1) colocalizes with myoferlin and pEGFR during EGF mediated receptor activation and shows no modulation at the protein level following myoferlin silencing. A, Immunofluorescence analysis of MYOF – CLH1 colocalization in basal conditions (CTRL) and during EGF stimulation. Displayed are mock-transfected cells. B, Immunofluorescence analysis of CLH1 – pEGFR colocalization during EGF mediated receptor activation in myoferlin deficient MDA-MB231 cells 48h post transfection. C, WB analysis of CLH1 expression following myoferlin depletion in MDA-MB231 cells. All images were accrued at X400 magnification, identical setting of photomultipliers, and are representative of at least 3 biological replicates; scale bars, 5  $\mu$ m.

### Myoferlin is critical for proper assembly of caveolin in caveolae

Previous studies reported the existence of an intimate relationship between caveolin (and particularly the caveolae) and myoferlin in the context of endocytosis [56]. In accordance with literature, we found that myoferlin was colocalized with caveolin both in control (basal condition) as well as in EGF-treated cells along the treatment time course (**Fig. 13A**). Further immunofluorescence analysis of pEGFR and caveolin in EGF-stimulated MDA-MB231 cells (**Fig. 13B**) showed evidence of colocalization of both proteins in mock-transfected cells, both in basal and EGF-stimulated conditions. In myoferlin-depleted cells, the colocalization was weaker and at later time points (60 and 120 minutes) pEGFR and caveolin did not colocalize.

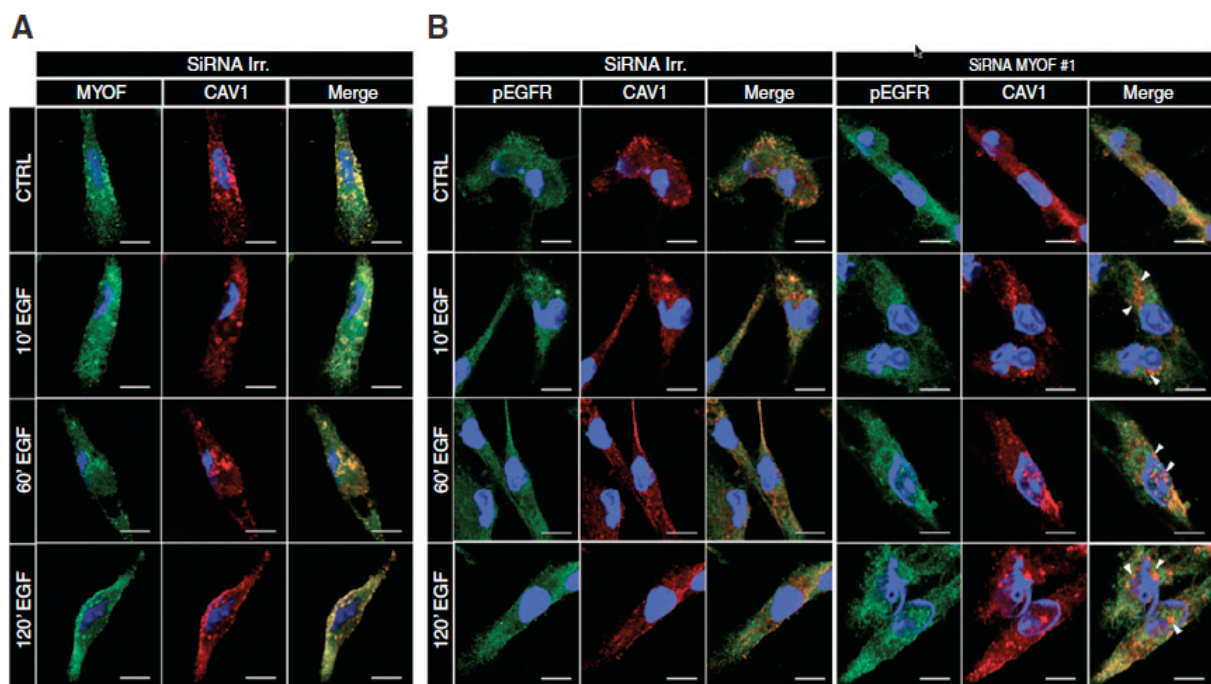


**Figure 13A-B:** Caveolin colocalizes with myoferlin and pEGFR during EGF-mediated receptor activation. A, immunofluorescence analysis of myoferlin and caveolin (CAV1) colocalization in basal conditions (CTRL) and during EGF stimulation. Displayed are mock-transfected cells. B, immunofluorescence analysis of CAV1–pEGFR colocalization during EGF-mediated receptor activation in myoferlin-deficient MDA-MB231 cells 48-hour posttransfection. White arrows indicate examples of several major differences in localization of the 2 proteins. All images were accrued at X400 magnification, identical setting of photomultipliers, and are representative of at least 3 biological replicates; scale bars, 5  $\mu$ m.

We also observed that caveolin foci in myoferlin-depleted cells were larger and more variable in size, which is particularly visible at later time points following EGF stimulation (**Fig. 14A**). Moreover, myoferlin silencing in non-stimulated MDA-MB231 cells resulted in a higher concentration of caveolin homo-oligomers (**Fig. 14B, left**), the presence of major aberrant molecular weight forms (in comparison with the control condition), and an enhanced enrichment of caveolin in lipid-raft microdomains (**Fig. 14B, right**). The latter pool of

caveolin was not found in the same fractions where myoferlin was present. The appearance of caveolin homo-oligomers with aberrant molecular weight was particularly emphasized after EGF stimulation in myoferlin-depleted cells (**Fig. 14C**). The present data suggest that the interaction between myoferlin and caveolin is essential for proper organization of caveolae and endocytosis of pEGFR. This is further supported by the data shown in **Figure 14D**, where siRNA-mediated depletion of caveolin in MDA-MB231 cells, similar to myoferlin silencing, induced an accumulation of pEGFR. In contrast, caveolin depletion was unable to inhibit the degradation of the EGFR upon EGF stimulation. Phospho-EGFR levels, although initially elevated, returned to basal levels at later stage.

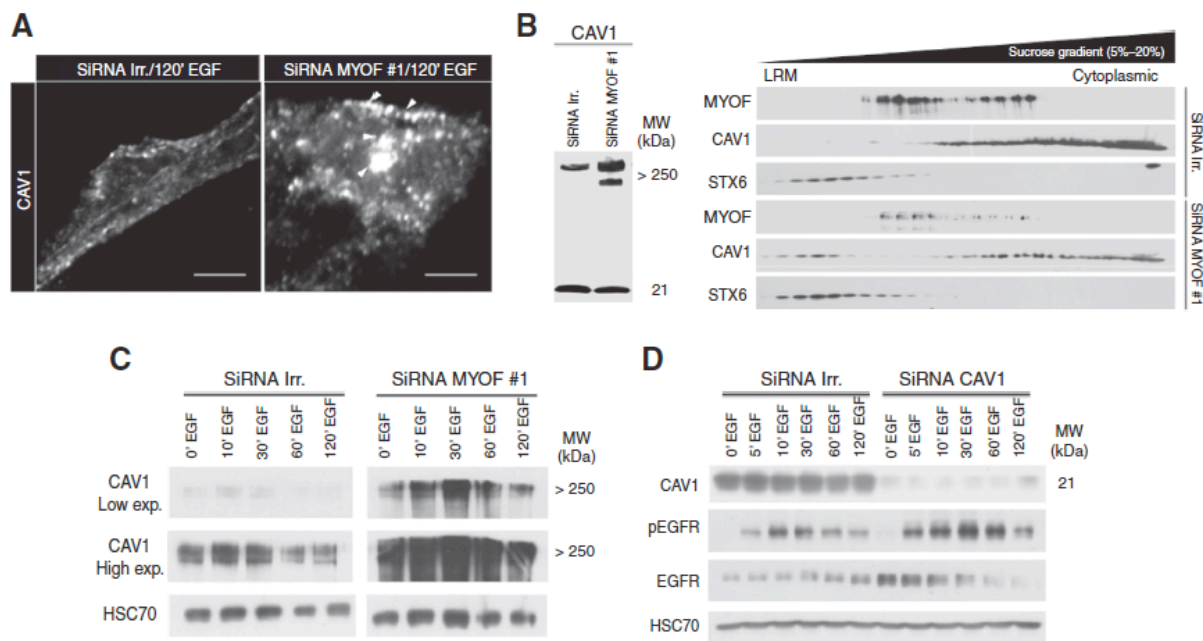


**Figure 14A-D:** Myoferlin affects the functional assembly of caveolin into caveolae. **A**, immunofluorescence analysis of caveolin in myoferlin-deficient MDA-MB231 cells 120-minute post-EGF stimulation. Arrows indicate large caveolin clusters accumulating in the myoferlin-depleted condition. Magnification, X400; scale bars, 5  $\mu$ m. **B**, left, Western blot analysis of caveolin in nondenaturing conditions (with or without MYOF depletion) shows high-molecular weight complexes corresponding to caveolin homomultimers. Right, sucrose-gradient fractionation of caveolin complexes in myoferlin depleted MDA-MB231 cells; LRM, lipid-raft microdomain fraction. Syntaxin 6 (STX6) is marker of lipid rafts. **C**, time-kinetics of high-molecular weight (>230 kDa) caveolin expression (homomultimers) in MDA-MB231 cells following myoferlin depletion and EGF stimulation. **D**, caveolin depletion in MDA-MB231 cells leads to a transient accumulation of pEGFR upon EGF stimulation 48-hour posttransfection. Displayed are caveolin monomers at approximately 21 kDa. All data are representative experiments from 3 biological replicates (**A–D**).

## **PART 3: Myoferlin and metabolism**

## Myoferlin regulates endosomal trafficking and tunes cancer cell metabolism

While studying the role of myoferlin in cancer, we observed that breast cancer cells silenced for myoferlin *in vitro* acidify the culture medium faster than the control-transfected counterparts. Our hypothesis was that myoferlin-silenced cells might generate more lactate due to intensified glycolysis. This has sparked our interest to ask the question if myoferlin is directly involved in the metabolism of cancer cells.

### **Myoferlin silencing in breast cancer cells leads to lactate accumulation and impaired mitochondrial activity**

Following our initial observation where pH indicator dye in culture medium turned from red to yellow 72-96h post-transfection, we have performed the measurement of lactate in the media of breast cancer cells using the NMR technique. We found that, in both MDA-MB231 and MDA-MB468 breast cancer cell lines, myoferlin depletion leads to a time-dependent accumulation of lactate in culture medium (**Fig 15A and B**)

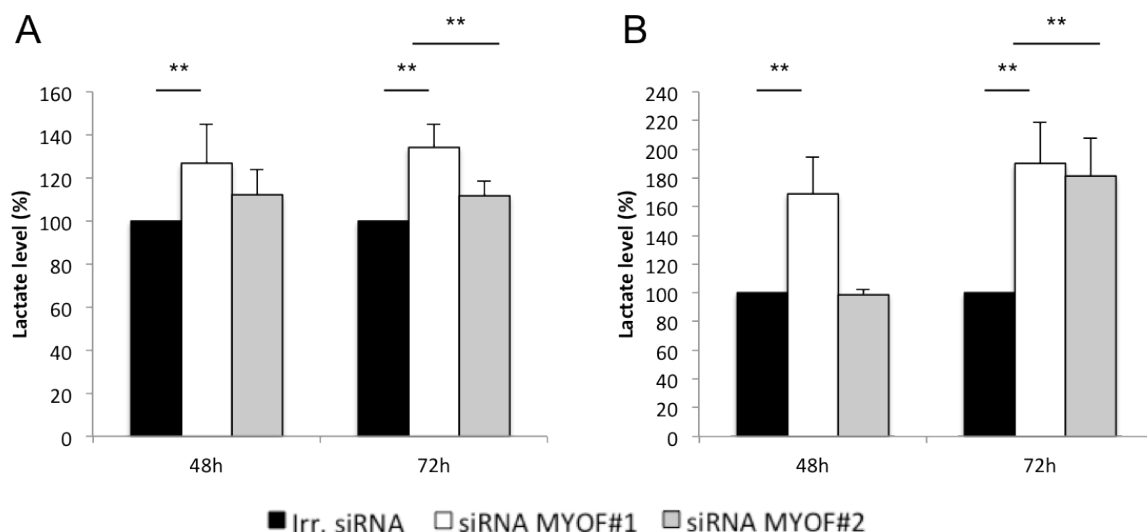


**Figure 15A-B:** Myoferlin depletion leads to lactate accumulation in culture medium of breast cancer cells. A, NMR measurement of lactate levels in culture media of MDA-MB231 and B, MDA-MB468 breast cancer cells following myoferlin silencing. Two different siRNAs directed against myoferlin were used. Error bars indicate SD of means from minimum 3 independent biological replicates. Statistical significance (p) was evaluated using an unpaired Student t-test (\* = p-value $\leq$ 0.05; \*\* = p-value $\leq$ 0.01)

We next sought to examine the effect of myoferlin silencing on the overall cellular metabolic activity of the same cancer cells, using the WST-1 assay. This assay is widely used to monitor proliferation of cultured cells. However, the WST-1 compound is reduced into formazan through the activity of the mitochondrial dehydrogenases, therefore reflecting the mitochondrial activity of the cells. As a result, we found that silencing of myoferlin leads to a progressive reduction of metabolic activity in both cell lines (**Fig. 15C and D**).

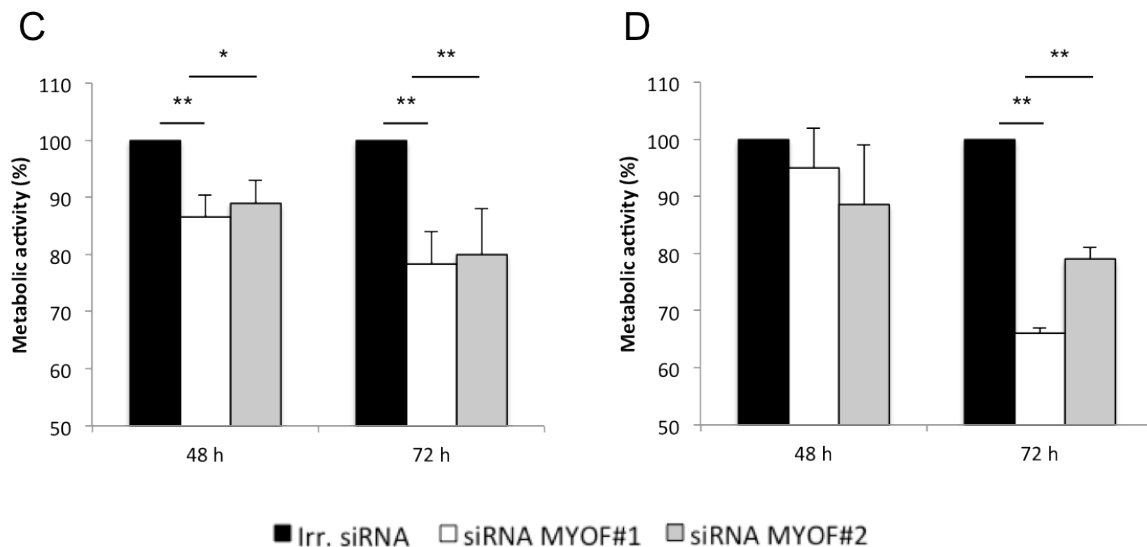


**Figure 15C-D:** Myoferlin depletion decreases metabolic activity of breast cancer cells. C, WST-1 analysis of MDA-MB231 and D, MDA-MB468 breast cancer cells following myoferlin silencing. Two different siRNAs directed against myoferlin were used. Error bars indicate SD of means from minimum 3 independent biological replicates. Statistical significance (p) was evaluated using an unpaired Student t-test (\* = p-value $\leq$ 0.05; \*\* = p-value $\leq$ 0.01)

Lactate accumulation and decrease in mitochondrial metabolic activity suggest an overall shift of the metabolic balance towards glycolysis, pointing at a possible mitochondrial dysfunction. We therefore turned our attention to cancer cell mitochondria and examined these functionally in the presence or absence of myoferlin.

### Loss of Myoferlin induces mitochondrial dysfunction in breast cancer cells

To test whether myoferlin depletion has a functional impact on mitochondria, we first isolated mitochondria from MDA-MB231 cells transfected with a siRNA against myoferlin or control siRNA. The quality control of the isolated fraction was performed accordingly and the results are shown in the Supplemental Data (**Sup. Fig. 2**). In order to obtain an initial picture of mitochondria state in absence of myoferlin, we subjected the mitochondria-enriched fraction to further western blot analysis. We specifically evaluated the expression levels of

NDUFB5 (subunit of complex 1), COX1 (subunit of complex 4) and the oligomycin sensitive subunit of ATP synthase, representing the different parts of the mitochondrial electron-transport respiratory chain. Mitofilin is an abundant protein of the mitochondrial inner membrane, which is an important structural organizer of the mitochondrial cristae [191]. As shown in the **Figure 16**, mitochondria of myoferlin-deficient cells displayed a marked decrease in the expression level of all the proteins tested.

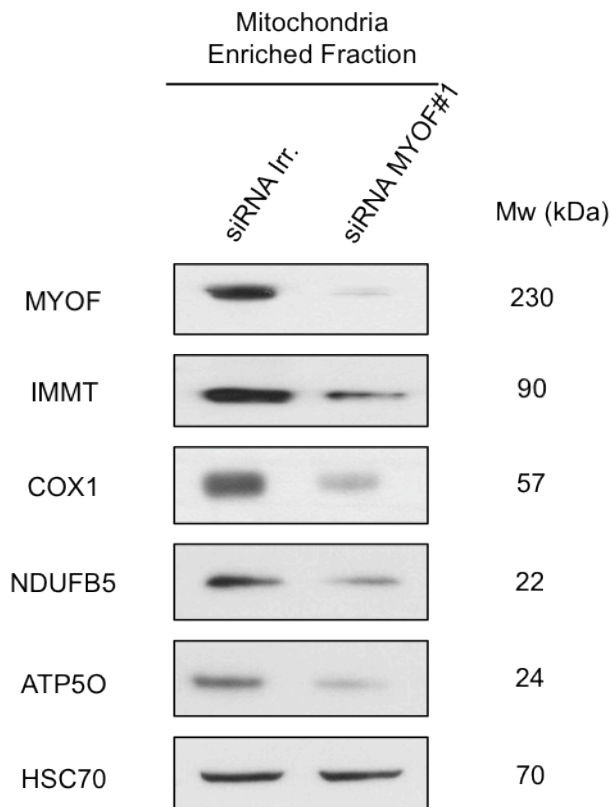


**Figure 16:** Myoferlin silencing affects the expression level of mitochondrial proteins. A, Western Blot analysis on mitochondria enriched fraction of MDA-MB231 reveals that expression level of several mitochondrial proteins is reduced upon MYOF silencing. HSC70 is used as loading control.

To further evaluate the impact of myoferlin silencing on mitochondria, we have performed imaging analysis using mitochondria specific dye (mitotracker) and antibody specific to human mitochondria (for details refer to Materials and Methods section). The mitotracker analysis (**Fig. 17A**) and immunofluorescence staining of mitochondria (**Fig. 17B**) showed that localization and appearance of mitochondria is affected in MDA-MB231 cells depleted of myoferlin.

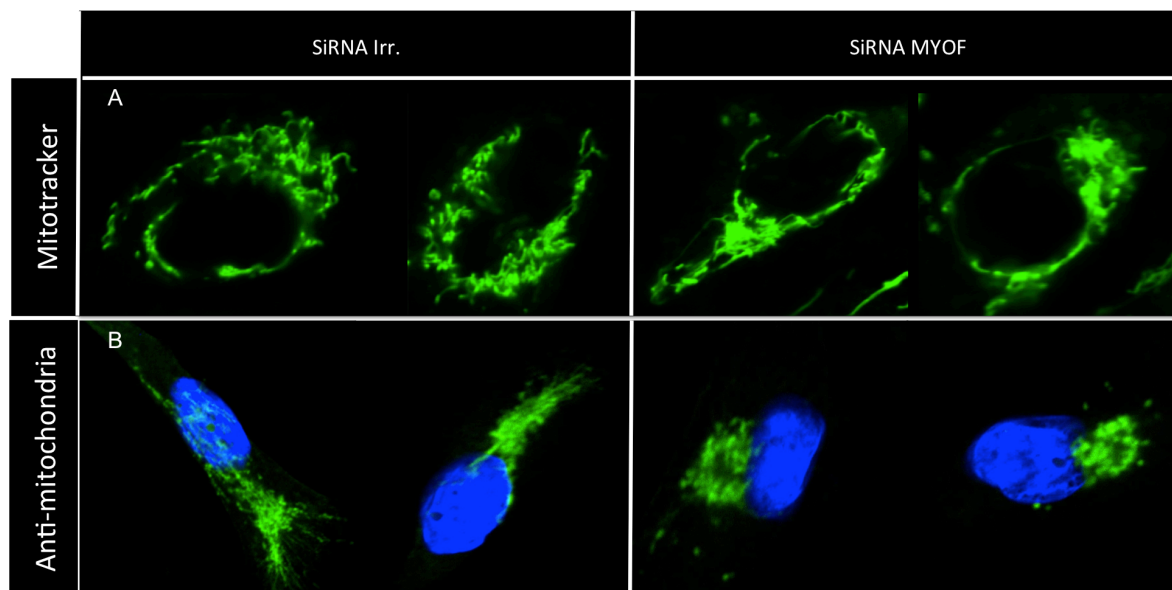


**Figure 17A-B:** Myoferlin silencing induces mitochondrial clustering. Confocal microscopy analysis of A, Mitotracker accumulation in MDA-MB231 cells 48 hours post-transfection with control siRNA (left panel) or siRNA against myoferlin (right panel). B, Immunofluorescence of anti-mitochondria reveals that myoferlin-deficient cells have a dotted mitochondrial appearance restricted to the discrete zone in the perinuclear region. Images were accrued at 400X magnification.

The myoferlin-depleted cancer cells displayed a condensed network of mitochondria, whereas the mitochondrial network in control cells appeared more diffused. The latter condition corresponded to a more typical appearance of normal, somewhat elongated mitochondria. In both conditions, the mitochondria appeared predominantly perinuclear. However, in myoferlin-deficient cells, a more prominent polarized distribution of mitochondria was observed using the mitotracker dye.

Following the observations made using the immunofluorescence technique, we sought to further investigate the role of myoferlin loss on mitochondrial activity. We therefore examined different key parameters of mitochondrial function: i) oxygen consumption ii) ATP production and iii) reactive oxygen species (ROS) generation. We first compared the cellular oxygen consumption rate in myoferlin-deficient versus control cells. We measured basal respiration of the cells in their culture medium (reported here as “routine respiration”), as well as in presence of oligomycin (referred here as “leak”) and FCCP (called “electron transport system” – ETSmax). Oligomycin is an inhibitor of mitochondrial ATP Synthase. Respiration in presence of this compound does not account for ATP production. FCCP is an uncoupling molecule which allows entry of the  $H^+$  back in the mitochondrial matrix and thus abolishes the proton gradient of mitochondria. Without the restriction of the proton gradient, uncoupled respiration is maximal and measuring oxygen consumption in presence of FCCP gives an indication of the maximal respiratory capacity of the cell. Our results, shown in **Figure 18**,

indicate that myoferlin silencing leads to a decrease in oxygen consumption rate, both basal and leak, and also to a reduction of the total capacity of the respiratory chain.

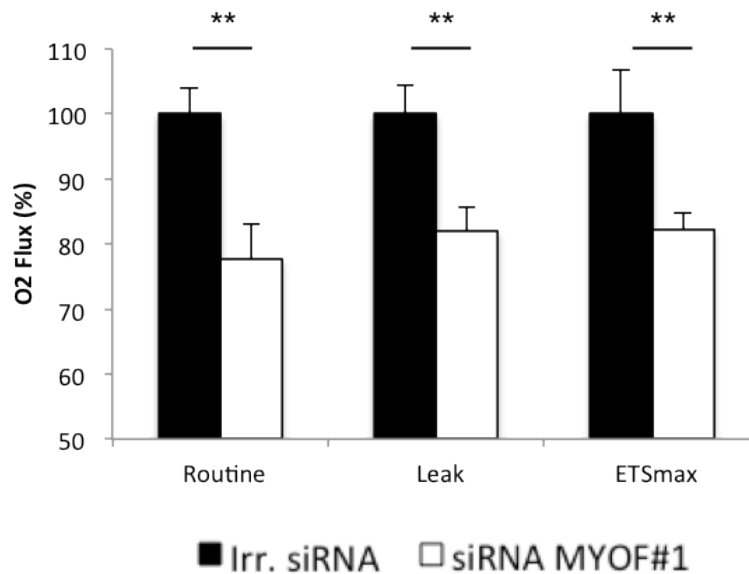


**Figure 18:** Loss of myoferlin impairs mitochondrial respiration in MDA-MB231 breast cancer cells. A, Oxygen consumption of MDA MB-231 in absence of myoferlin. Cellular respiration was measured in culture medium (Routine), in presence of oligomycine (Leak) or after uncoupling with FCCP (ETSmax). All values were corrected for residual oxygen consumption obtained in presence of rotenone. For further details see Materials and Methods. Error bars indicate SD of means from minimum 3 independent biological replicates. Statistical significance (p) was evaluated using an unpaired Student t-test (\* = p-value $\leq$ 0.05; \*\* = p-value $\leq$ 0.01)

Having observed a significant decrease of mitochondrial respiration, we next examined if this defect would lead to an overall decrease of the ATP level. Indeed, measurements of cellular ATP levels indicated that MDA-MB231 cells lacking myoferlin have less ATP (**Fig. 19A**). Having in mind that mitochondrial dysfunction generally leads to an induction of oxidative stress, we also examined if myoferlin-deficient cells have an elevated ROS production. Surprisingly, we found that level of the ROS precursor, superoxide anion, was significantly lower in myoferlin-depleted cells as compared to controls (**Fig. 19B**).

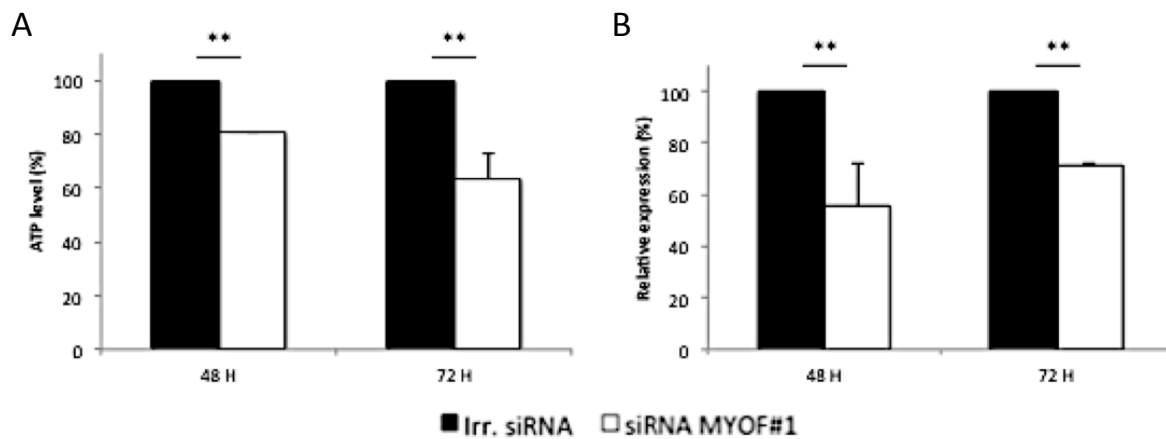
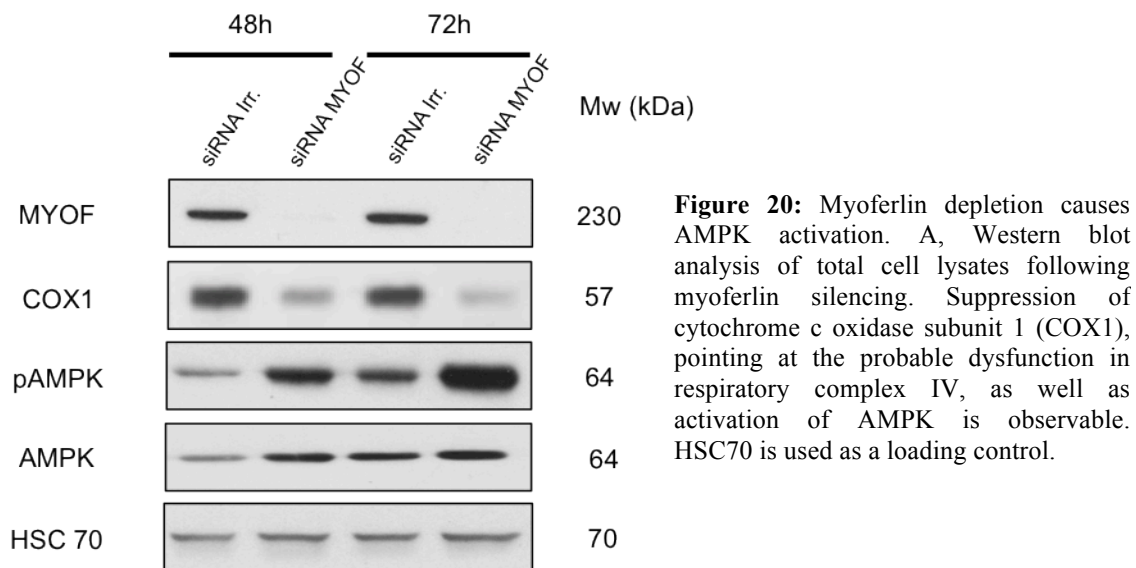


**Figure 19A-B:** Loss of myoferlin leads to lower ATP and ROS levels. A, Measurement of ATP and B, ROS levels in MDA-MB231 cells following myoferlin depletion. Error bars indicate SD of means from minimum 3 independent biological replicates. Statistical significance (p) was evaluated using an unpaired Student t-test (\* = p-value $\leq$ 0.05; \*\* = p-value $\leq$ 0.01)

Mitochondrial dysfunction and impairment of ATP production leads to changes in cell metabolism. Following our observation that myoferlin deficiency leads to mitochondrial dysfunction and an overall decrease of energy production, we hypothesized that the cancer cell must initiate alternative pathways to compensate for this loss. An important actor in such metabolic reprogramming is the AMP activated protein kinase (AMPK).

#### **Myoferlin depletion activates AMPK and induces a metabolic shift towards glycolysis**

Following our rationale of metabolic adaptation, we found that silencing of myoferlin leads to a considerable increase in the phosphorylated form of AMPK (**Fig 20**), while the total expression levels of this protein are also increased. This result suggests that AMPK signaling pathway is strongly activated when myoferlin is depleted from cancer cells. Interestingly, the degree of phosphorylation also increases with the time and correlates with a severe decrease in the expression level of the cytochrome c oxidase subunit 1 (**Fig. 20**), observable on total cell lysates.



The activation of AMPK following myoferlin knockdown was a consistent feature in the different cancer cell lines we tested (**Fig. 21**).

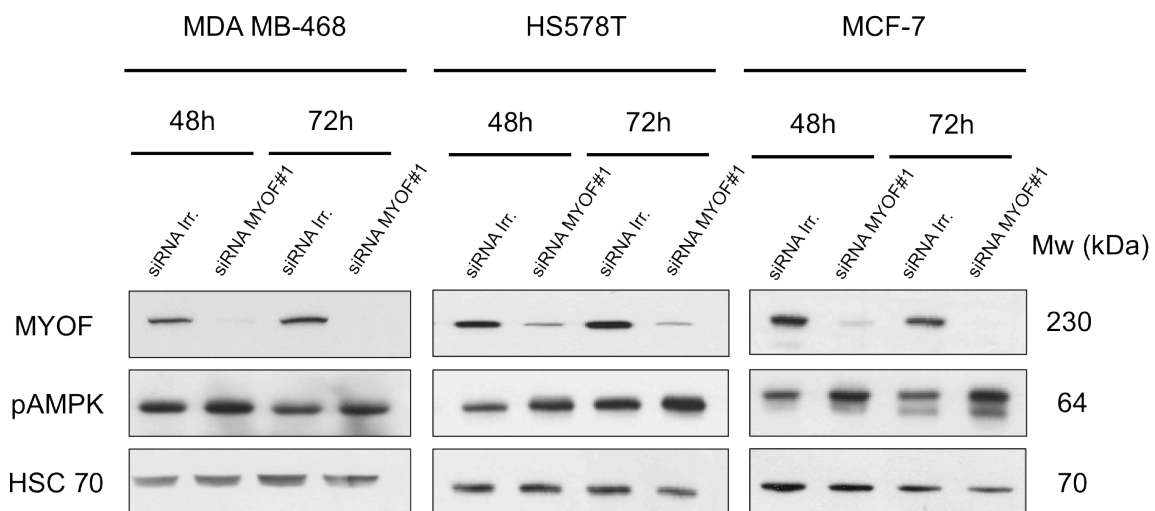


**Figure 21:** AMPK activation following myoferlin silencing is a common feature of several breast cancer cell lines.

Activation of AMPK signaling pathway generally leads to an increase in glycolysis and lipid oxidation which are used to generate ATP. To check if myoferlin-depleted cells are redirecting their metabolism towards one of these pathways, we evaluated the expression of several key proteins involved in metabolic processes. As shown in **Figure 22**, phosphorylation of AMPK following myoferlin silencing leads to the subsequent phosphorylation of a downstream target, the acetyl-coA carboxylase (ACC). The phosphorylation status of AMPK and acetyl-CoA carboxylase is an important indicator of

AMPK activity. ACC is a relevant regulator of fatty acid metabolism, controlling the fate of malonyl-coA that results either in the inhibition of beta-oxidation or the activation of lipid biosynthesis. Phosphorylation by AMPK leads to inhibition of the protein, which will then favor beta-oxidation instead of lipid biosynthesis. Similar to AMPK activation, myoferlin-depleted cells show a marked increase in the phosphorylated form of pyruvate dehydrogenase (PDH). Consistent with this observation, we also observed an increase in the pyruvate dehydrogenase kinase (PDHK1), the responsible kinase for pyruvate dehydrogenase phosphorylation. Increase in the pPDH/PDH ratio reflects a progressive inactivation of the pyruvate dehydrogenase, causing a decrease in the conversion of pyruvate into acetyl CoA. Acetyl CoA produced by this step is usually processed in the citric acid cycle to sustain cellular respiration. This pathway is now at least in part inhibited due to a decrease in mitochondrial function. Biochemically, this situation stimulates a hypoxic state and we therefore sought to verify if HIF-1 $\alpha$  is also up-regulated. Indeed, acute deletion of myoferlin in MDA-MB231 results in increased HIF-1 $\alpha$  protein levels under normoxic conditions.

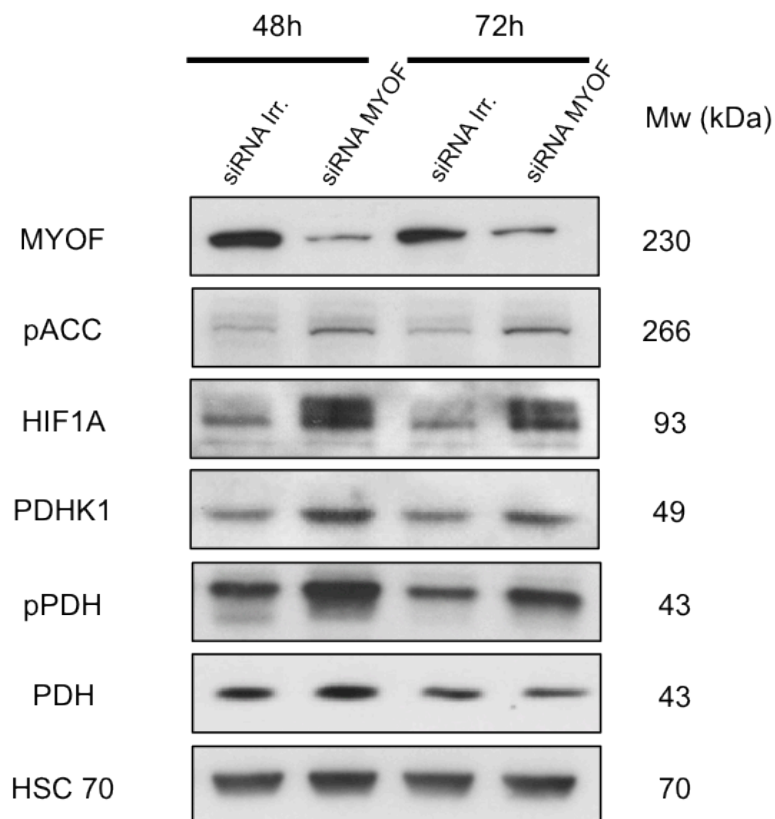


**Figure 22:** Myoferlin silencing results in a metabolic shift towards glycolysis and inhibition of lipid synthesis. Western blot analysis of MDA-MB231 cells shows that myoferlin depletion and resulting AMPK activation leads to an inhibition of lipid synthesis and to decreased pyruvate entry into the TCA cycle. This is respectively evidenced by increase in pACC and pPDH/PDH ratio. Glycolytic shift is further supported by stabilization of the transcription factor HIF1A. HSC70 is used as a loading control.

Lactate accumulation, impairment of mitochondrial function and AMPK activation strongly point at metabolic reprogramming of myoferlin-depleted cancer cells. The salvage mechanism (at least *in vitro*) suggests an overall shift towards glycolysis. We next sought to examine if this potential escape mechanism could be used to selectively target these cells in order to enhance apoptosis.

### **Myoferlin silencing sensitizes cells to drugs targeting metabolism**

Mitochondrial dysfunction generally leads to increase in apoptosis. We therefore evaluated whether loss of myoferlin is associated with apoptosis and cell death. To this end, we have applied a double approach. We have first employed annexin-V/PI staining that distinguishes early and late apoptosis as well as necrosis. The measurement showed that myoferlin-depleted cells displayed a modest increase in early and late apoptosis compared to control cells (**Fig. 23A**). The second approach consisted of measuring the mitochondrial membrane potential, which usually decreases in damaged and is completely absent in non-functional mitochondria. The latter group is found in cells that have either undergone or are undergoing apoptosis. The approach applied here consisted of measuring the ability of the mitochondria to take up and retain tetra-methyl-rhodamine ester (TMRE) [192]. Analogously to the observations made with annexin-V assay, the proportion of cells with fully depolarized mitochondria was higher in myoferlin depleted breast cancer cells (**Fig. 23B**).

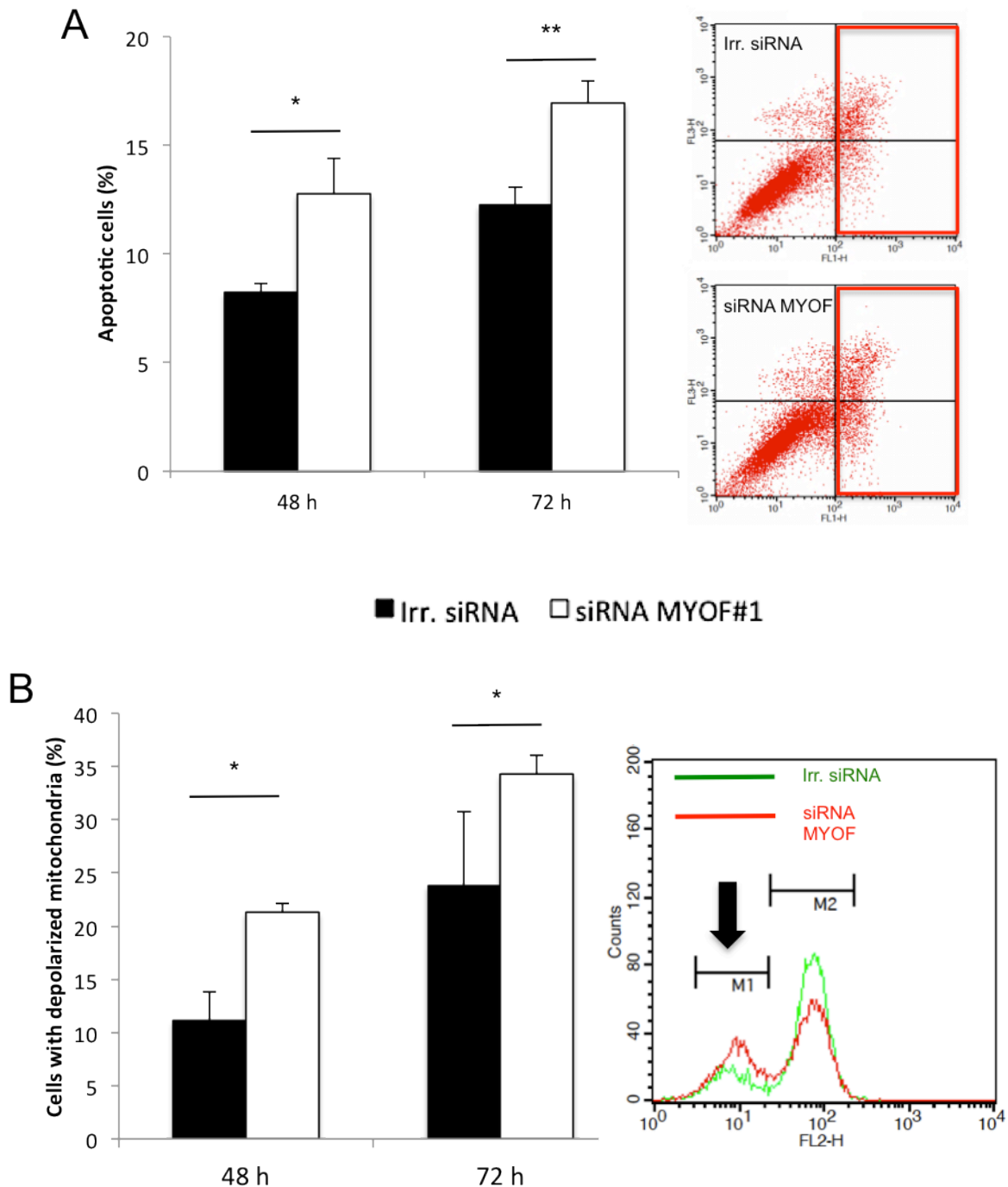


**Figure 23A-B:** Myoferlin silencing induces cell death. A, Apoptosis induction (annexin-V assay) of myoferlin-depleted MDA-MB231 cells measured by flow cytometry. Representative images are given on the right. Early apoptotic cells (annexin V<sup>+</sup>/PI<sup>-</sup>, bottom right) and late apoptotic cells (annexin V<sup>+</sup>/PI<sup>+</sup>, upper right) were summed together to yield a unique value (expressed as percentage) of apoptotic cells. B, Flow cytometry analysis of TMRE accumulation in MDA-MB231. In absence of myoferlin, the number of cells with depolarized mitochondria (right panel, bold arrow) is higher. Error bars indicate SD of means from minimum 3 independent biological replicates. Statistical significance (p) was evaluated using an unpaired Student t-test (\* = p-value $\leq$ 0.05; \*\* = p-value $\leq$ 0.01).

Based on the outlined data, we further hypothesized that cancer cells lacking myoferlin may have adapted their metabolism by activating AMPK and switching to

glycolysis. We further sought to test if blocking AMPK activation or forcing cells to continue through the tricarboxylic acid cycle and oxidative phosphorylation may enhance cell death. The results show that redirecting cell metabolism towards oxidative phosphorylation with dichloroacetic acid, an inhibitor of PDH kinase, significantly enhanced the effect of myoferlin silencing on both apoptosis and mitochondrial depolarization (**Fig. 24A and B**). Furthermore, inhibiting AMPK activation with drosomorphin (compound C) in myoferlin-deficient cells led to an enhanced pro-apoptotic death and to a significant increase in mitochondria depolarization in comparison to control cells (**Fig. 24C and D**).

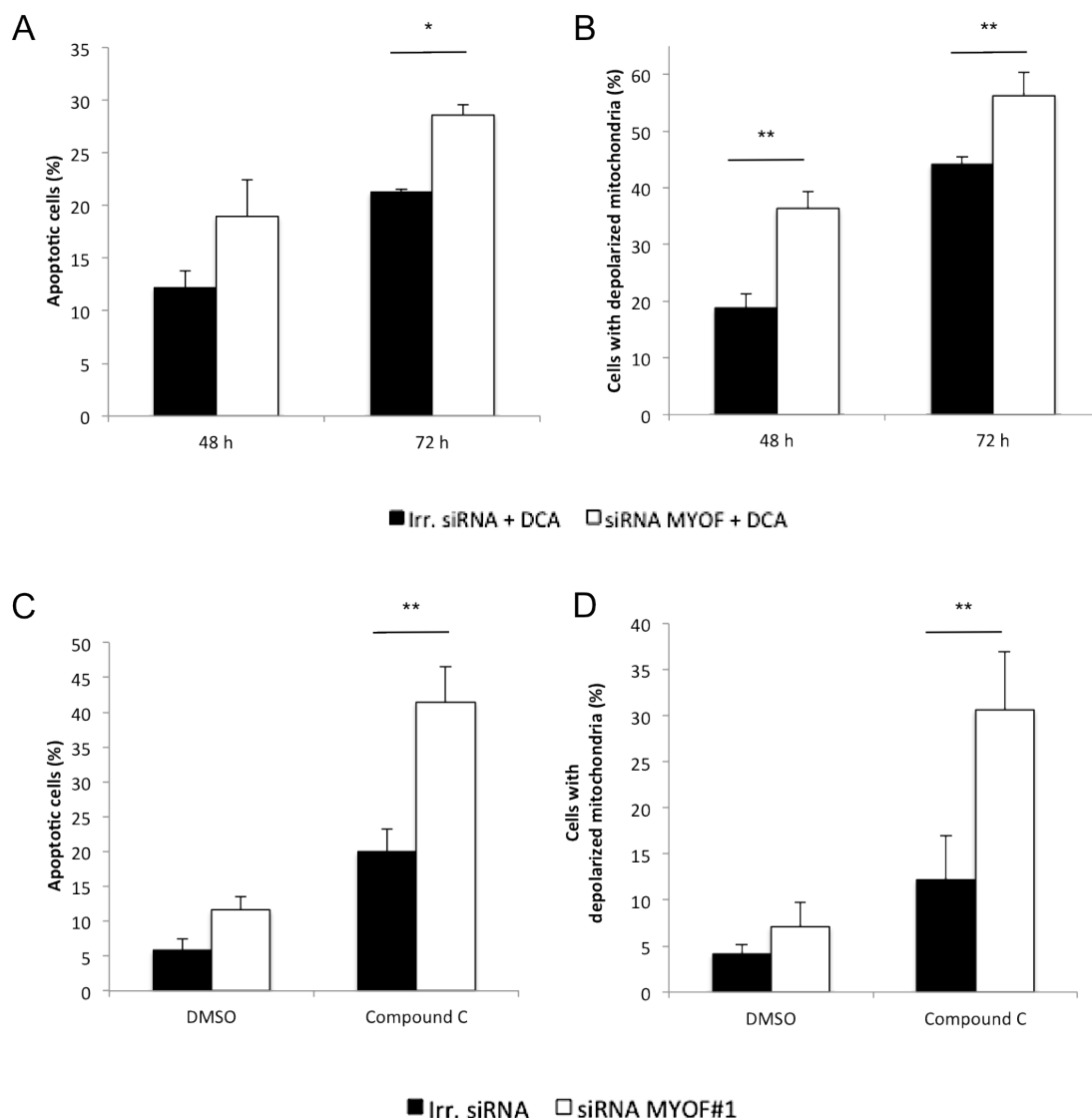


**Figure 24A-D:** Myoferlin depletion sensitizes MDA-MB231 cells to glycolysis and AMPK inhibitors. A, C, Apoptosis induction (annexin-V assay) of myoferlin-depleted MDA-MB231 is enhanced in presence of dichloroacetic acid (A) and Compound C (C). Early and late apoptotic cells were summed together to yield a unique percentage of apoptotic cells. B, D Analysis of mitochondrial membrane depolarization using TMRE in MDA-MB231 cells. DCA (C) or Compound C (D) treatment of myoferlin-depleted cells enhances mitochondrial depolarization. Error bars indicate SD of means from minimum 3 independent biological replicates. Statistical significance: \* = p-value  $\leq$  0.05; \*\* = p-value  $\leq$  0.01.

Taken together, these results strengthen the notion that AMPK activation and the subsequent increase in glycolysis may in part act as compensatory mechanisms to counterbalance the mitochondrial dysfunction induced by myoferlin loss. In order to gain a more significant mechanistic insight into how myoferlin may affect the cell metabolism and mitochondrial function, we have evaluated the structural changes in the cells following myoferlin suppression.

### **Myoferlin colocalizes with endosomal system and trafficking vesicles**

We have previously shown that myoferlin is expressed mainly in the cytosol, where it colocalizes with caveolin, and at the cell membrane of MDA-MB231 cells. Here we further asked the question if myoferlin colocalizes with mitochondria. To test this, we performed co-immuno staining of myoferlin and mitochondria. As shown in **Figure 25**, despite the abundant expression of myoferlin in MDA-MB231 cells, a clear colocalization with mitochondria was not evident.

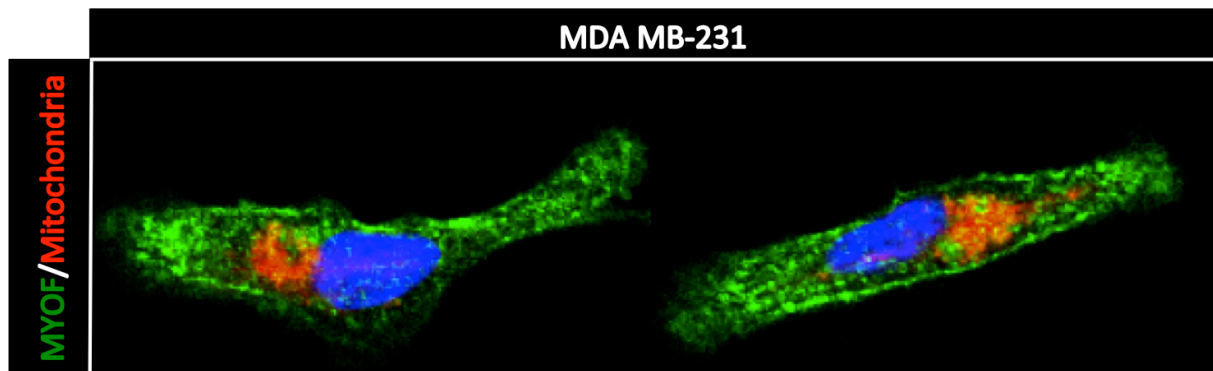


**Figure 25:** Myoferlin does not colocalize with mitochondria. Immunofluorescence analysis of MYOF (green) and mitochondria (red) reveals that myoferlin and mitochondria do not specifically cluster together. Images were accrued at X400 magnification.

In order to further evaluate the precise subcellular localization of myoferlin, we performed an immunogold staining followed by transmission electron microscopy (TEM) analysis. Specificity of the staining was confirmed using MDA-MB231 cells which were stably or transiently transfected with shRNA/siRNA against myoferlin. We could not detect any gold particle in both of these conditions (data not shown). In wild-type cells, staining for myoferlin was mainly located in the cytosol of the cell (**Fig. 26**). The majority of the mitochondria observed were negative for myoferlin. However, in some occasions, a punctual signal was observed in close vicinity of the organelle membrane, precluding an absolute exclusion of the possibility that myoferlin may be a constituent of mitochondria (**Sup. Fig. 2**).

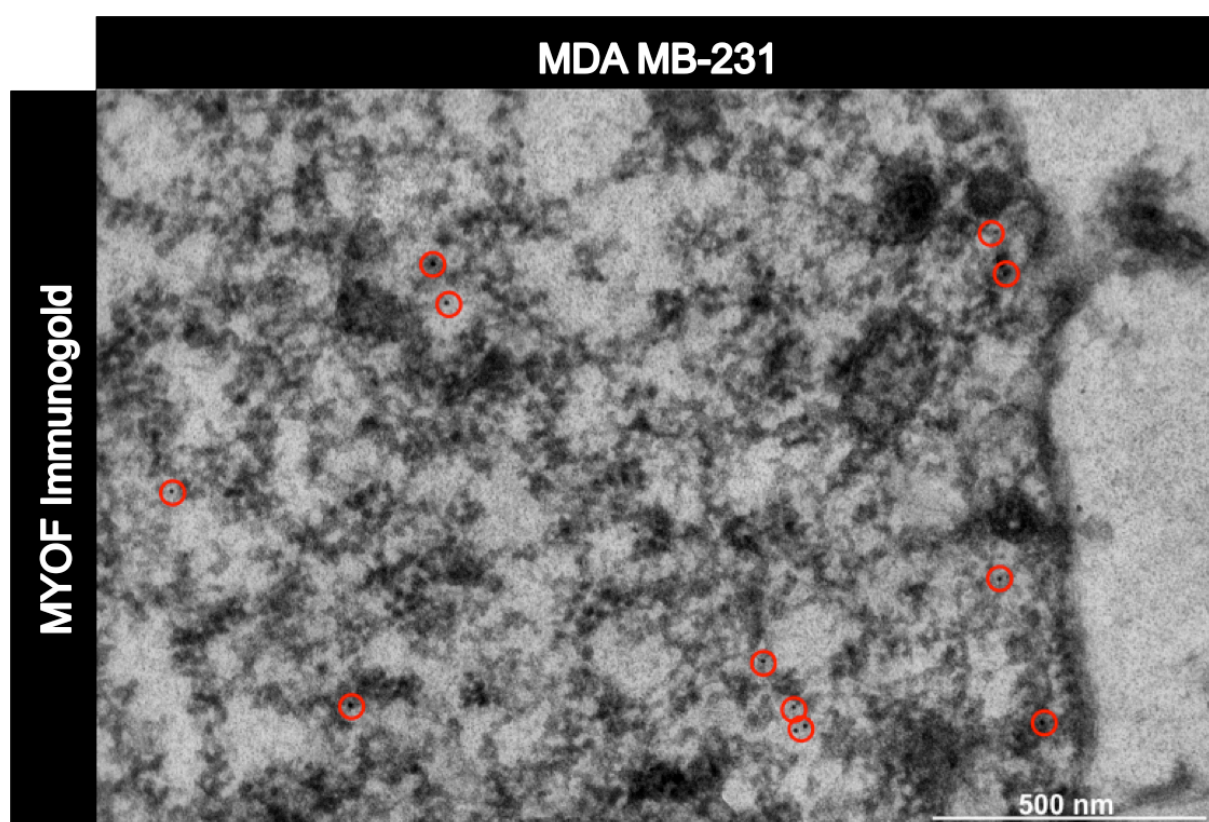


**Figure 26:** Myoferlin is highly expressed in the cytosol of MDA-MB231 breast cancer cells. Immunogold & TEM performed with an anti-myoferlin antibody shows an abundant cytosolic staining.

Of the significantly labeled section of the cell noteworthy is the entire endosomal system which was strongly positive for myoferlin. Myoferlin was present in both early- and late-endosomes as well as their potential anchor site on the plasma membrane, strengthening the role of myoferlin in membrane fusion and repair processes (**Fig 27A**). Surprisingly, some myoferlin signal was detected in the nucleus and the nucleolus of MDA-MB231 (**Fig 27B**).

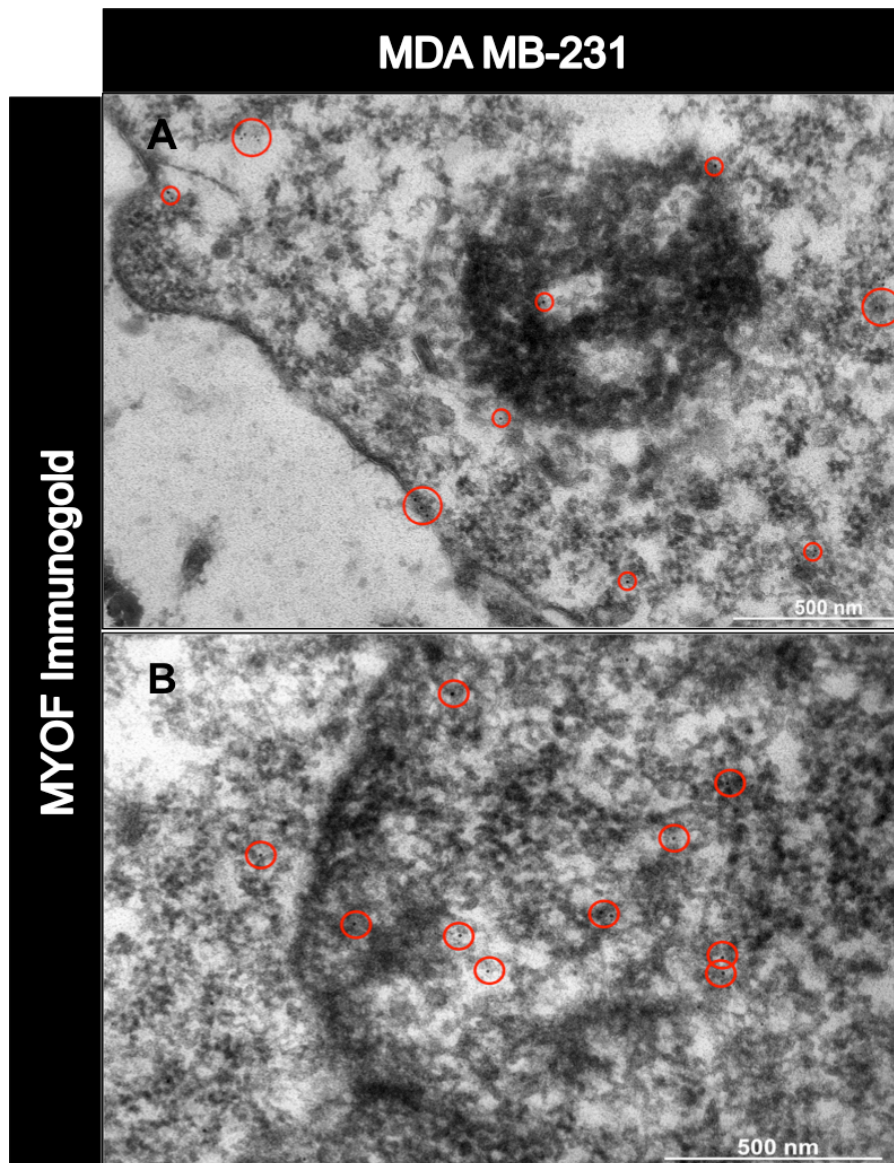


**Figure 27A-B:** Myoferlin subcellular localization in MDA-MB231 breast cancer cells. A, TEM analysis of immunogold myoferlin staining highlights significant colocalization of the protein with the endosomal system. Different types of endosomes as well as plasma membrane were strongly positive for myoferlin. B, Myoferlin is present in the nucleus of the breast cancer cells, especially in interchromatin regions.

Expectedly, myoferlin was further detected in intracellular caveolae (**Fig. 28A and B**) and in clathrin coated vesicles (**Fig. 28 C and D**), confirming our previous results obtained by immunofluorescence (**Fig. 12A and 13A**). Caveolin is well known to be involved in

metabolic regulation of both stromal and cancer cells. In addition, we have observed in our EGFR study that myoferlin silencing affects caveolin function with respect to EGFR signaling in MDA-MB231 cells. We therefore asked the question if impaired association between myoferlin and caveolin could in part explain the metabolic consequences observed upon myoferlin silencing.

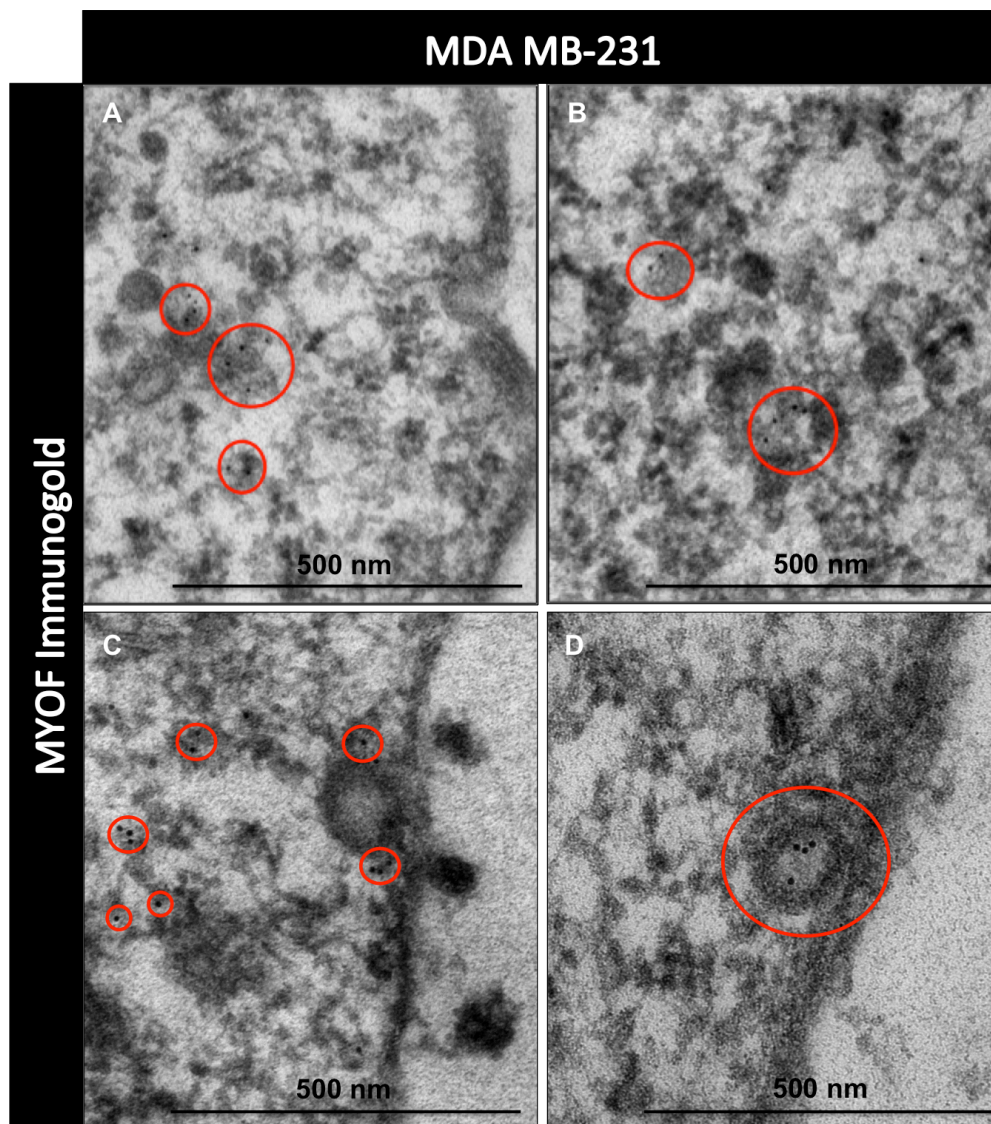


**Figure 28A-D:** Myoferlin is present in caveolae and clathrin vesicles of MDA MB-231 breast cancer cells. A-D, TEM following immunogold staining reveals myoferlin expression in both caveolae (A,B) and clathrin coated vesicles (C,D).

### Myoferlin interacts with caveolin-1 in caveolae and is essential for caveolin oligomerization

To test whether caveolin-1 and myoferlin are able to interact together, we next performed an immunoprecipitation of myoferlin followed by Western blot against caveolin-1. Results in **Figure 29A** show that caveolin monomers, detected at ~21 kDa, do not precipitate with myoferlin. However, high molecular weight complexes of caveolin were trapped by the myoferlin antibody, suggesting that myoferlin is more likely to interact with caveolin oligomers rather than with the monomeric form of the protein. High-order oligomers of caveolin, consisting of 14-16 monomers, are thought to facilitate the invagination and release of caveolae into the cytoplasm [193]. Phosphorylation of caveolin on residue Y14 has been reported to cause destabilization of these high molecular weight complexes [194]. Since we have previously demonstrated that silencing of myoferlin affects the organization of caveolin into oligomers (**Fig. 14**), we hypothesized that this effect could be due to an impaired phosphorylation of caveolin in absence of myoferlin. Western blot analysis of transiently transfected MDA-MB231 cells revealed that phosphorylation of the caveolin monomer was not affected by myoferlin silencing. In contrast to this, the phosphorylated level of the caveolin oligomers was dramatically decreased in myoferlin-silenced cells in comparison with the control cells (**Fig. 29B**). Thus, accumulation of caveolin oligomers upon myoferlin removal is directly linked to the decrease of caveolin phosphorylation.

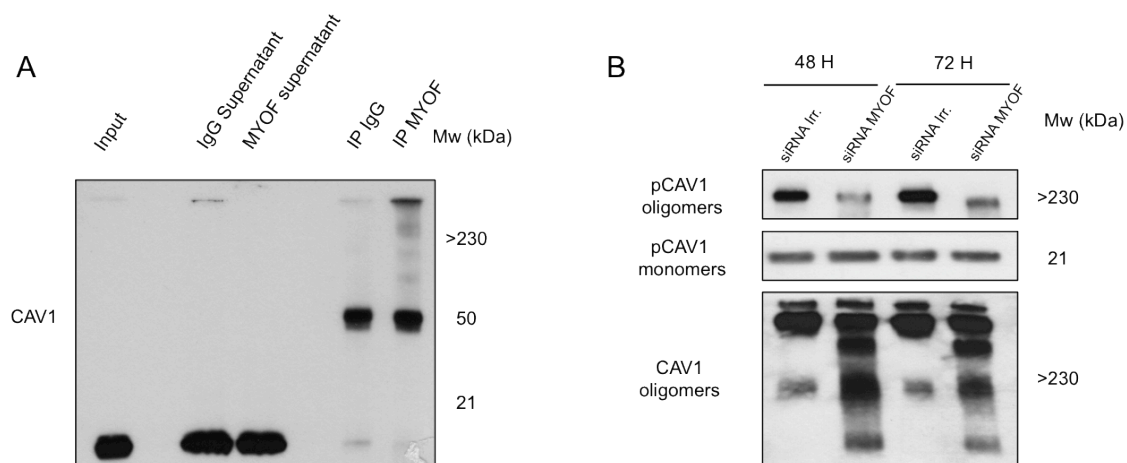


**Figure 29A-B:** Myoferlin interacts with oligomerized caveolin-1. A, Immunoprecipitation of myoferlin followed by western blot analysis of caveolin suggests that myoferlin interacts with high molecular weight oligomers. B, Western blot analysis of caveolin in non-denaturing conditions (with or without myoferlin depletion) shows high-molecular weight complexes corresponding to caveolin homomultimers. In absence of myoferlin, these complexes are mainly composed of the non-phosphorylated form of the protein.

### Myoferlin silencing impairs microvilli formation and endosome traffic

While exploring the ultrastructural changes in the myoferlin-depleted cells, we noticed that cells lacking myoferlin showed less microvilli than the control cells (**Fig. 30A and B**). In control cells, we readily observed enlarged lysosomes which may have resulted through fusion of several late-degrading vesicles (**Fig. 30C**). This was not observed in myoferlin-depleted cells, where overall less lysosomes were present and of generally smaller size (**Fig. 30D**).

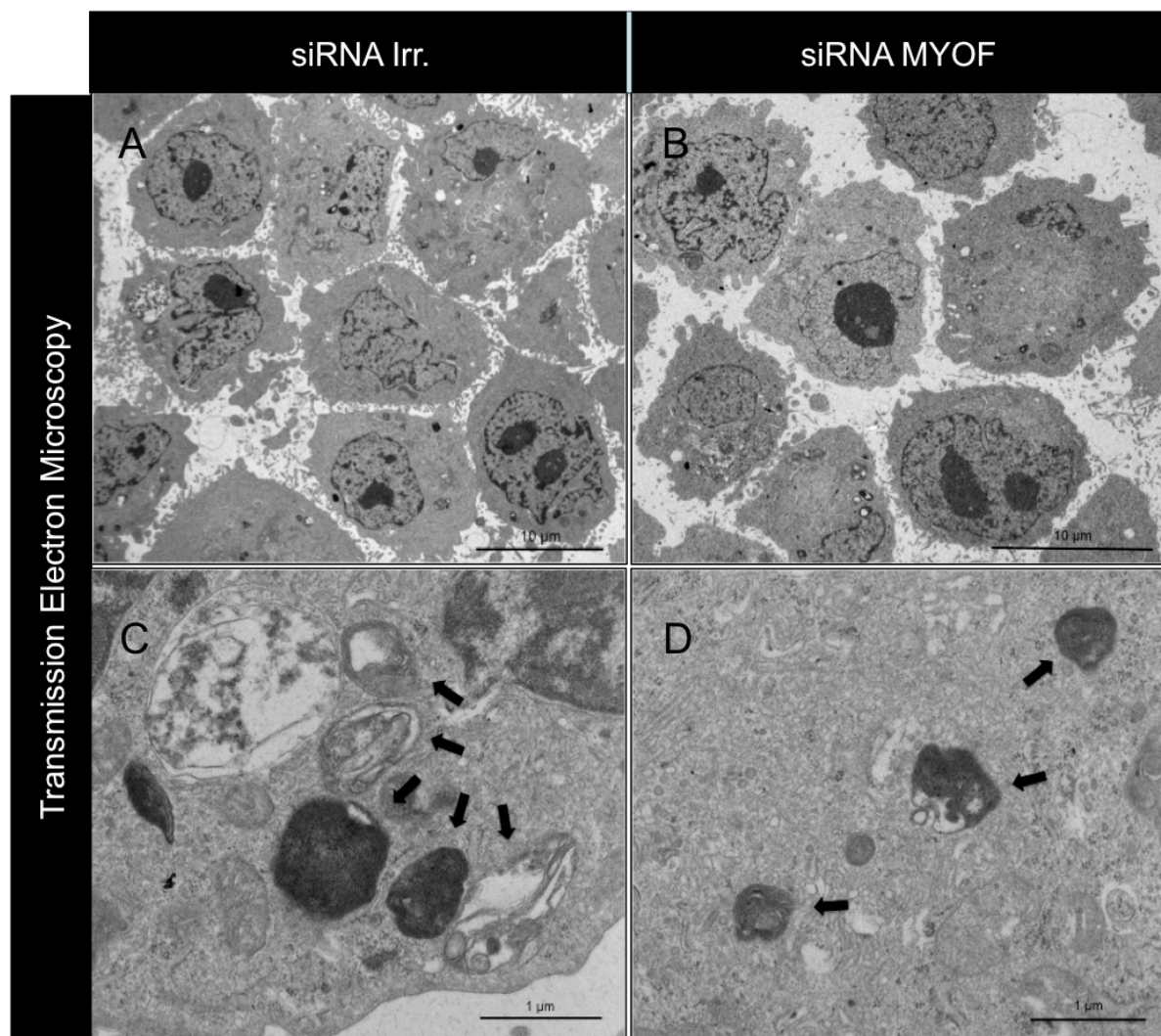


**Figure 30A-D:** Myoferlin depletion causes reduction in number of microvilli and smaller lysosomes. TEM analysis of myoferlin-deficient cells. Shown are MDA-MB231 breast cancer cells. A, B, Microvilli. C, D Lysosomes.

We further focused our attention on two types of small intracellular structures: the caveolae and the clathrin coated vesicles. In cells lacking myoferlin, a significant accumulation of caveolae next to the plasma membrane was observable (**Fig. 31D**). This localization suggests that these vesicles are not able to fuse with the plasma membrane and

are therefore trapped in its vicinity. Concerning the clathrin-coated vesicles, their number did not seem to be different between the two conditions. However, majority of these vesicles were “closed” in absence of myoferlin (**Fig. 31B and D**), whereas an increased number of open vesicles, fusing with the membrane, were readily observable in the control cells (**Fig. 31A and C**). A semiquantitative evaluation indicated that 75% of the clathrin vesicles are found in a “closed state” in myoferlin-depleted cells, while 75% of vesicles are in “open state” in control cells.

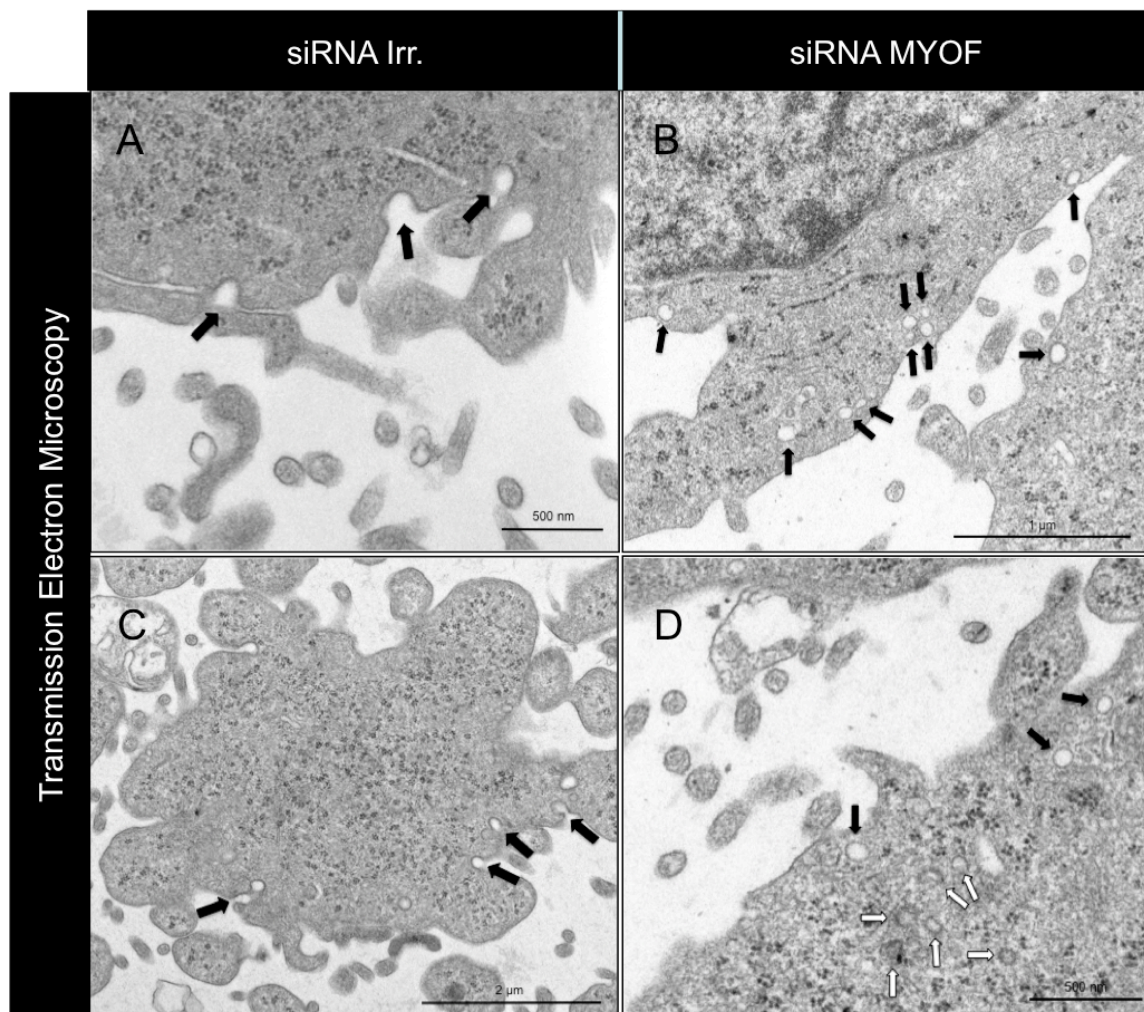


**Figure 31A-D:** Myoferlin silencing results in accumulation of vesicles in the vicinity of the plasma membrane. Control MDA-MB231 cells display a high number of fusing clathrin coated vesicles (A and C, black arrows) whereas these vesicles were observed accumulating nearby the membrane in a closed state in myoferlin-silenced cells (B and D, black arrows). Cells lacking myoferlin also display an important accumulation of caveolae in the vicinity of the membrane (D, white arrows).

### AMPK activation following myoferlin silencing is caveolin dependent

In order to further evaluate the contribution of caveolin to the metabolic phenotype observed in absence of myoferlin, we co-silenced myoferlin and caveolin in MDA-MB231 cells (**Fig. 32**). Expectedly, myoferlin knockdown induced a clear activation of AMPK, the overexpression of HIF-1 $\alpha$  and the down-regulation of cytochrome c oxidase. Caveolin silencing alone did not affect the levels of these proteins. However, co-silencing of caveolin and myoferlin specifically abolished the overexpression of p-AMPK and HIF-1 $\alpha$ , restoring their expression levels but had no effect on COX1 decrease. These results suggest that caveolin-1 plays an important role in the AMPK-mediated metabolic response to the loss of myoferlin, but not on its impact on mitochondrial function.

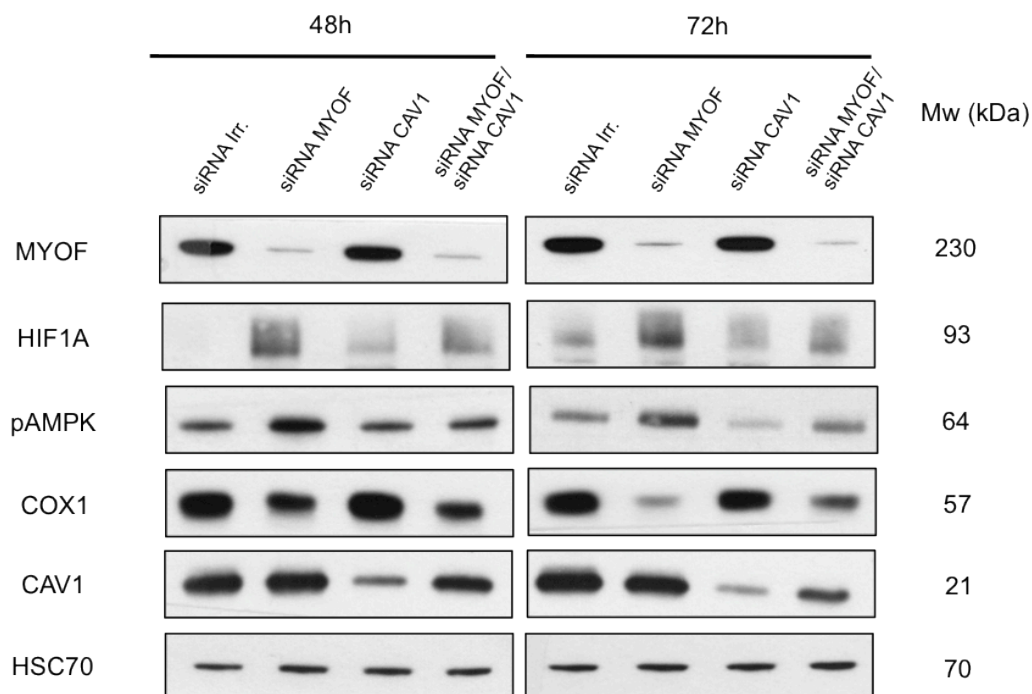


**Figure 32:** Caveolin-1 regulates AMPK following the loss of myoferlin. Western blot analysis of co-transfected MDA-MB231 cells shows that concomitant silencing of myoferlin and caveolin abolishes both the activation of AMPK and stabilization of HIF-1 $\alpha$ . Decrease in COX1 is not affected by caveolin-1 silencing.

### Myoferlin silencing reduces tumor growth and metastasis *in vivo*

Myoferlin-depleted and control cells (both shRNA based constructs) were engrafted in NOD-SCID mice and the tumor volume was measured on a weekly basis for a period of 4 weeks. In the first week no measurement was performed because the tumors were too small in size. The results show that myoferlin-silenced tumors grew at a similar rate as the control ones, however the size difference between the both remained significantly different (**Fig. 33**). The volumes of control tumors were approximately 35% larger than the ones in myoferlin silenced tumors. Once control tumors reached a defined volume ( $\pm 250 \text{ mm}^3$ ), tumors (both control and shMYOF) were surgically removed and the mice were monitored for 6 weeks for the development of distant metastases.

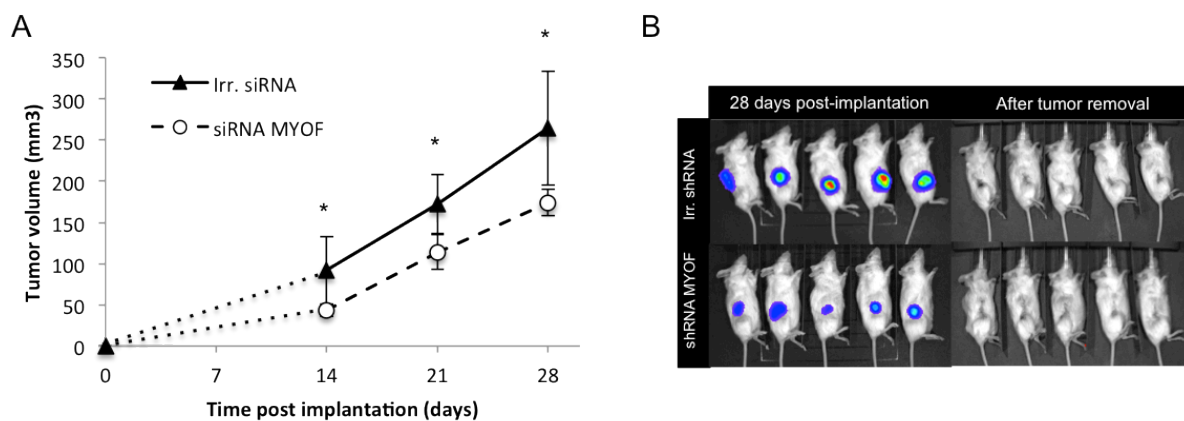


**Figure 33A-B:** Myoferlin decreases tumor growth *in vivo*. A, Volumes ( $\text{mm}^3$ ) of primary tumors were measured weekly following the xenografting. Dotted line is an extrapolation – no volume measurements were performed during this period. B, Bioluminescence imaging of control and shMYOF xenografts at day 28 post tumor engraftment. Error bars indicate SD of means from 10 animals/condition/experiment. A representative experiment is shown. Statistical significance: \* =  $p\text{-value} \leq 0.05$ .

Histological evaluation of dissected tumors revealed significant differences between the control and myoferlin-depleted xenografts. Control tumors displayed a large necrotic core which was completely absent in the myoferlin silenced xenografts (**Fig. 34A**). Furthermore the edges of the myoferlin silenced tumors were clearly delineated from the surrounding stroma. This was not the case in control tumors where cells infiltrating muscle and fat tissue were readily observable. To confirm this we used vimentin staining which specifically stained cancer cells (**Fig. 34B**). Interestingly, we observed that control tumors in contrast to myoferlin depleted ones contained regions reassembling lipid droplets. We confirmed this observation by employing Oil-Red-O staining (**Fig. 34C**).

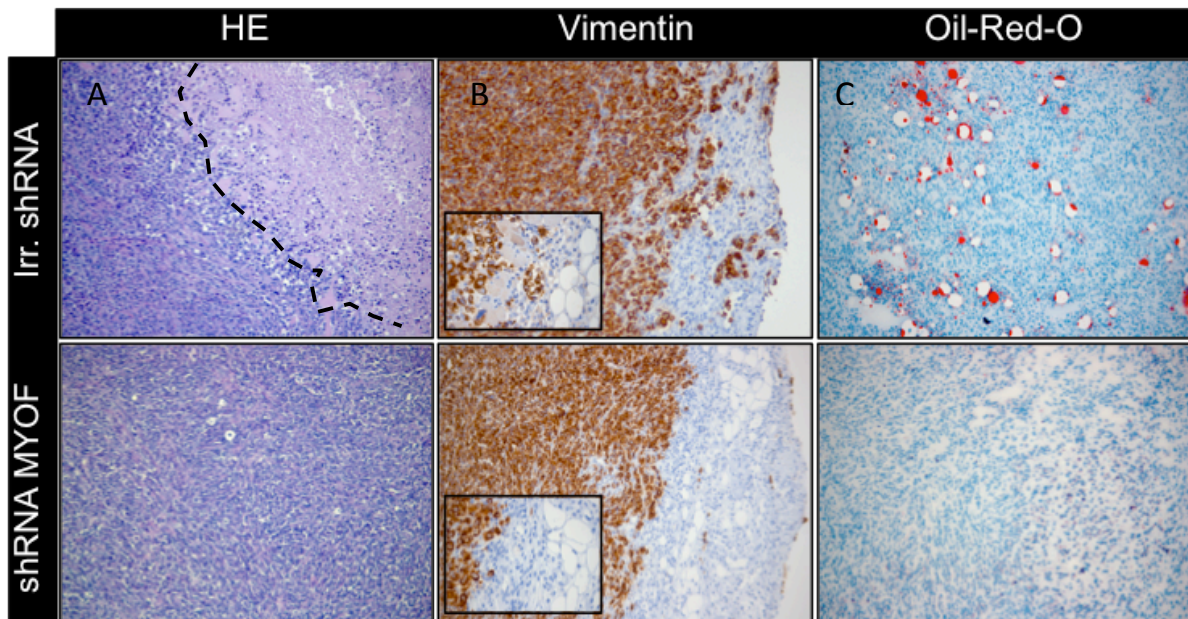


**Figure 34A-C:** Myoferlin depletion reduces necrosis, invasion and lipid accumulation *in vivo*. A, Representative hematoxylin and eosin (H&E) staining of formalin-fixed paraffin-embedded (FFPE) MDA-MB231 tumors. Dotted line: control xenografts displayed a necrotic region in the center of the tumor. B, Vimentin staining of FFPE tumor xenografts. Myoferlin-depleted tumors are well delimited and non-invasive whereas control tumors invade the surrounding muscle and fat tissues. C, Oil-Red-O staining of fresh-frozen xenograft tumors highlights loss of lipid droplets (in red) in myoferlin-depleted condition. All images were taken at 100X magnification. Zooms of invasive regions were performed at 400X magnification.

Following the histological observations, we next sought to examine whether cells isolated from the xenograft tumors show any difference in mitochondrial respiration. As shown in the **Figure 35**, myoferlin-deficient cells isolated from tumors showed a  $\approx 20\%$  decrease in electron transport chain capacity.

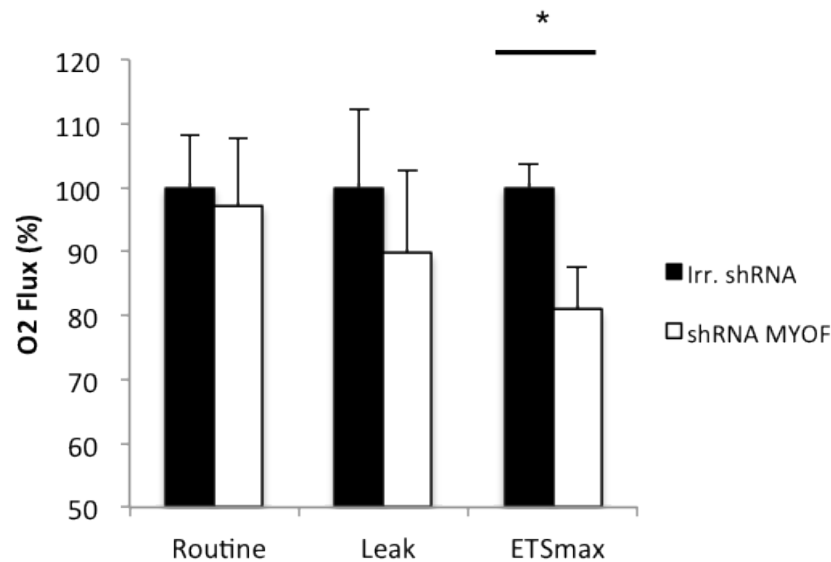


**Figure 35:** Loss of myoferlin induces mitochondrial dysfunction *in vivo*. Oxygen consumption of isolated cancer cells from xenografted control or myoferlin-silenced tumors. Cellular respiration was measured in culture medium (Routine), in presence of oligomycine (Leak) or after uncoupling with FCCP (ETSmax). All values were corrected for residual oxygen consumption obtained in presence of rotenone. For further details refer to Materials and Methods. Error bars indicate SD of means from minimum 3 animals. Statistical significance (p) was evaluated using an unpaired Student t-test (\* = p-value $\leq$ 0.05)

Following the evaluation of myoferlin impact on primary tumor growth, we next assessed the importance of this protein in the process of metastasis development. A bioluminescent signal in lung region was detected in control mice shortly after the operation, while this was not the case for the cohort with myoferlin-silenced tumors. Six weeks post-operation, majority of control mice developed overt lung metastasis and exhibited positive lymph nodes as assessed by a strong bioluminescent signal (**Fig 36A**). In contrast to this, in myoferlin-silenced tumors only few mice showed a weak signal in the chest region. At 6 weeks post surgery, the mice were sacrificed and the lungs were subjected to further histological evaluation. We evaluated serial section of the entire lung for tumoral foci and as evidenced by positive for vimentin staining. The results show that control mice had indeed developed large metastatic foci (**Fig. 36B and C**). Lungs from mice with myoferlin-silenced tumors were mainly negative for vimentin staining. Only few single cancer cells were detected and we did not observe any foci of more than 20 cells.

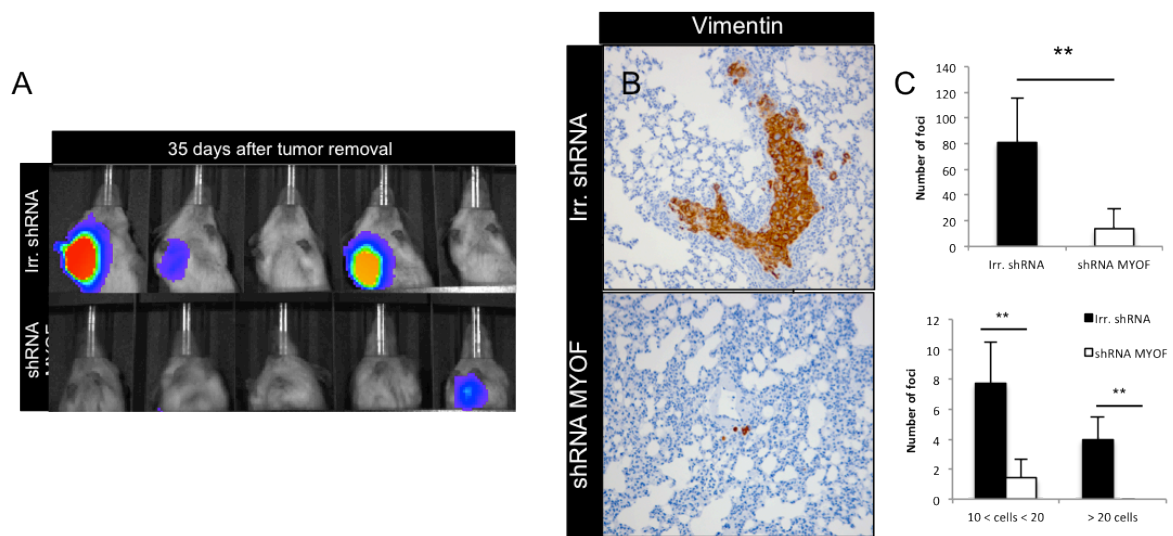


**Figure 36A-C:** Myoferlin silencing reduces lung-metastasis formation. A, Bioluminescent imaging of xenografted mice. Positive axillary lymph nodes and lung metastases resulted in higher bioluminescent signal in the control animals. B, Vimentin IHC in lungs shows that metastasis formation is significantly less developed in animals previously xenografted with myoferlin-silenced tumors. Images were accrued at 100X magnification. C, Quantification of lung metastatic foci. Statistical significance (p): \*\* = p-value ≤ 0.01).

# **Discussion**

Breast cancer is a multifaceted disease comprising several cancer subtypes, which are fundamentally different from each other. Owing to seminal gene-expression profiling studies [195, 196] we distinguish basal-like (triple-negative), luminal A, luminal B (both HR+), normal-like and HER2-like (HER2+/HR-) subtypes. Today we do not yet understand the exact origins of these different breast cancer subtypes, however we know well that they are associated with major differences in tumor invasiveness, metastatic behaviors and ultimately patient outcome. In the current work we describe myoferlin, a novel protein of relevance in cancer, which is expressed in all breast cancer subtypes. We report here for the first time that myoferlin expression significantly correlates with patient outcome. Luminal A and luminal B patients with high myoferlin expression have a better clinical prognosis. Patients with the triple-negative and HER2+ breast cancer subtypes have poor prognosis when expressing high myoferlin levels. This dual behavior is surprising and to our knowledge we have not observed similar for any other tumor-associated proteins. Although we are currently unable to explain this myoferlin behavior, the current study shows that myoferlin is broadly involved in cancer and may therefore assume different roles in varying tumor types. For example, triple-negative cancers are known to exhibit high EGFR [197] and caveolin-1 [198] expression. Furthermore, metabolic switch from oxidative phosphorylation to glucose metabolism has been shown relevant for stem-cell and EMT phenotype in basal-like breast cancer [199]. We show here that myoferlin assumes critical role in regulating EGFR function, caveolin oligomerization and metabolism – all possibly relevant for a significant negative correlation with patient outcome in triple-negative breast cancer. Along these lines, we discuss below myoferlin involvement in each of these processes in particular.

EGFR is a receptor commonly associated with human tumors. Ligand binding and dimerization causes autophosphorylation of the intracytoplasmic domains and activation of the intracellular tyrosine kinase. Activated EGFR (pEGFR) stimulates a number of different signal transduction pathways, which play important roles in various cellular processes such as cell proliferation and migration. Our study shows for the first time that myoferlin is overexpressed at the protein level in all human breast adenocarcinomas analyzed and that myoferlin knockdown in breast cancer cells interferes with EGF-induced cell migration and EMT. Moreover, our data designate an unexpected link between myoferlin and EGFR in breast cancer cells, where myoferlin intervenes in the control of EGFR activity and signaling. Consistent with the previous report of Bernatchez and colleagues [56] in endothelial cells, we show that myoferlin colocalizes with caveolin in breast cancer cells, both in basal condition and upon EGF stimulation. As the major component of membrane caveolae, caveolin

interacts with a variety of partners such as integrins and RTK receptors and functions as a regulatory platform for their respective postligand signaling . Because of the frequent deletion of caveolin gene in cancers, including breast cancer, caveolin has been considered as a potential tumor suppressor [200]. Caveolin scaffolding has been previously shown to induce EGFR sequestration in tumor cells. In particular, Lajoie and colleagues [201] propose that the sensitivity of cancer cells to EGF stimulus can be controlled by 2 membrane domains: on one hand, caveolin that concentrates EGFR and blocks it from signaling and on the other hand, the galectin lattice that holds EGFR at the membrane and favors its mitogenic signaling. Despite the prevailing evidence that caveolin acts as a tumor suppressor, it is noteworthy that its overexpression has been also associated with the metastatic potential of lung and prostate cancer cells [202-204]. This study provides an answer to these apparently contradictory findings by pointing for the first time to myoferlin as an important regulator of caveolin scaffold in breast cancer cells. We show that myoferlin suppression results in enhanced clustering of caveolin oligomers in lipid-raft microdomains as well as the emergence of smaller oligomers of aberrant size. The literature suggested that this disorganization is caused by a decreased phosphorylation of caveolin oligomers. In fact, caveolin phosphorylation causes destabilization of high molecular weight oligomers by inducing changes in tertiary structure of the protein [194]. Therefore, phosphorylation of the protein, usually by Src kinases, tightly controls vesicle interactions with the plasma membrane. In our case, the decrease in phosphorylation level of caveolin oligomers observed following myoferlin depletion suggest an excessive stabilization of oligomers. This hypothesis is in agreement with the accumulation of caveolae-type of vesicles nearby the plasma membrane as observed in electron microscopy. This observation is of particular relevance for the subsequent consequence of myoferlin depletion, including the ones affecting metabolism. With respect to EGFR, our data notably show that myoferlin (but not caveolin) depletion is sufficient to block its degradation and to stop the attenuation of EGFR phosphorylation upon EGF stimulation. We found that in breast cancer cells myoferlin depletion does not affect EGFR endocytosis rate, suggesting that this protein is dispensable at this early step. As the internalization proceeds, the cargo (in this case EGFR) needs to be targeted in the cell for activating downstream effectors and subsequently to be neutralized via proteasomal and lysosomal degradation [81]. Previous studies suggest that proteasomal degradation precedes and is necessary for the lysosomal targeting of the receptor [205-207]. A recent multiparametric image analysis study reveals a predominant role of caveolin in endosomal progression rather than internalization of EGFR [208]. The immunogold staining and TEM confirmed that

myoferlin is strongly expressed in clathrin vesicles and in caveolae/lipid rafts, but also in other components of the endosomal system (early and late endosomes and endolysosomes). As a consequence, silencing myoferlin severely affects vesicular trafficking, notably preventing the formation of high sized lysosomes (resulting from the fusion of multiple degrading vesicles) and leading to an accumulation of small endocytic vesicles at the vicinity of the plasma membrane. Aberrant vesicle trafficking, especially degrading vesicles, has already been suggested in the context of myoferlin-dependent RTK regulation (IGFR1, VEGFR2, TIE2), leading to increased degradation of the receptors [44, 54, 55].

Our results indicate that permanent phosphorylation of EGFR in cells lacking myoferlin has detrimental effects on the EGFR-controlled biologic processes. The length of signaling has an impact on which cellular processes are activated downstream. Similar has been reported with Raf kinase [209], where high-intensity Raf signal causes cell-cycle arrest; this is in contrast to the normally assumed proliferation function. Recently, Rush and colleagues [210] have shown that high endosomal accumulation of activated EGFR induces apoptosis in MDA-MB468 cells. The authors have used monensin to block endosomal trafficking of EGFR. As EGFR accumulation and activation pattern shown in the current study largely exceeds the magnitude of EGFR accumulation shown previously [210], it is reasonable to propose that cell death is probably the terminal outcome of myoferlin depletion.

One of the most striking biologic effects observed here was the inability of breast cancer cells to respond to EGF-stimulus to migrate (MDA-MB231 and MDA-MB468) or undergo EMT (MDA-MB468). Li and colleagues [60] reported recently that MDA-MB231 underwent a spontaneous reverse EMT in the absence of myoferlin. However, similar data published by the same authors elsewhere [211] partially dispute their recently published results (e.g., vimentin levels after myoferlin depletion; ref. 14). We were unable to observe similar effects in MDA MB231 cells as shown in ref. 14; neither cell attachment nor vimentin levels are affected upon myoferlin silencing (detailed in Supplementary Data, **Sup. Fig. 4**). Interestingly, Li and colleagues [60] and Eisenberg and colleagues [59] both showed that short hairpin RNA (shRNA)-mediated myoferlin depletion impairs MDA-MB231 cells' invasion; however, it has no effect on cell migration or proliferation. Our invasion and proliferation data are in agreement with the literature [59, 60]. However, opposite to the previous findings, we show that myoferlin silencing exhibits a strong inhibitory effect on the ability of MDA-MB231 cells to migrate. Although unable at this stage to explain for these discrepancies, we think that experimental differences and adaptation processes when using shRNAs [59, 60] in contrast with siRNAs (present study) might play an important role. First,

previous studies [59, 60] did not use any coating of Transwell inserts when conducting migration experiments; we have used denatured protein matrix coating (gelatin) to provide environment for the cells to attach and subsequently migrate through the insert. Second, adaptation processes may arise with stable transfected cell lines, which in turn may mask the true phenotype [212, 213]. Finally, recent studies from the same group suggest that cells lacking myoferlin changed their migratory phenotype from single to collective migration [61].

We observed that silencing of myoferlin in MDA-MB231 cells leads to an accumulation of lactate in the culture medium of the cells grown *in vitro*. This increased production of lactate correlates with a decrease in mitochondrial activity of myoferlin-silenced cells, suggesting that an important change occurs in their metabolism. Following this initial observation, we have shown here for the first time that myoferlin silencing decreases cellular oxygen consumption and ATP levels. This is accompanied by a general decrease in ROS production and down-regulation of important members of respiratory chain. Keeping this in mind, we have asked the question how myoferlin may modulate mitochondrial function. Our data suggest that myoferlin does not colocalize with mitochondria, nor we are aware of any proteomic datasets which describe myoferlin as a mitochondrial protein. These data suggest that the mitochondrial function is probably indirectly affected by myoferlin depletion. One strong indication of how this may happen comes from the TEM results. As mentioned above, myoferlin was found abundantly expressed in every compartment of the endosomal system and myoferlin depletion resulted in major impairment of vesicle trafficking. The latter is key to receptor internalization (as shown here with EGFR) but is also relevant for nutrient uptake and in particular fatty acids and cholesterol levels in the cell. Impairment of metabolite trafficking will inevitably affect mitochondria, which are extremely sensitive to minor changes in metabolites. Trafficking vesicles, especially caveolae are enriched in sphingolipids and cholesterol, have an essential role in regulating cell metabolism via regulation of lipid trafficking and cholesterol transport between organelles [214, 215].

Recent study by Bosch et al. demonstrated that caveolin-1 regulates mitochondrial membrane cholesterol levels that in turn can affect mitochondrial function [115]. In absence of CAV1, cholesterol accumulates in mitochondrial membrane, reducing its fluidity, and leads to the organelle's dysfunction. At the cellular level, CAV1-deficient cells rely mainly on glycolysis and become highly susceptible to apoptosis when the availability of glucose is reduced (using 2-DG) or when oxidative phosphorylation is stimulated (using DCA). The phenotypic effects observed by Bosch et al. are reminiscent of the ones we observe when we silence myoferlin in MDA-MB231 cells: an altered mitochondrial function which leads to an

increase in apoptosis, despite a compensatory increase in glycolysis. Mitochondrial dysfunction and apoptosis are exacerbated when we shift the glucose metabolism to OXPHOS with DCA treatment. Therefore, an analogy between specialized roles for myoferlin similar to what is observed for caveolin is tempting and should be further explored.

The current work shows that in absence of myoferlin, the PI3K/AKT signaling pathway is activated, and this effect is reinforced under EGF stimulation. PI3K/AKT pathway is commonly activated in glycolytic tumors and will result in decreased mitochondrial metabolism in favour of glycolysis [216]. Therefore, aberrant activation of this pathway through defects in endosomal trafficking of EGFR represents a possible way how myoferlin could regulate mitochondrial function. The current study shows that myoferlin-deficient cells activate the AMPK, which is the kinase that regulates energy homeostasis. Lactate accumulation and impairment of mitochondrial function following myoferlin depletion suggest that the cells will reprogram their metabolism mainly towards glycolysis that is the only nutrient available in excess *in vitro*. The observation of the ongoing Warburg effect is further evidenced by inhibition of the pyruvate dehydrogenase complex (PDH) and stabilization of the hypoxia inducible factor 1-alpha (HIF-1 $\alpha$ ). Increased phosphorylation of the regulatory enzyme acetylCoA carboxylase suggests that fatty acid oxydation may also be enhanced in myoferlin-deficient cells.

A recent study, focusing on the metabolic adaptation of AMPK-knockout mice, demonstrated that AMPK negatively regulates the Warburg effect, and that loss of AMPK enhances tumor growth via HIF-1 $\alpha$  mediated increase of glycolysis [178]. However rapid inhibition of PDH by AMPK has been demonstrated to cause induction of the Warburg effect in cancer cells under nutrient deprivation condition [182]. This effect was further coupled to a reduced mitochondrial oxidative phosphorylation and a decreased sensitivity to apoptosis of HeLa cells. In the current study, the resulting phenotype in absence of myoferlin, featuring impaired vesicular trafficking, is comparable to a situation of nutrient deprivation [214]. Therefore it is not far reached to assume that activation of AMPK and increased Warburg effect are initial adaptive measures for cancer cell to escape apoptosis. Therefore, blocking this rescue mechanism by forcing the cells to produce energy through oxidative phosphorylation or by inhibiting AMPK phosphorylation significantly increases cell death. AMPK-mediated increase in glycolysis is generally considered to counteract increased oxidative stress [217]. In our case, we have found that cellular ROS production was decreased in myoferlin-deficient cells. We believe that this decrease in ROS production reflects the general decrease of mitochondrial activity in cancer cells. Measuring ROS production at

earlier timepoints would therefore be helpful to determine whether AMPK activation in absence of myoferlin is mediated by a transient ROS accumulation.

The present data highlight that AMPK activation and subsequent metabolic shift to glycolysis are mediated by caveolin-1. We demonstrated this through co-silencing of myoferlin and caveolin-1, which leads to a decrease in AMPK activation and HIF1 $\alpha$  stabilization. Similar to these findings, recent data showed that deletion of caveolin-1 significantly alters AMPK activation which is induced by fasting/cold treatment in mouse brown adipose tissue. This is preventing the subsequent activation of  $\beta$ -oxidation that normally occurs under these conditions [218]. Links between caveolin-1 and AMPK have further been reported in endothelial cells, where the group of Vavvas showed that oxidative-stress induced phosphorylation of caveolin-1 is inhibited by AMPK through peroxiredoxin [219]. Interestingly, we also observe a situation where high levels of activated AMPK correlates with low levels of phosphorylated caveolin-1 oligomers. Taken together, these results underline a potential interaction between these two proteins in stress situations.

Using murine *in vivo* studies, we demonstrate that myoferlin silencing in cancer cells reduces tumor growth in a model of breast cancer. Concomitant studies on murine lung cancer [62] and on human breast cancer [61] also strengthen the important role of myoferlin in tumor progression. In the latter, the authors reported that tumors lacking myoferlin were smaller, well delineated, homogeneous and less invasive. Our results are in agreement with these findings and in addition, we show that control tumors exhibit lipid droplets positive to Oil-Red-O staining, which is not the case in myoferlin-depleted tumors. Given the metabolic phenotype of myoferlin-silenced breast cancer *in vitro*, we think that cells that have been stably silenced for myoferlin (using shRNA) have already adapted their metabolism towards increased glycolysis and  $\beta$ -oxidation. This may have happened during the selection steps of generating stable clones. Cells isolated from xenografted tumors show here a reduced capacity of the mitochondrial respiratory chain. We were unable to detect the activation of AMPK in animal tumors deficient of myoferlin, suggesting the possibility that the activation of this key enzyme is a transient phenomenon that has probably occurred in the early steps of adaptation. Another relevant observation is the absence of necrosis in myoferlin-silenced tumors. We are currently exploring the status of HIF-1 $\alpha$  in the same tumors as well as the evidence of increased angiogenesis.

Several studies, including ours, have stated that cells lacking myoferlin are less invasive [59-61]. Decrease in microvilli formation and impairment of cell migration in myoferlin-depleted cells are in agreement with this. We hypothesized that loss of myoferlin

could influence metastases formation. Using an *in vivo* model of lung metastasis development, we report for the first time that mice injected with cells lacking myoferlin develop significantly fewer and smaller lung metastases than the control cohort. Further studies are ongoing in our lab to further test the hypothesis that this observation is related to the modified metabolism in primary tumors.

# **Conclusions and perspectives**

## **Conclusions & perspectives**

The current work provides the first report that myoferlin is overexpressed in a large cohort of human breast cancer and that silencing of myoferlin impedes breast cancer cells to respond to EGF-induced cell migration and epithelial-to-mesenchymal transition. Mechanistically, myoferlin controls the degradation of the EGFR after its activation and internalization in breast cancer cells. Both effects were induced as a result of impaired degradation of phosphorylated EGFR via dysfunctional plasma membrane caveolae and alteration of caveolin-1 homo-oligomerization. This observation proves important the second important function of myoferlin to control cell metabolism. Namely, we show here for the first time that myoferlin is important regulator of the endosomal system and that loss of myoferlin alters mitochondrial function and cell metabolism. This response is dependent on the aberrant oligomerization of caveolin-1 and improper caveolae assembly, potentially caused by differences in phosphorylation of the protein. *In vivo*, myoferlin depletion reduced tumor development in both chicken chorioallantoic membrane and mouse xenograft model of human breast cancer. From a histological point of view, the mice xenograft tumors depleted in myoferlin display no necrosis and contain particularly fewer lipid droplets, suggesting *in vivo* metabolic adaptation. Animals injected with myoferlin-deficient cells also develop significantly less lung metastasis than the control group, highlighting for the first time the importance of myoferlin in process of tumor dissemination.

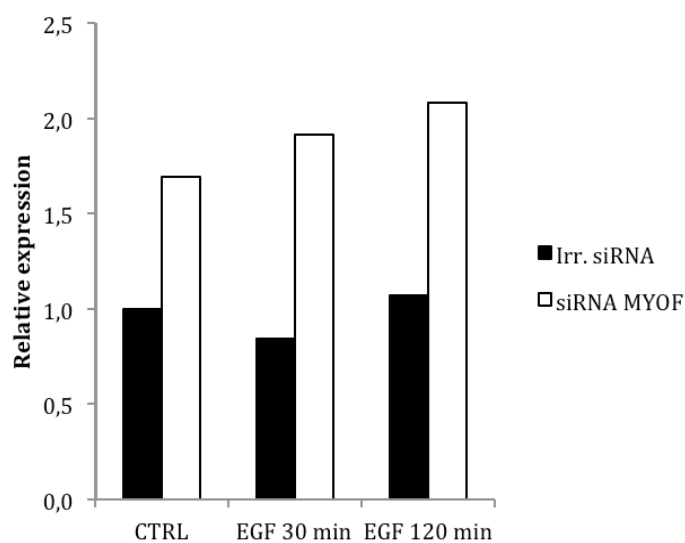
# **Supplementary figures**

Gene symbol	Accession No.	No. of unique peptides	Sequence coverage	Protein score
AEBP1	Q8IU7	4	6%	113
AGRIN	O00468	3	2%	80
AMPN	P15144	3	8%	161
AATM	P00505	2	9%	45
ATLA3	Q6DD88	1	9%	91
CAN1	P07384	2	5%	77
CAN2	P17655	2	5%	62
CD276	Q5ZPR3	2	6%	161
COCA1	Q9Y6C2	4	7%	184
EMIL1	Q99715	16	11%	512
FINC	P02751	13	10%	770
GGT1	P19440	2	8%	67
GGT2	P36268	1	8%	44
ITAV	P06756	3	6%	115
IBP3	P17936	2	9%	65
LAMA5	O15230	5	4%	78
LRC15	Q8TF66	2	8%	126
MRC2	Q9UBG0	2	3%	78
MYOF	Q9NZM1	3	7%	45
CADM1	Q9BY67	2	7%	104
OLFML1	Q6UWY5	2	5%	58
POSTN	Q15063	11	21%	616
TENA	P24821	10	8%	380
TSP1	P07996	3	7%	139
TIMP1	P01033	2	14%	89
BGH3	Q15582	4	12%	136
TM9S3	Q9HD45	1	3%	66
CU129	Q96M42	1	14%	38
CSPG2	P13611	4	2%	181

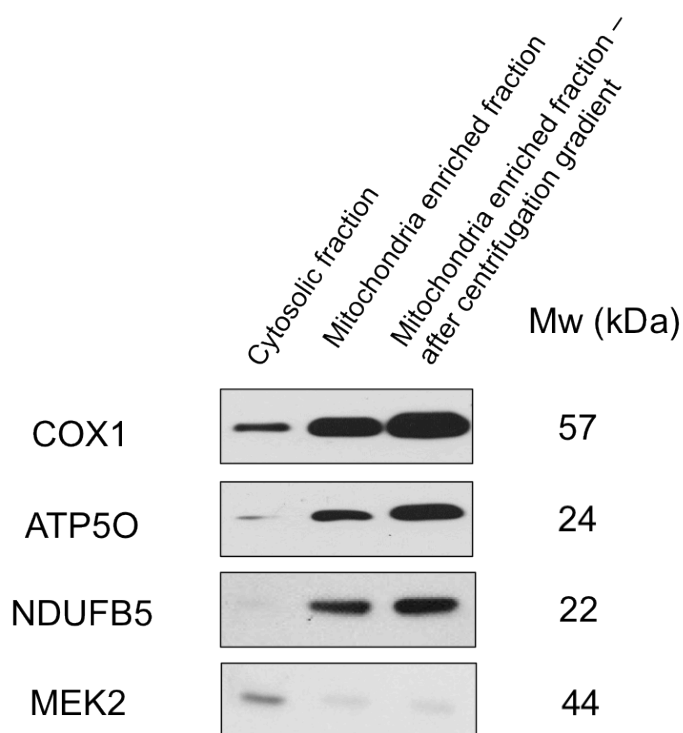
**Supplementary table 1:** Average values (n=3) indicating the number of unique peptides, sequence coverage and score (Mascot; for details see [www.matrixscience.com](http://www.matrixscience.com)) that were observed in the Swissprot database for each of the respective proteins reported in the Table 1

Gene symbol	Accession No.	Glycopeptide Sequence (deamidated consensus site)	Precursor m/z value (charge)	Peptide score
AEBP1	Q8IUX7	GVVTDEQGIPIANATISVSGINHGVK	859.78 (3+)	45
AGRN	O00468	NELMLNSSLMR	670.83 (2+)	80
AMPN	P15144	AEFNITLIHPK	642.38 (2+)	54
		VPVTLALNNTLFIEER	972.19 (2+)	96
		GPSTPLPEDPNWNVTEFHTTPK	822.38 (3+)	34
ATLA3	Q6DD88	ELGGAIDFGAAYVLEQASSHIGNSTQATVR	1021.78 (3+)	34
CD276	Q5ZPR3	VVLGANGTYSCLVR	755.36 (2+)	62
		TALFPDLLAQGNASLR	844.40 (2+)	99
COCA1	Q99715	MLEAYNLTEK	614.82 (2+)	58
		EAGNITTDGYEILGK	791.40 (2+)	64
		NLQVYNATSNLSLVK	826.39 (2+)	59
EMIL1	Q9Y6C2	LGALNSSLQLLEDR	765.42 (2+)	68
		ETNTTSQMQAALLEK	841.39 (2+)	65
		LEQLGGLLANVSGELGGR	892.51 (2+)	92
FINC	P02751	DQCIVDDITYNVNDTFHK	1099.48 (2+)	78
		LDAPTNLQFVNETDSTVLVR	1117.06 (2+)	115
		HEEGHMLNCTCFGQGR	650.55 (3+)	56
GGT1	P19440	LAFATMFNSSEQSQK	853.36 (2+)	98
GGT2	P36268	LHNQLLPNVTTVER	817.99 (2+)	42
ITAV	P06756	ANTTQPGIVEGGQVLK	806.90 (2+)	55
		ISSLQTTEKNDTVAGQGER	1017.91 (2+)	61
		TAADTTGLQPILNQFTPANISR	777.39 (3+)	98
IBP3	P17936	GLCVNASAVSR	567.88 (2+)	63
		AYLLPAPPAPGNASESEEDR	695.72 (3+)	31
LAMAS	O15230	LNASIAADLQSQLR	715.39 (2+)	80
LRC15	Q8TF66	MILANLQNISLQNNR	823.35 (2+)	107
MRC2	Q9UBG0	VTPACNTSLPAQR	708.33 (2+)	78
		GTDPSPSPSPALPPAPGTELSYLNQTFR	972.12 (3+)	35
CADM1	Q98Y67	FQLLNFSSELK	707.41 (2+)	89
OLFML1	Q6UWY5	TLLNASCDNMLMGIK	857.34 (2+)	64
POSTN	Q15063	EVNDTLLVNEK	694.34 (2+)	85
TENA	P24821	VEAAQNLTLPGLSLR	735.40 (2+)	92
		LLETVEYNISGAER	797.89 (2+)	102
		LNYSLPTGQWVGVLPR	965.03 (2+)	79
		LNWTAADQAYEHFIIQVQEANK	864.11 (3+)	38
		GFESEPVSGSFTTALDGPVGLVTANITDSEALAR	1176.23 (3+)	73
		GPNCSEPECVGNCHLR	628.90 (3+)	56
TSP1	P07996	VVNSTTGPEHLR	456.59 (3+)	50
TIMP1	P01033	FVGTPEVNTLYQR	877.35 (2+)	70
TM953	Q9HD45	IVDVNLTSEGK	588.33 (2+)	66
CSPG2	P13611	FENQTFPPPSR	746.83 (2+)	55

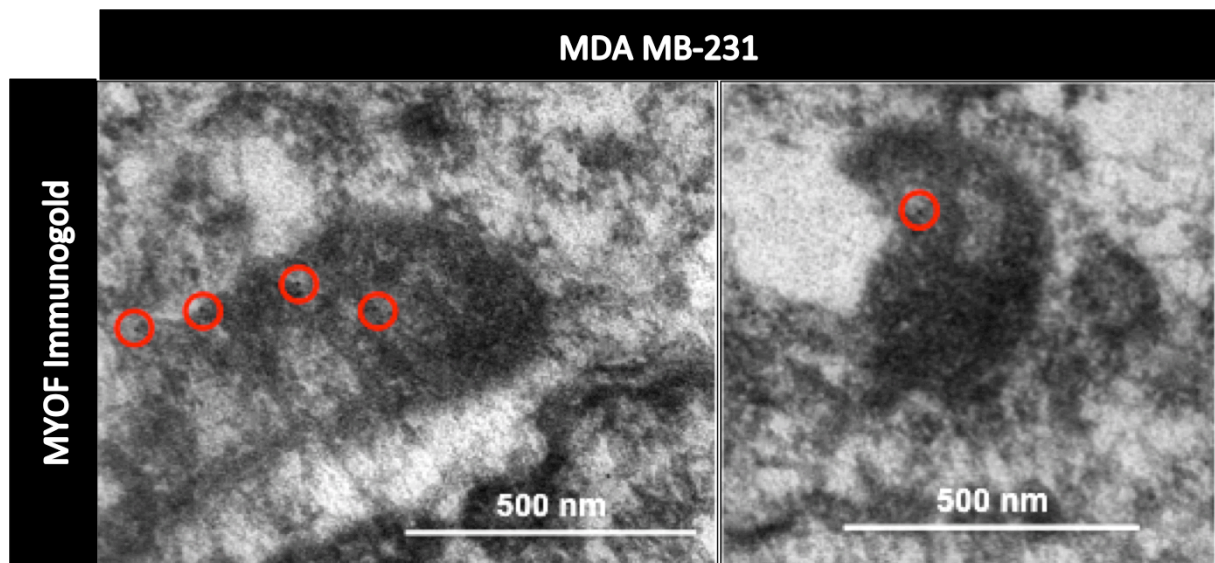
**Supplementary table 2:** Glycosylated peptides observed for the proteins displayed in the Table 1. The table provides an overview of the exact peptide sequence, the corresponding N-glycosylation consensus site, the number of patients that have tested positive (T indicates tumoral and N the normal state; the number refers to the patient listed in the Table A3), the observed mass and peptide charge as well as the score (Mascot).



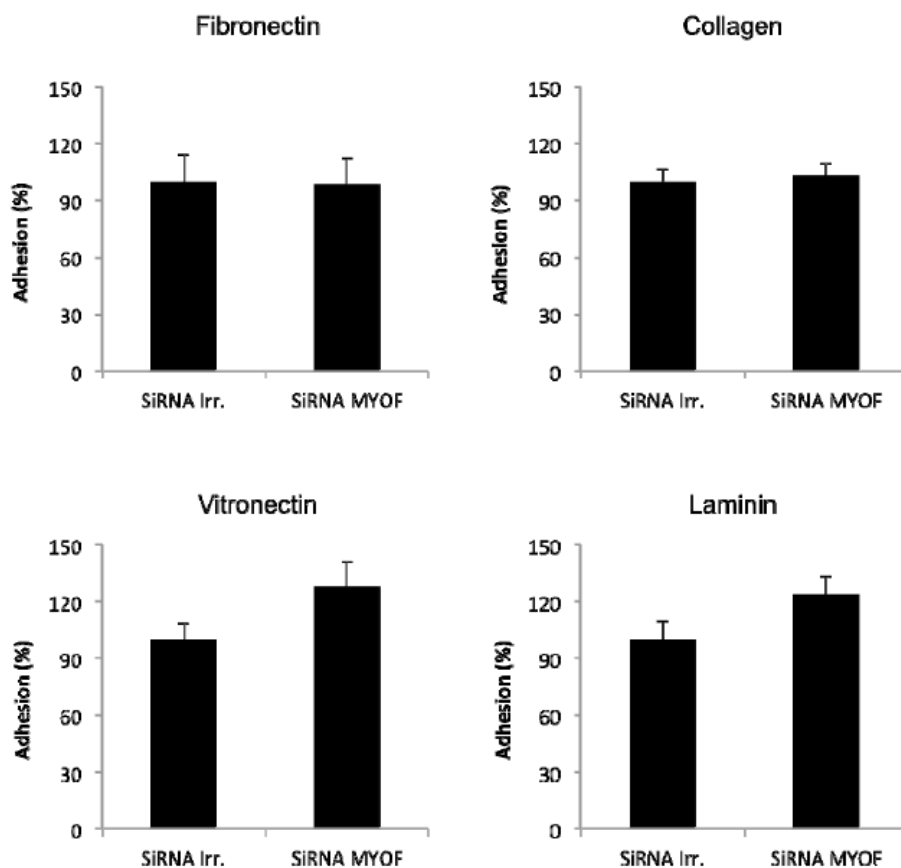
**Supplementary figure 1:** Silencing of myoferlin affects EGFR at the transcriptional level. RT-qPCR analysis of MDA-MB231 stimulated or not with EGF shows an increase in EGFR mRNA after myoferlin silencing.



**Supplementary figure 2:** Mitochondria isolation from MDA-MB231 cells. Western blot analysis of mitochondria enriched samples. COX1, ATP5O and NDUFB5 are used as mitochondrial markers. MEK2 is a cytosolic protein.



**Supplementary figure 3:** Myoferlin localization in mitochondria. Although majority of the observed mitochondria were negative for myoferlin staining, signal could be detected in some organelles.



**Supplementary figure 4:** Cellular adhesion assay on selected extracellular matrix proteins. Myoferlin depletion in MDA-MB231 cells does not influence their in vitro adhesion properties on fibronectin, collagen, vitronectin and laminin matrices. Error bars indicate standard deviation of means from three biological replicates.

# References

1. *Cancer diagnostics: discovery and clinical applications* Clinical Chemistry, 2002. **48**.
2. *Recent advances in cancer biomarkers.* Clin Biochem, 2004. **37**: p. s1 - s402.
3. *Biomarkers and clinical proteomics.* Mol Cell Proteomics, 2006. **5**.
4. *Proteomics and biomarkers.* J Proteome Res, 2005. **4**: p. 1053-1456.
5. Castronovo, V., et al., *Identification of specific reachable molecular targets in human breast cancer using a versatile ex vivo proteomic method.* Proteomics, 2007. **7**(8): p. 1188-96.
6. Castronovo, V., et al., *A chemical proteomics approach for the identification of accessible antigens expressed in human kidney cancer.* Mol Cell Proteomics, 2006. **5**(11): p. 2083-91.
7. Turtoi, A., et al., *Novel comprehensive approach for accessible biomarker identification and absolute quantification from precious human tissues.* J Proteome Res, 2011. **10**(7): p. 3160-82.
8. Conrotto, P., et al., *Identification of new accessible tumor antigens in human colon cancer by ex vivo protein biotinylation and comparative mass spectrometry analysis.* Int J Cancer, 2008. **123**(12): p. 2856-64.
9. Turtoi, A., et al., *Sparc-like protein 1 is a new marker of human glioma progression.* J Proteome Res, 2012. **11**(10): p. 5011-21.
10. Wollscheid, B., et al., *Mass-spectrometric identification and relative quantification of N-linked cell surface glycoproteins.* Nat Biotechnol, 2009. **27**(4): p. 378-86.
11. Naeem, A., M. Saleemuddin, and R.H. Khan, *Glycoprotein targeting and other applications of lectins in biotechnology.* Curr Protein Pept Sci, 2007. **8**(3): p. 261-71.
12. Zhang, H., et al., *Identification and quantification of N-linked glycoproteins using hydrazide chemistry, stable isotope labeling and mass spectrometry.* Nat Biotechnol, 2003. **21**(6): p. 660-6.
13. Tian, Y., et al., *Solid-phase extraction of N-linked glycopeptides.* Nat Protoc, 2007. **2**(2): p. 334-9.
14. Zhang, H., *Glycoproteomics using chemical immobilization.* Curr Protoc Protein Sci, 2007. **Chapter 24**: p. Unit 24 3.
15. Sun, B., et al., *Shotgun glycopeptide capture approach coupled with mass spectrometry for comprehensive glycoproteomics.* Mol Cell Proteomics, 2007. **6**(1): p. 141-9.
16. Chen, R., et al., *Glycoproteomics analysis of human liver tissue by combination of multiple enzyme digestion and hydrazide chemistry.* J Proteome Res, 2009. **8**(2): p. 651-61.
17. Turtoi, A., et al., *Identification of novel accessible proteins bearing diagnostic and therapeutic potential in human pancreatic ductal adenocarcinoma.* J Proteome Res, 2011. **10**(9): p. 4302-13.
18. Doherty, K.R., et al., *Normal myoblast fusion requires myoferlin.* Development, 2005. **132**(24): p. 5565-75.
19. Cipta, S. and H.H. Patel, *Molecular bandages: inside-out, outside-in repair of cellular membranes. Focus on "Myoferlin is critical for endocytosis in endothelial cells".* Am J Physiol Cell Physiol, 2009. **297**(3): p. C481-3.
20. Ward, S. and J. Miwa, *Characterization of temperature-sensitive, fertilization-defective mutants of the nematode caenorhabditis elegans.* Genetics, 1978. **88**(2): p. 285-303.
21. Nelson, G.A., T.M. Roberts, and S. Ward, *Caenorhabditis elegans spermatozoan locomotion: amoeboid movement with almost no actin.* J Cell Biol, 1982. **92**(1): p. 121-31.

22. Achanzar, W.E. and S. Ward, *A nematode gene required for sperm vesicle fusion*. J Cell Sci, 1997. **110** ( Pt 9): p. 1073-81.
23. Ohsako, T., K. Hirai, and M.T. Yamamoto, *The Drosophila misfire gene has an essential role in sperm activation during fertilization*. Genes Genet Syst, 2003. **78**(3): p. 253-66.
24. Smith, M.K. and B.T. Wakimoto, *Complex regulation and multiple developmental functions of misfire, the Drosophila melanogaster ferlin gene*. BMC Dev Biol, 2007. **7**: p. 21.
25. Lek, A., et al., *Phylogenetic analysis of ferlin genes reveals ancient eukaryotic origins*. BMC Evol Biol, 2010. **10**: p. 231.
26. Dacks, J.B. and M.C. Field, *Evolution of the eukaryotic membrane-trafficking system: origin, tempo and mode*. J Cell Sci, 2007. **120**(Pt 17): p. 2977-85.
27. Lek, A., et al., *Ferlins: regulators of vesicle fusion for auditory neurotransmission, receptor trafficking and membrane repair*. Traffic, 2012. **13**(2): p. 185-94.
28. McNeil, P.L. and T. Kirchhausen, *An emergency response team for membrane repair*. Nat Rev Mol Cell Biol, 2005. **6**(6): p. 499-505.
29. Shin, O.H., et al., *Evolutionarily conserved multiple C2 domain proteins with two transmembrane regions (MCTPs) and unusual Ca<sup>2+</sup> binding properties*. J Biol Chem, 2005. **280**(2): p. 1641-51.
30. Yamazaki, T., et al., *Arabidopsis synaptotagmin SYT1, a type I signal-anchor protein, requires tandem C2 domains for delivery to the plasma membrane*. J Biol Chem, 2010. **285**(30): p. 23165-76.
31. Washington, N.L. and S. Ward, *FER-1 regulates Ca<sup>2+</sup> -mediated membrane fusion during C. elegans spermatogenesis*. J Cell Sci, 2006. **119**(Pt 12): p. 2552-62.
32. Sea Urchin Genome Sequencing, C., et al., *The genome of the sea urchin Strongylocentrotus purpuratus*. Science, 2006. **314**(5801): p. 941-52.
33. Anderson, L.V., et al., *Dysferlin is a plasma membrane protein and is expressed early in human development*. Hum Mol Genet, 1999. **8**(5): p. 855-61.
34. Vandre, D.D., et al., *Dysferlin is expressed in human placenta but does not associate with caveolin*. Biol Reprod, 2007. **77**(3): p. 533-42.
35. Robinson, J.M., et al., *While dysferlin and myoferlin are coexpressed in the human placenta, only dysferlin expression is responsive to trophoblast fusion in model systems*. Biol Reprod, 2009. **81**(1): p. 33-9.
36. Liu, J., et al., *Dysferlin, a novel skeletal muscle gene, is mutated in Miyoshi myopathy and limb girdle muscular dystrophy*. Nat Genet, 1998. **20**(1): p. 31-6.
37. Wenzel, K., et al., *Dysfunction of dysferlin-deficient hearts*. J Mol Med (Berl), 2007. **85**(11): p. 1203-14.
38. Kuru, S., et al., *[A patient with limb girdle muscular dystrophy type 2B (LGMD2B) manifesting cardiomyopathy]*. Rinsho Shinkeigaku, 2004. **44**(6): p. 375-8.
39. Bansal, D., et al., *Defective membrane repair in dysferlin-deficient muscular dystrophy*. Nature, 2003. **423**(6936): p. 168-72.
40. Matsuda, C., et al., *The sarcolemmal proteins dysferlin and caveolin-3 interact in skeletal muscle*. Hum Mol Genet, 2001. **10**(17): p. 1761-6.
41. Huang, Y., et al., *Calpain 3 is a modulator of the dysferlin protein complex in skeletal muscle*. Hum Mol Genet, 2008. **17**(12): p. 1855-66.
42. Lennon, N.J., et al., *Dysferlin interacts with annexins A1 and A2 and mediates sarcolemmal wound-healing*. J Biol Chem, 2003. **278**(50): p. 50466-73.
43. Demonbreun, A.R., et al., *Impaired muscle growth and response to insulin-like growth factor 1 in dysferlin-mediated muscular dystrophy*. Hum Mol Genet, 2011. **20**(4): p. 779-89.

44. Demonbreun, A.R., et al., *Myoferlin is required for insulin-like growth factor response and muscle growth*. *FASEB J*, 2010. **24**(4): p. 1284-95.
45. Sharma, A., et al., *A new role for the muscle repair protein dysferlin in endothelial cell adhesion and angiogenesis*. *Arterioscler Thromb Vasc Biol*, 2010. **30**(11): p. 2196-204.
46. Yasunaga, S., et al., *OTOF encodes multiple long and short isoforms: genetic evidence that the long ones underlie recessive deafness DFNB9*. *Am J Hum Genet*, 2000. **67**(3): p. 591-600.
47. Roux, I., et al., *Otoferlin, defective in a human deafness form, is essential for exocytosis at the auditory ribbon synapse*. *Cell*, 2006. **127**(2): p. 277-89.
48. Yasunaga, S., et al., *A mutation in OTOF, encoding otoferlin, a FER-1-like protein, causes DFNB9, a nonsyndromic form of deafness*. *Nat Genet*, 1999. **21**(4): p. 363-9.
49. Johnson, C.P. and E.R. Chapman, *Otoferlin is a calcium sensor that directly regulates SNARE-mediated membrane fusion*. *J Cell Biol*, 2010. **191**(1): p. 187-97.
50. Davis, D.B., et al., *Myoferlin, a candidate gene and potential modifier of muscular dystrophy*. *Hum Mol Genet*, 2000. **9**(2): p. 217-26.
51. Britton, S., et al., *The third human FER-1-like protein is highly similar to dysferlin*. *Genomics*, 2000. **68**(3): p. 313-21.
52. Martens, S. and H.T. McMahon, *Mechanisms of membrane fusion: disparate players and common principles*. *Nat Rev Mol Cell Biol*, 2008. **9**(7): p. 543-56.
53. Demonbreun, A.R., et al., *Myoferlin regulation by NFAT in muscle injury, regeneration and repair*. *J Cell Sci*, 2010. **123**(Pt 14): p. 2413-22.
54. Bernatchez, P.N., et al., *Myoferlin regulates vascular endothelial growth factor receptor-2 stability and function*. *J Biol Chem*, 2007. **282**(42): p. 30745-53.
55. Yu, C., et al., *Myoferlin gene silencing decreases Tie-2 expression in vitro and angiogenesis in vivo*. *Vascul Pharmacol*, 2011. **55**(1-3): p. 26-33.
56. Bernatchez, P.N., et al., *Myoferlin is critical for endocytosis in endothelial cells*. *Am J Physiol Cell Physiol*, 2009. **297**(3): p. C484-92.
57. Difilippantonio, S., et al., *Gene expression profiles in human non-small and small-cell lung cancers*. *Eur J Cancer*, 2003. **39**(13): p. 1936-47.
58. Abba, M.C., et al., *Gene expression signature of estrogen receptor alpha status in breast cancer*. *BMC Genomics*, 2005. **6**: p. 37.
59. Eisenberg, M.C., et al., *Mechanistic modeling of the effects of myoferlin on tumor cell invasion*. *Proc Natl Acad Sci U S A*, 2011. **108**(50): p. 20078-83.
60. Li, R., et al., *Myoferlin depletion in breast cancer cells promotes mesenchymal to epithelial shape change and stalls invasion*. *PLoS One*, 2012. **7**(6): p. e39766.
61. Volakis, L.I., et al., *Loss of myoferlin redirects breast cancer cell motility towards collective migration*. *PLoS One*, 2014. **9**(2): p. e86110.
62. Leung, C., et al., *Expression of myoferlin in human and murine carcinoma tumors: role in membrane repair, cell proliferation, and tumorigenesis*. *Am J Pathol*, 2013. **182**(5): p. 1900-9.
63. Rodriguez-Boulau, E. and S.K. Powell, *Polarity of epithelial and neuronal cells*. *Annu Rev Cell Biol*, 1992. **8**: p. 395-427.
64. Marrs, J.A., et al., *Plasticity in epithelial cell phenotype: modulation by expression of different cadherin cell adhesion molecules*. *J Cell Biol*, 1995. **129**(2): p. 507-19.
65. Nelson, W.J., et al., *Regulation of epithelial cell polarity: a view from the cell surface*. *Cold Spring Harb Symp Quant Biol*, 1992. **57**: p. 621-30.
66. Yeaman, C., K.K. Grindstaff, and W.J. Nelson, *New perspectives on mechanisms involved in generating epithelial cell polarity*. *Physiol Rev*, 1999. **79**(1): p. 73-98.

67. Goldenring, J.R., *A central role for vesicle trafficking in epithelial neoplasia: intracellular highways to carcinogenesis*. Nat Rev Cancer, 2013. **13**(11): p. 813-20.
68. Singh, B., et al., *Transformation of polarized epithelial cells by apical mistrafficking of epiregulin*. Proc Natl Acad Sci U S A, 2013. **110**(22): p. 8960-5.
69. Muller, P.A., et al., *Mutant p53 drives invasion by promoting integrin recycling*. Cell, 2009. **139**(7): p. 1327-41.
70. Hayashi, D., et al., *Deficiency of claudin-18 causes paracellular H<sup>+</sup> leakage, up-regulation of interleukin-1beta, and atrophic gastritis in mice*. Gastroenterology, 2012. **142**(2): p. 292-304.
71. Ivanov, A.I., A. Nusrat, and C.A. Parkos, *The epithelium in inflammatory bowel disease: potential role of endocytosis of junctional proteins in barrier disruption*. Novartis Found Symp, 2004. **263**: p. 115-24; discussion 124-32, 211-8.
72. Lioni, M., et al., *Dysregulation of claudin-7 leads to loss of E-cadherin expression and the increased invasion of esophageal squamous cell carcinoma cells*. Am J Pathol, 2007. **170**(2): p. 709-21.
73. Casaletto, J.B. and A.I. McClatchey, *Spatial regulation of receptor tyrosine kinases in development and cancer*. Nat Rev Cancer, 2012. **12**(6): p. 387-400.
74. Mellman, I. and W.J. Nelson, *Coordinated protein sorting, targeting and distribution in polarized cells*. Nat Rev Mol Cell Biol, 2008. **9**(11): p. 833-45.
75. Goh, L.K., et al., *Multiple mechanisms collectively regulate clathrin-mediated endocytosis of the epidermal growth factor receptor*. J Cell Biol, 2010. **189**(5): p. 871-83.
76. Haber, D.A., N.S. Gray, and J. Baselga, *The evolving war on cancer*. Cell, 2011. **145**(1): p. 19-24.
77. Goldstein, N.I., et al., *Biological efficacy of a chimeric antibody to the epidermal growth factor receptor in a human tumor xenograft model*. Clin Cancer Res, 1995. **1**(11): p. 1311-8.
78. Agus, D.B., et al., *Targeting ligand-activated ErbB2 signaling inhibits breast and prostate tumor growth*. Cancer Cell, 2002. **2**(2): p. 127-37.
79. Scaltriti, M., et al., *Expression of p95HER2, a truncated form of the HER2 receptor, and response to anti-HER2 therapies in breast cancer*. J Natl Cancer Inst, 2007. **99**(8): p. 628-38.
80. Yarden, Y. and G. Pines, *The ERBB network: at last, cancer therapy meets systems biology*. Nat Rev Cancer, 2012. **12**(8): p. 553-63.
81. Sigismund, S., et al., *Clathrin-independent endocytosis of ubiquitinated cargos*. Proc Natl Acad Sci U S A, 2005. **102**(8): p. 2760-5.
82. Sigismund, S., et al., *Clathrin-mediated internalization is essential for sustained EGFR signaling but dispensable for degradation*. Dev Cell, 2008. **15**(2): p. 209-19.
83. Caswell, P.T., et al., *Rab25 associates with alpha5beta1 integrin to promote invasive migration in 3D microenvironments*. Dev Cell, 2007. **13**(4): p. 496-510.
84. Hu, J., et al., *Cdc42-interacting protein 4 is a Src substrate that regulates invadopodia and invasiveness of breast tumors by promoting MT1-MMP endocytosis*. J Cell Sci, 2011. **124**(Pt 10): p. 1739-51.
85. Fisher, K.E., et al., *MT1-MMP- and Cdc42-dependent signaling co-regulate cell invasion and tunnel formation in 3D collagen matrices*. J Cell Sci, 2009. **122**(Pt 24): p. 4558-69.
86. Hattula, K., et al., *Characterization of the Rab8-specific membrane traffic route linked to protrusion formation*. J Cell Sci, 2006. **119**(Pt 23): p. 4866-77.
87. Rainero, E., et al., *Diacylglycerol kinase alpha controls RCP-dependent integrin trafficking to promote invasive migration*. J Cell Biol, 2012. **196**(2): p. 277-95.

88. Pellinen, T., et al., *Small GTPase Rab21 regulates cell adhesion and controls endosomal traffic of beta1-integrins*. J Cell Biol, 2006. **173**(5): p. 767-80.
89. Wang, E., et al., *Apical and basolateral endocytic pathways of MDCK cells meet in acidic common endosomes distinct from a nearly-neutral apical recycling endosome*. Traffic, 2000. **1**(6): p. 480-93.
90. Roman, L.M. and H. Garoff, *Alteration of the cytoplasmic domain of the membrane-spanning glycoprotein p62 of Semliki Forest virus does not affect its polar distribution in established lines of Madin-Darby canine kidney cells*. J Cell Biol, 1986. **103**(6 Pt 2): p. 2607-18.
91. Sotgia, F., et al., *Caveolin-1 and cancer metabolism in the tumor microenvironment: markers, models, and mechanisms*. Annu Rev Pathol, 2012. **7**: p. 423-67.
92. Turtoi, A., et al., *Myoferlin is a key regulator of EGFR activity in breast cancer*. Cancer Res, 2013. **73**(17): p. 5438-48.
93. Palade, G.E., *An electron microscope study of the mitochondrial structure*. J Histochem Cytochem, 1953. **1**(4): p. 188-211.
94. Williams, T.M. and M.P. Lisanti, *The caveolin proteins*. Genome Biol, 2004. **5**(3): p. 214.
95. Song, K.S., et al., *Expression of caveolin-3 in skeletal, cardiac, and smooth muscle cells. Caveolin-3 is a component of the sarcolemma and co-fractionates with dystrophin and dystrophin-associated glycoproteins*. J Biol Chem, 1996. **271**(25): p. 15160-5.
96. Monier, S., et al., *VIP21-caveolin, a membrane protein constituent of the caveolar coat, oligomerizes in vivo and in vitro*. Mol Biol Cell, 1995. **6**(7): p. 911-27.
97. Monier, S., et al., *Oligomerization of VIP21-caveolin in vitro is stabilized by long chain fatty acylation or cholesterol*. FEBS Lett, 1996. **388**(2-3): p. 143-9.
98. Sargiacomo, M., et al., *Signal transducing molecules and glycosyl-phosphatidylinositol-linked proteins form a caveolin-rich insoluble complex in MDCK cells*. J Cell Biol, 1993. **122**(4): p. 789-807.
99. Ros-Baro, A., et al., *Lipid rafts are required for GLUT4 internalization in adipose cells*. Proc Natl Acad Sci U S A, 2001. **98**(21): p. 12050-5.
100. Karlsson, M., et al., *Insulin induces translocation of glucose transporter GLUT4 to plasma membrane caveolae in adipocytes*. FASEB J, 2002. **16**(2): p. 249-51.
101. Scherer, P.E., et al., *Induction of caveolin during adipogenesis and association of GLUT4 with caveolin-rich vesicles*. J Cell Biol, 1994. **127**(5): p. 1233-43.
102. Rauch, M.C., et al., *Hexose transporters GLUT1 and GLUT3 are colocalized with hexokinase I in caveolae microdomains of rat spermatogenic cells*. J Cell Physiol, 2006. **207**(2): p. 397-406.
103. Ost, A., et al., *Triacylglycerol is synthesized in a specific subclass of caveolae in primary adipocytes*. J Biol Chem, 2005. **280**(1): p. 5-8.
104. Trigatti, B.L., R.G. Anderson, and G.E. Gerber, *Identification of caveolin-1 as a fatty acid binding protein*. Biochem Biophys Res Commun, 1999. **255**(1): p. 34-9.
105. Ortgren, U., et al., *Separation and characterization of caveolae subclasses in the plasma membrane of primary adipocytes; segregation of specific proteins and functions*. FEBS J, 2006. **273**(14): p. 3381-92.
106. Covey, S.D., et al., *Cholesterol depletion inhibits fatty acid uptake without affecting CD36 or caveolin-1 distribution in adipocytes*. Biochem Biophys Res Commun, 2007. **355**(1): p. 67-71.
107. Murata, M., et al., *VIP21/caveolin is a cholesterol-binding protein*. Proc Natl Acad Sci U S A, 1995. **92**(22): p. 10339-43.

108. Bist, A., P.E. Fielding, and C.J. Fielding, *Two sterol regulatory element-like sequences mediate up-regulation of caveolin gene transcription in response to low density lipoprotein free cholesterol*. Proc Natl Acad Sci U S A, 1997. **94**(20): p. 10693-8.
109. Uittenbogaard, A., et al., *Cholesteryl ester is transported from caveolae to internal membranes as part of a caveolin-annexin II lipid-protein complex*. J Biol Chem, 2002. **277**(7): p. 4925-31.
110. Frank, P.G., et al., *Caveolin-1 and regulation of cellular cholesterol homeostasis*. Am J Physiol Heart Circ Physiol, 2006. **291**(2): p. H677-86.
111. Pol, A., et al., *A caveolin dominant negative mutant associates with lipid bodies and induces intracellular cholesterol imbalance*. J Cell Biol, 2001. **152**(5): p. 1057-70.
112. Fielding, P.E. and C.J. Fielding, *Plasma membrane caveolae mediate the efflux of cellular free cholesterol*. Biochemistry, 1995. **34**(44): p. 14288-92.
113. Pol, A., et al., *Cholesterol and fatty acids regulate dynamic caveolin trafficking through the Golgi complex and between the cell surface and lipid bodies*. Mol Biol Cell, 2005. **16**(4): p. 2091-105.
114. Asterholm, I.W., et al., *Altered mitochondrial function and metabolic inflexibility associated with loss of caveolin-1*. Cell Metab, 2012. **15**(2): p. 171-85.
115. Bosch, M., et al., *Caveolin-1 deficiency causes cholesterol-dependent mitochondrial dysfunction and apoptotic susceptibility*. Curr Biol, 2011. **21**(8): p. 681-6.
116. Bosch, M., et al., *Mitochondrial cholesterol: a connection between caveolin, metabolism, and disease*. Traffic, 2011. **12**(11): p. 1483-9.
117. Mastrodonato, M., et al., *Altered distribution of caveolin-1 in early liver steatosis*. Eur J Clin Invest, 2011. **41**(6): p. 642-51.
118. Fridolfsson, H.N., et al., *Mitochondria-localized caveolin in adaptation to cellular stress and injury*. FASEB J, 2012. **26**(11): p. 4637-49.
119. Fiucci, G., et al., *Caveolin-1 inhibits anchorage-independent growth, anoikis and invasiveness in MCF-7 human breast cancer cells*. Oncogene, 2002. **21**(15): p. 2365-75.
120. Lu, Z., et al., *Downregulation of caveolin-1 function by EGF leads to the loss of E-cadherin, increased transcriptional activity of beta-catenin, and enhanced tumor cell invasion*. Cancer Cell, 2003. **4**(6): p. 499-515.
121. Sloan, E.K., K.L. Stanley, and R.L. Anderson, *Caveolin-1 inhibits breast cancer growth and metastasis*. Oncogene, 2004. **23**(47): p. 7893-7.
122. Yamaguchi, H., et al., *Lipid rafts and caveolin-1 are required for invadopodia formation and extracellular matrix degradation by human breast cancer cells*. Cancer Res, 2009. **69**(22): p. 8594-602.
123. Salatino, M., et al., *Progesterin-induced caveolin-1 expression mediates breast cancer cell proliferation*. Oncogene, 2006. **25**(59): p. 7723-39.
124. Timme, T.L., et al., *Caveolin-1 is regulated by c-myc and suppresses c-myc-induced apoptosis*. Oncogene, 2000. **19**(29): p. 3256-65.
125. Razani, B., et al., *Caveolin-1 expression is down-regulated in cells transformed by the human papilloma virus in a p53-dependent manner. Replacement of caveolin-1 expression suppresses HPV-mediated cell transformation*. Biochemistry, 2000. **39**(45): p. 13916-24.
126. Witkiewicz, A.K., et al., *An absence of stromal caveolin-1 expression predicts early tumor recurrence and poor clinical outcome in human breast cancers*. Am J Pathol, 2009. **174**(6): p. 2023-34.
127. Witkiewicz, A.K., et al., *Stromal caveolin-1 levels predict early DCIS progression to invasive breast cancer*. Cancer Biol Ther, 2009. **8**(11): p. 1071-9.

128. Sloan, E.K., et al., *Stromal cell expression of caveolin-1 predicts outcome in breast cancer*. Am J Pathol, 2009. **174**(6): p. 2035-43.
129. Di Vizio, D., et al., *An absence of stromal caveolin-1 is associated with advanced prostate cancer, metastatic disease and epithelial Akt activation*. Cell Cycle, 2009. **8**(15): p. 2420-4.
130. Mercier, I., et al., *Human breast cancer-associated fibroblasts (CAFs) show caveolin-1 downregulation and RB tumor suppressor functional inactivation: Implications for the response to hormonal therapy*. Cancer Biol Ther, 2008. **7**(8): p. 1212-25.
131. Warburg, O., *The metabolism of tumors*. 1930.
132. Warburg, O., *On the origin of cancer cells*. Science, 1956. **123**: p. 309-314.
133. Czernin, J. and M.E. Phelps, *Positron emission tomography scanning: current and future applications*. Annu Rev Med, 2002. **53**: p. 89-112.
134. Mochiki, E., et al., *Evaluation of 18F-2-deoxy-2-fluoro-D-glucose positron emission tomography for gastric cancer*. World J Surg, 2004. **28**(3): p. 247-53.
135. Walenta, S., et al., *High lactate levels predict likelihood of metastases, tumor recurrence, and restricted patient survival in human cervical cancers*. Cancer Res, 2000. **60**(4): p. 916-21.
136. Schwickert, G., et al., *Correlation of high lactate levels in human cervical cancer with incidence of metastasis*. Cancer Res, 1995. **55**(21): p. 4757-9.
137. Altenberg, B. and K.O. Greulich, *Genes of glycolysis are ubiquitously overexpressed in 24 cancer classes*. Genomics, 2004. **84**(6): p. 1014-20.
138. Hatzivassiliou, G., et al., *ATP citrate lyase inhibition can suppress tumor cell growth*. Cancer Cell, 2005. **8**(4): p. 311-21.
139. Gillies, R.J. and R.A. Gatenby, *Adaptive landscapes and emergent phenotypes: why do cancers have high glycolysis?* J Bioenerg Biomembr, 2007. **39**(3): p. 251-7.
140. Abel, F., et al., *Imbalance of the mitochondrial pro- and anti-apoptotic mediators in neuroblastoma tumours with unfavourable biology*. Eur J Cancer, 2005. **41**(4): p. 635-46.
141. Cavalli, L.R., M. Varella-Garcia, and B.C. Liang, *Diminished tumorigenic phenotype after depletion of mitochondrial DNA*. Cell Growth Differ, 1997. **8**(11): p. 1189-98.
142. Morais, R., et al., *Tumor-forming ability in athymic nude mice of human cell lines devoid of mitochondrial DNA*. Cancer Res, 1994. **54**(14): p. 3889-96.
143. Ishikawa, K., et al., *ROS-generating mitochondrial DNA mutations can regulate tumor cell metastasis*. Science, 2008. **320**(5876): p. 661-4.
144. Petros, J.A., et al., *mtDNA mutations increase tumorigenicity in prostate cancer*. Proc Natl Acad Sci U S A, 2005. **102**(3): p. 719-24.
145. Shidara, Y., et al., *Positive contribution of pathogenic mutations in the mitochondrial genome to the promotion of cancer by prevention from apoptosis*. Cancer Res, 2005. **65**(5): p. 1655-63.
146. Baysal, B.E., et al., *Mutations in SDHD, a mitochondrial complex II gene, in hereditary paraganglioma*. Science, 2000. **287**(5454): p. 848-51.
147. Niemann, S. and U. Muller, *Mutations in SDHC cause autosomal dominant paraganglioma, type 3*. Nat Genet, 2000. **26**(3): p. 268-70.
148. Xiao, M., et al., *Inhibition of alpha-KG-dependent histone and DNA demethylases by fumarate and succinate that are accumulated in mutations of FH and SDH tumor suppressors*. Genes Dev, 2012. **26**(12): p. 1326-38.
149. Frezza, C., et al., *Haem oxygenase is synthetically lethal with the tumour suppressor fumarate hydratase*. Nature, 2011. **477**(7363): p. 225-8.

150. Ward, P.S., et al., *The common feature of leukemia-associated IDH1 and IDH2 mutations is a neomorphic enzyme activity converting alpha-ketoglutarate to 2-hydroxyglutarate*. *Cancer Cell*, 2010. **17**(3): p. 225-34.
151. Dang, L., et al., *Cancer-associated IDH1 mutations produce 2-hydroxyglutarate*. *Nature*, 2009. **462**(7274): p. 739-44.
152. Lu, C., et al., *IDH mutation impairs histone demethylation and results in a block to cell differentiation*. *Nature*, 2012. **483**(7390): p. 474-8.
153. McCormack, J.G., A.P. Halestrap, and R.M. Denton, *Role of calcium ions in regulation of mammalian intramitochondrial metabolism*. *Physiol Rev*, 1990. **70**(2): p. 391-425.
154. Amuthan, G., et al., *Mitochondria-to-nucleus stress signaling induces phenotypic changes, tumor progression and cell invasion*. *EMBO J*, 2001. **20**(8): p. 1910-20.
155. DeBerardinis, R.J., et al., *The biology of cancer: metabolic reprogramming fuels cell growth and proliferation*. *Cell Metab*, 2008. **7**(1): p. 11-20.
156. Deberardinis, R.J., J.J. Lum, and C.B. Thompson, *Phosphatidylinositol 3-kinase-dependent modulation of carnitine palmitoyltransferase 1A expression regulates lipid metabolism during hematopoietic cell growth*. *J Biol Chem*, 2006. **281**(49): p. 37372-80.
157. Kurelac, I., G. Romeo, and G. Gasparre, *Mitochondrial metabolism and cancer*. *Mitochondrion*, 2011. **11**(4): p. 635-7.
158. Papandreou, I., et al., *HIF-1 mediates adaptation to hypoxia by actively downregulating mitochondrial oxygen consumption*. *Cell Metab*, 2006. **3**(3): p. 187-97.
159. Semenza, G.L., et al., *Hypoxia response elements in the aldolase A, enolase 1, and lactate dehydrogenase A gene promoters contain essential binding sites for hypoxia-inducible factor 1*. *J Biol Chem*, 1996. **271**(51): p. 32529-37.
160. Jones, R.G., et al., *AMP-activated protein kinase induces a p53-dependent metabolic checkpoint*. *Mol Cell*, 2005. **18**(3): p. 283-93.
161. Feng, Z., et al., *The coordinate regulation of the p53 and mTOR pathways in cells*. *Proc Natl Acad Sci U S A*, 2005. **102**(23): p. 8204-9.
162. Hardie, D.G., *AMP-activated/SNF1 protein kinases: conserved guardians of cellular energy*. *Nat Rev Mol Cell Biol*, 2007. **8**(10): p. 774-85.
163. Mihaylova, M.M. and R.J. Shaw, *The AMPK signalling pathway coordinates cell growth, autophagy and metabolism*. *Nat Cell Biol*, 2011. **13**(9): p. 1016-23.
164. Hardie, D.G., F.A. Ross, and S.A. Hawley, *AMPK: a nutrient and energy sensor that maintains energy homeostasis*. *Nat Rev Mol Cell Biol*, 2012. **13**(4): p. 251-62.
165. Kalender, A., et al., *Metformin, independent of AMPK, inhibits mTORC1 in a rag GTPase-dependent manner*. *Cell Metab*, 2010. **11**(5): p. 390-401.
166. Davies, S.P., A.T. Sim, and D.G. Hardie, *Location and function of three sites phosphorylated on rat acetyl-CoA carboxylase by the AMP-activated protein kinase*. *Eur J Biochem*, 1990. **187**(1): p. 183-90.
167. Sato, R., J.L. Goldstein, and M.S. Brown, *Replacement of serine-871 of hamster 3-hydroxy-3-methylglutaryl-CoA reductase prevents phosphorylation by AMP-activated kinase and blocks inhibition of sterol synthesis induced by ATP depletion*. *Proc Natl Acad Sci U S A*, 1993. **90**(20): p. 9261-5.
168. Watt, M.J., et al., *Regulation of HSL serine phosphorylation in skeletal muscle and adipose tissue*. *Am J Physiol Endocrinol Metab*, 2006. **290**(3): p. E500-8.
169. Das, S.K., et al., *Adipose triglyceride lipase contributes to cancer-associated cachexia*. *Science*, 2011. **333**(6039): p. 233-8.

170. Marsin, A.S., et al., *Phosphorylation and activation of heart PFK-2 by AMPK has a role in the stimulation of glycolysis during ischaemia*. *Curr Biol*, 2000. **10**(20): p. 1247-55.
171. McGee, S.L., et al., *AMP-activated protein kinase regulates GLUT4 transcription by phosphorylating histone deacetylase 5*. *Diabetes*, 2008. **57**(4): p. 860-7.
172. Decensi, A., et al., *Metformin and cancer risk in diabetic patients: a systematic review and meta-analysis*. *Cancer Prev Res (Phila)*, 2010. **3**(11): p. 1451-61.
173. Evans, J.M., et al., *Metformin and reduced risk of cancer in diabetic patients*. *BMJ*, 2005. **330**(7503): p. 1304-5.
174. Rosilio, C., et al., *The metabolic perturbators metformin, phenformin and AICAR interfere with the growth and survival of murine PTEN-deficient T cell lymphomas and human T-ALL/T-LL cancer cells*. *Cancer Lett*, 2013. **336**(1): p. 114-26.
175. Faubert, B., et al., *The AMP-activated protein kinase (AMPK) and cancer: Many faces of a metabolic regulator*. *Cancer Lett*, 2014.
176. Hadad, S.M., et al., *Histological evaluation of AMPK signalling in primary breast cancer*. *BMC Cancer*, 2009. **9**: p. 307.
177. Conde, E., et al., *Specific pattern of LKB1 and phospho-acetyl-CoA carboxylase protein immunostaining in human normal tissues and lung carcinomas*. *Hum Pathol*, 2007. **38**(9): p. 1351-60.
178. Faubert, B., et al., *AMPK is a negative regulator of the Warburg effect and suppresses tumor growth in vivo*. *Cell Metab*, 2013. **17**(1): p. 113-24.
179. Liu, L., et al., *Deregulated MYC expression induces dependence upon AMPK-related kinase 5*. *Nature*, 2012. **483**(7391): p. 608-12.
180. Luo, Z., M. Zang, and W. Guo, *AMPK as a metabolic tumor suppressor: control of metabolism and cell growth*. *Future Oncol*, 2010. **6**(3): p. 457-70.
181. Leprieux, G., et al., *The eEF2 kinase confers resistance to nutrient deprivation by blocking translation elongation*. *Cell*, 2013. **153**(5): p. 1064-79.
182. Wu, C.A., et al., *Nutrient deprivation induces the Warburg effect through ROS/AMPK-dependent activation of pyruvate dehydrogenase kinase*. *Biochim Biophys Acta*, 2013. **1833**(5): p. 1147-56.
183. Dumont, B., et al., *Differential proteomic analysis of a human breast tumor and its matched bone metastasis identifies cell membrane and extracellular proteins associated with bone metastasis*. *J Proteome Res*, 2012. **11**(4): p. 2247-60.
184. Emi, N., T. Friedmann, and J.K. Yee, *Pseudotype formation of murine leukemia virus with the G protein of vesicular stomatitis virus*. *J Virol*, 1991. **65**(3): p. 1202-7.
185. Bonnomet, A., et al., *A dynamic in vivo model of epithelial-to-mesenchymal transitions in circulating tumor cells and metastases of breast cancer*. *Oncogene*, 2012. **31**(33): p. 3741-53.
186. Vargo-Gogola, T. and J.M. Rosen, *Modelling breast cancer: one size does not fit all*. *Nat Rev Cancer*, 2007. **7**(9): p. 659-72.
187. Ringner, M., et al., *GOBO: gene expression-based outcome for breast cancer online*. *PLoS One*, 2011. **6**(3): p. e17911.
188. Grande, M., et al., *Transforming growth factor-beta and epidermal growth factor synergistically stimulate epithelial to mesenchymal transition (EMT) through a MEK-dependent mechanism in primary cultured pig thyrocytes*. *J Cell Sci*, 2002. **115**(Pt 22): p. 4227-36.
189. Lee, M.Y., et al., *Epithelial-mesenchymal transition in cervical cancer: correlation with tumor progression, epidermal growth factor receptor overexpression, and snail up-regulation*. *Clin Cancer Res*, 2008. **14**(15): p. 4743-50.

190. Price, J.T., et al., *Epidermal growth factor promotes MDA-MB-231 breast cancer cell migration through a phosphatidylinositol 3'-kinase and phospholipase C-dependent mechanism*. *Cancer Res*, 1999. **59**(21): p. 5475-8.
191. John, G.B., et al., *The mitochondrial inner membrane protein mitofilin controls cristae morphology*. *Mol Biol Cell*, 2005. **16**(3): p. 1543-54.
192. Berridge, M.V., P.M. Herst, and A.S. Tan, *Tetrazolium dyes as tools in cell biology: new insights into their cellular reduction*. *Biotechnol Annu Rev*, 2005. **11**: p. 127-52.
193. Machleidt, T., et al., *Multiple domains in caveolin-1 control its intracellular traffic*. *J Cell Biol*, 2000. **148**(1): p. 17-28.
194. Shajahan, A.N., et al., *Role of Src-induced dynamin-2 phosphorylation in caveolae-mediated endocytosis in endothelial cells*. *J Biol Chem*, 2004. **279**(19): p. 20392-400.
195. Perou, C.M., et al., *Molecular portraits of human breast tumours*. *Nature*, 2000. **406**(6797): p. 747-52.
196. Sorlie, T., et al., *Gene expression patterns of breast carcinomas distinguish tumor subclasses with clinical implications*. *Proc Natl Acad Sci U S A*, 2001. **98**(19): p. 10869-74.
197. Reis-Filho, J.S., et al., *EGFR amplification and lack of activating mutations in metaplastic breast carcinomas*. *J Pathol*, 2006. **209**(4): p. 445-53.
198. Savage, K., et al., *Caveolin 1 is overexpressed and amplified in a subset of basal-like and metaplastic breast carcinomas: a morphologic, ultrastructural, immunohistochemical, and in situ hybridization analysis*. *Clin Cancer Res*, 2007. **13**(1): p. 90-101.
199. Dong, C., et al., *Loss of FBP1 by Snail-mediated repression provides metabolic advantages in basal-like breast cancer*. *Cancer Cell*, 2013. **23**(3): p. 316-31.
200. Williams, T.M. and M.P. Lisanti, *Caveolin-1 in oncogenic transformation, cancer, and metastasis*. *Am J Physiol Cell Physiol*, 2005. **288**(3): p. C494-506.
201. Lajoie, P., et al., *Plasma membrane domain organization regulates EGFR signaling in tumor cells*. *J Cell Biol*, 2007. **179**(2): p. 341-56.
202. Li, L., et al., *Caveolin-1 mediates testosterone-stimulated survival/clonal growth and promotes metastatic activities in prostate cancer cells*. *Cancer Res*, 2001. **61**(11): p. 4386-92.
203. Tahir, S.A., et al., *Secreted caveolin-1 stimulates cell survival/clonal growth and contributes to metastasis in androgen-insensitive prostate cancer*. *Cancer Res*, 2001. **61**(10): p. 3882-5.
204. Ho, C.C., et al., *Up-regulated caveolin-1 accentuates the metastasis capability of lung adenocarcinoma by inducing filopodia formation*. *Am J Pathol*, 2002. **161**(5): p. 1647-56.
205. Alwan, H.A., E.J. van Zoelen, and J.E. van Leeuwen, *Ligand-induced lysosomal epidermal growth factor receptor (EGFR) degradation is preceded by proteasome-dependent EGFR de-ubiquitination*. *J Biol Chem*, 2003. **278**(37): p. 35781-90.
206. Longva, K.E., et al., *Ubiquitination and proteasomal activity is required for transport of the EGF receptor to inner membranes of multivesicular bodies*. *J Cell Biol*, 2002. **156**(5): p. 843-54.
207. Roepstorff, K., et al., *Differential effects of EGFR ligands on endocytic sorting of the receptor*. *Traffic*, 2009. **10**(8): p. 1115-27.
208. Schmidt-Glenewinkel, H., et al., *Multiparametric image analysis reveals role of Caveolin1 in endosomal progression rather than internalization of EGFR*. *FEBS Lett*, 2012. **586**(8): p. 1179-89.
209. Sewing, A., et al., *High-intensity Raf signal causes cell cycle arrest mediated by p21Cip1*. *Mol Cell Biol*, 1997. **17**(9): p. 5588-97.

210. Rush, J.S., et al., *Endosomal accumulation of the activated epidermal growth factor receptor (EGFR) induces apoptosis*. J Biol Chem, 2012. **287**(1): p. 712-22.
211. Li, R., *The expression and effect of Myoferlin depletion in breast cancer cells (dissertation)*. Columbus (OH): Ohio State University, 2012.
212. Chakraborty, J., et al., *Gain of cellular adaptation due to prolonged p53 impairment leads to functional switchover from p53 to p73 during DNA damage in acute myeloid leukemia cells*. J Biol Chem, 2010. **285**(43): p. 33104-12.
213. Kok, K.H., T. Lei, and D.Y. Jin, *siRNA and shRNA screens advance key understanding of host factors required for HIV-1 replication*. Retrovirology, 2009. **6**: p. 78.
214. Ortegren, U., et al., *A new role for caveolae as metabolic platforms*. Trends Endocrinol Metab, 2007. **18**(9): p. 344-9.
215. Pilch, P.F. and L. Liu, *Fat caves: caveolae, lipid trafficking and lipid metabolism in adipocytes*. Trends Endocrinol Metab, 2011. **22**(8): p. 318-24.
216. Gogvadze, V., S. Orrenius, and B. Zhivotovsky, *Mitochondria in cancer cells: what is so special about them?* Trends Cell Biol, 2008. **18**(4): p. 165-73.
217. Wu, S.B. and Y.H. Wei, *AMPK-mediated increase of glycolysis as an adaptive response to oxidative stress in human cells: implication of the cell survival in mitochondrial diseases*. Biochim Biophys Acta, 2012. **1822**(2): p. 233-47.
218. Cohen, A.W., et al., *Caveolin-1 expression is essential for proper nonshivering thermogenesis in brown adipose tissue*. Diabetes, 2005. **54**(3): p. 679-86.
219. Takeuchi, K., et al., *AMP-dependent kinase inhibits oxidative stress-induced caveolin-1 phosphorylation and endocytosis by suppressing the dissociation between c-Abl and Prdx1 proteins in endothelial cells*. J Biol Chem, 2013. **288**(28): p. 20581-91.

# **Publications**

## List of publications

Turtoi A\*, **Blomme A\***, Bellahcène A, Gilles C, Hennequière V, Peixoto P, Bianchi E, Noel A, De Pauw E, Lifrange E, Delvenne P, Castronovo V. 2013. Myoferlin as a key regulator of EGFR activity in breast cancer. *Cancer research* 73 (17): 5438-5448.

Turtoi A, **Blomme A**, Debois D, Somja J, Delvaux D, Patsos G, Di Valentin E, Peulen O, Mutijima EN, De Pauw E, Delvenne P, Detry O, Castronovo V. 2013. Organized proteomic heterogeneity in colorectal cancer liver metastases and implications for therapies. *Hepatology* doi: 10.1002/hep.26608

Warnock G, Turtoi A, **Blomme A**, Bretin F, Bahri MA, Lemaire C, Libert LC, Seret AE, Luxen A, Castronovo V, Plenevaux AR. 2013. In vivo PET/CT in a human glioblastoma chicken chorioallantoic membrane model: a new tool for oncology and radiotracer development. *Journal of Nuclear Medicine* 54 (10): 1782-1788.

Turtoi A, Dumont B, Greffe Y, **Blomme A**, Mazzucchelli G, Delvenne P, Mutijima EN, Lifrange E, De Pauw E, Castronovo V. 2011. Novel Comprehensive Approach for Accessible Biomarker Identification and Absolute Quantification from Precious Human Tissues. *Journal of Proteome Research* 10 (7): 3160-3182.

Gérin S., Mathy G., **Blomme A.**, Franck F., Sluse F.E., Plasticity of the mitoproteome to nitrogen sources (nitrate and ammonium) in *Chlamydomonas reinhardtii*: The logic of Aox1 gene localization., *Biochim. Biophys. Acta*, 2010, 1767(6-7), 994-1003.

Mathy G., Cardol P., Dinant M., **Blomme A.**, Gérin S., Ghysels B., Cloes M., De Pauw E., Leprince P., Remacle C., Sluse-Goffart C., Franck F., Matagne R.F., Sluse F.E., Proteomic and functional characterization of a *Chlamydomonas reinhardtii* mutant lacking the mitochondrial alternative oxidase 1., *J. Proteome Res.*, 2010, 9(6), 2825-2838.